Concatenated Space-Time Codes in Rayleigh Fading Channels

Geoffrey James Byers

Submitted in fulfillment of the academic requirements
for the degree of MSc Eng
in the School of Electrical and Electronic Engineering
at the University of Natal, Durban, South Africa

March 6, 2002

Abstract

The rapid growth of wireless subscribers and services as well as the increased use of internet services, suggest that wireless internet access will increase rapidly over the next few years. This will require the provision of high data rate wireless communication services. However the problem of a limited and expensive radio spectrum coupled with the problem of the wireless fading channel makes it difficult to provide these services. For these reasons, the research area of high data rate, bandwidth efficient and reliable wireless communications is currently receiving much attention.

Concatenated codes are a class of forward error correction codes which consist of two or more constituent codes. These codes achieve reliable communications very close to the Shannon limit provided that sufficient diversity, such as temporal or spatial diversity, is available. Space-time trellis codes (STTCs) merge channel coding and transmit antenna diversity to improve system capacity and performance. The main focus of this dissertation is on STTCs and concatenated STTCs in quasi-static and rapid Rayleigh fading channels.

Analytical bounds are useful in determining the behaviour of a code at high SNRs where it becomes difficult to generate simulation results. A novel method is proposed to analyse the performance of STTCs and the accuracy of this analysis is compared to simulation results where it is shown to closely approximate system performance.

The field of concatenated STTCs has already received much attention and has shown improved performance over conventional STTCs. It was recently shown that double concatenated convolutional codes in AWGN channels outperform simple concatenated codes. Motivated by this, two double concatenated STTC structures are proposed and their per-

formance is compared to that of a simple concatenated STTCs. It is shown that double concatenated STTCs outperform simple concatenated STTCs in rapid Rayleigh fading channels. An analytical model for this system in rapid fading is developed which combines the proposed analytical method for STTCs with existing analytical techniques for concatenated convolutional codes.

The final part of this dissertation considers a direct-sequence/slow-frequency-hopped (DS/ SFH) code division multiple access (CDMA) system with turbo coding and multiple transmit antennas. The system model is modified to include a more realistic, time correlated Rayleigh fading channel and the use of side information is incorporated to improve the performance of the turbo decoder. Simulation results are presented for this system and it is shown that the use of transmit antenna diversity and side information can be used to improve system performance.

Preface

The research work presented in this dissertation was performed by Mr Geoffrey Byers, under the supervision of Prof. Fambirai Takawira, at the University of Natal's school of Electrical and Electronic Engineering, in the Centre of Radio Access Technologies. This work was partially sponsored by Alcatel Altech Telecoms and Telkom SA Ltd as part of the Centre of Excellence programme.

Parts of this dissertation have been presented by the student at the IEEE COMSIG '2000 conference in Cape Town, South Africa and the SATNAC '2001 conference at the Wild Coast Sun, South Africa and have been submitted to the IEEE ICC '2002 conference to be held in New York, USA.

The entire dissertation, unless otherwise indicated, is the student's own original work and has not been submitted in part, or in whole, to any other University for degree purposes.

Acknowledgements

I wish to thank my supervisor, Prof. Fambirai Takawira, for his invaluable guidance, help and support. His willingness to always set aside his time to assist me in any way has been most appreciated. His valuable input into my research and constant encouragement has been of paramount importance to the success of this dissertation.

My parents and brother are owed many thanks for their support and their keen interest in my work. They have always encouraged me in whatever challenge I have taken up in my life and my MSc was no exception. I would like to thank my mother for proof reading parts of this dissertation.

Thanks are owed to Telkom SA Ltd and Alcatel Altech Telecoms for their much appreciated and enjoyed financial support and for providing the equipment necessary for completion of my MSc.

I would like to thank Miss Brigitte Le Bretton, Mr Bruce Harrisson, Dr Kesh Govinder and Mr Rob Gous for their help in one way or another over the past two years.

Finally I would like to thank my postgraduate colleagues for their help and friendship and for providing many hours of entertainment which helped create a most enjoyable working environment.

Contents

List of Figures

Chapter 1

Introduction

1.1 General

Predictions of "wireless catching up with wireline" are already evident today with the number of worldwide wireless subscribers expected to exceed 1 billion by the year 2002 [1]. Many factors are driving the wireless internet and wireless information revolution. A computer literate society which is becoming more reliant on data and information has emerged. Personal and business lifestyles are placing increased demands on both travel and mobility. Technology has provided high speed and cost effective mobile systems which are small, powerful and application rich. The market has shown a rapid growth in the use of internet and mobile services along with the growth of electronic commerce and increased use of portable computers. These factors have increased the demand for high data rate wireless communication services.

Many different second generation (2G) wireless systems have been developed, such as Global System for Mobile Communication (GSM) and IS-95 code division multiple access (CDMA). Third generation (3G) cellular systems aim to provide access to a diverse range of services for anyone, anywhere, anytime and at the lowest possible cost and merge existing cellular systems into a seamless radio infrastructure.

In order to coordinate global standardization of 3G systems, the International Telecom-

munications Union (ITU) formed the International Mobile Telecommunications for the 21st century (IMT-2000) program. The goal of this program is to allow wireless access to the global telecommunication infrastructure through both satellite and terrestrial systems, serving fixed and mobile users in public and private networks. Various standardisation bodies have agreed that global standards should specify the services and interfaces necessary for international compatibility and that regional standards should then be allowed to specify the details. In this way different IMT-2000 systems can exist between regions based on a common framework.

Some major objectives of IMT-2000 and differences from 2G systems are as follows: use of a common global frequency band; small pocket terminals with worldwide roaming; optimisation of a common radio interface for multiple operating environments; high transmission speed allowing for both circuit and packet switched as well as multimedia services; compatibility of IMT-2000 services with fixed network services; spectrum efficiency, quality and flexibility.

There are a number of IMT-2000 terrestrial radio interfaces. These are Universal Mobile Telecommunications System (UMTS), CDMA2000 and Universal Terrestrial Radio Access Time Division Duplex (UTRA TDD). UMTS or wideband code division multiple access (WCDMA) is likely to be used in most future 3G systems. It is being developed under European Telecommunications Standards Institute (ETSI) and is intended for the evolution of the (GSM) networks. The UMTS terrestrial radio access (UTRA) system is the radio part of the UMTS standard and has been specified to operate in a large variety of environments. Future development of IMT-2000 aims to include re-configurable terminals, downloading of services and applications, broadband satellite systems and space-time techniques. Space-time techniques allow for increased system capacity and bandwidth efficiency.

Network operators are constantly competing for the very limited radio spectrum which is essential to the provision of the described services. High demand generally results in high cost where recently $17.2 billion was raised for the PCS licenses auctioned in the United States of America. The extremely high cost of bandwidth has motivated network

operators and equipment suppliers to develop systems which squeeze every possible bit out of the available bandwidth.

The demand for high capacity wireless communication systems is evident, but the high cost of the limited radio spectrum is a major obstacle to the provision of high date rate services. The ability of future wireless systems to deliver high quality, high data rate and bandwidth efficient services is integral to future progress and development of wireless communication systems.

1.2 Digital communication systems

This section describes the main components of a digital communications system. Various methods used to improve system performance are discussed and lastly the field of space-time coding is introduced.

1.2.1 An overview

The goal of a communication system is to send a message from a source to one or more destinations such that the recovered message is an identical replica of the original message. A basic communication system [2], consisting of a transmitter, a channel and a receiver, is shown in Fig. 1.1.
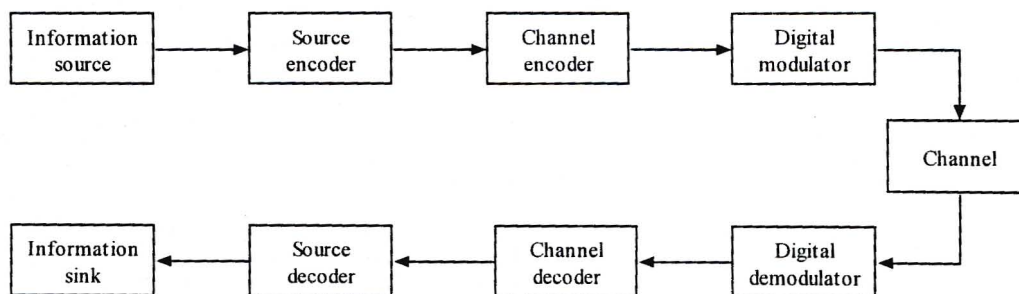
Figure 1.1: A communications system.

The original message could take an analog (continuous time) or digital (discrete time)

form. The source encoder constructs an information bit stream from the original message using as few bits as possible. This process is often referred to as compression. By adding redundancy to the information or uncoded bits by encoding them, they are protected against channel impairments. The digital modulator converts the encoded bits into a continuous time signal waveform which is suitable for transmission over the channel.

The communication channel between the transmitter and receiver corrupts the transmitted signal in a random like manner. In a wireless channel three main processes corrupt the transmitted signal, namely time-varying multipath fading, additive Gaussian noise (AWGN) and cochannel interference.

The demodulator provides an estimate of the encoded bit stream using the received signal. These estimates are then decoded where the most likely information bit sequence is chosen based on the code used. Finally the source decoder reconstructs an estimate of the original message from the decoded information bits.

Corruption of the transmitted signal by the channel causes errors in the demodulated signal. These errors may be corrected by the channel decoder, but this is not always the case. The rate of bit errors in the information stream or bit error rate (BER) gives a measure of the performance of the channel encoder and modulator.

The bandwidth efficiency and uncoded bit rate of a communication system are often described in terms of capacity. This is the ratio of data rate in bps to the bandwidth in Hz used. Thus capacity has units bps/Hz where a high capacity is synonymous with high bandwidth efficiency.

1.2.2 Error correcting codes

The uncoded bit stream is generally divided into frames and transmitted one frame at a time. There are two main approaches to correcting errors in a transmitted frame. Automatic repeat request (ARQ) will request the transmitter to resend the entire frame if the receiver detects any errors. This technique is well suited to reliable channels as the probability of error is small and hence the number of retransmissions is low. In harsher

channels, such as the wireless channel, ARQ is not a suitable technique as the frame may need to be resent several times before it is received correctly. In these harsher channels forward error correction (FEC) is used where the receiver attempts to correct errors within the frame. A variety of FEC codes exist, namely block codes, convolutional codes and concatenated codes. These FEC codes improve system performance at the cost of increased system bandwidth.

Block codes, which were developed first, map a block of k information bits to a block of n encoded bits where $k < n$. These codes allow a limited number of errors to be detected and a limited number of errors to be corrected. Block codes encountered in practice include; Hamming codes, Hadamard codes, Golay codes, cyclic Hamming codes, cyclic Golay codes, maximum–length shift register codes, Bose-Chaudhuri-Hocquenghem (BCH) codes [2]. Reed-Solomon (RS) codes [3], which fall under non-binary BCH codes, have good distance properties and allow for protection against burst errors. There exist efficient hard decision decoding algorithms, making these codes practical for a realistic system.

Convolutional codes were originally proposed by Elias [4]. They are different from block codes as data is not grouped into large blocks, but instead data is continuously encoded by passing k information bits at a time through a linear m-stage shift register. At each time instant, n encoded bits are calculated as a function of the current k information bits and the m shift register stages. Convolutional codes were first decoded using sequential decoding, but the first optimal (maximum-likelihood) decoder was proposed by Viterbi in 1967. The Viterbi algorithm [5] allowed for practical decoding and many applications were developed as a result of this algorithm. A big advantage of convolutional codes over block codes is the existence of soft-decision decoding algorithms such as the soft decision Viterbi algorithm and the maximum a posteriori (MAP) algorithm.

The first concatenated code proposed was proposed by D. Forney in 1966 [6] where the output of a RS code was then convolutionally encoded. This combined the good low SNR performance of convolutional codes with the good burst error protection properties of RS codes. In NASA's Galileo mission, a block interleaver was placed between the RS and

convolutional codes to spread out long error bursts. In 1993 a new class of concatenated codes were proposed by Berrou, Glavieux and Thitimajshima and were given the name turbo codes [7, 8]. Turbo codes were shown to achieve reliable communications at SNRs close to the Shannon limit in AWGN channels. The basic structure, which is described in detail in chapter 4, consists of two recursive systematic convolutional codes concatenated in parallel, separated by a pseudo-random interleaver. These codes are decoded using a suboptimal, yet powerful, iterative decoding algorithm which can be implemented with realisable complexity. The algorithm exchanges extrinsic information between decoders which allows the decoding process to be iterated several times, decreasing the number of errors on each iteration.

1.2.3 Modulation

The conversion of the encoded bit stream to its analog representation can be done in many different ways. A host of modulation techniques [9, chap. 6] are available such as binary and M-ary amplitude, frequency and phase shift-keying. These modulation techniques are chosen on the basis of system bandwidth and fading characteristics of the channel.

1.2.4 Combined coding and modulation

By treating the encoder and modulator as a single entity, large performance gains are obtained. With Trellis Coded Modulation (TCM) [10] the encoder/modulator combination is designed to increase the Euclidean distance rather than the Hamming distance between sequences of symbols. In this way coding gain is achieved through signal set expansion with no increase in system power or bandwidth. The concept of TCM combined with turbo coding was investigated in [11, 12, 13] and these systems showed improved performance over conventional TCM schemes.

In a wireless channel deep fades are often experienced. When only one path exists between the transmitter and receiver and this path experiences a deep fade, it is almost impossible to achieve reliable communications. To overcome this problem various diversity techniques

have been considered and this is the topic of the next section.

1.2.5 Diversity

In a wireless channel the transmitted signal is severely distorted due to multipath fading caused by destructive addition of multipaths and by interference from other users in multiple access systems. A signal experiencing a deep fade is highly susceptible to noise and this makes it difficult for the receiver to correctly determine the transmitted signal. Thus improving the performance of the channel encoder or modulator or combination thereof is not sufficient to achieve reliable communications. If multiple copies of the original signal are transmitted over independently fading sub channels, the probability of each signal undergoing a deep fade is greatly reduced. The receiver then combines the signals from each sub channel to obtain a closer approximation of the original transmitted signal.

In a realistic system diversity techniques are only useful if there is low correlation between the multiple sub channels. Therefore when selecting a diversity technique one take into account the characteristics of the communications channel. Many diversity techniques exist [14, Chap. 7] and can be divided into three main categories namely time, frequency and space and direction diversity as shown in Fig. 1.2. A good overview of the application of these techniques to cellular systems is given in [15] where it was concluded that it is essential to use space diversity in 3G systems.
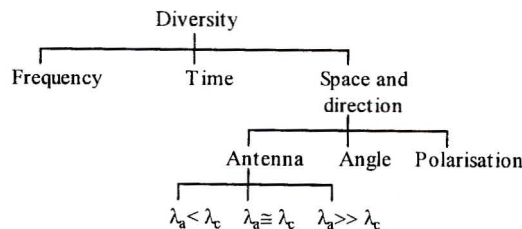
Figure 1.2: Classification of diversity techniques.

Time or temporal diversity makes use of channel coding and interleaving to spread the information over time. This diversity technique is only effective if the channel is time variant, such as with rapid fading channels, and it provides little diversity gain in slow

fading channels. Frequency diversity requires the channel to be frequency selective and works well if the frequency separation between sub channels is greater than the coherence bandwidth. For both time diversity using FEC codes and frequency diversity, performance gain is achieved at the cost of increased system bandwidth.

Space and direction diversity includes antenna, angle and polarization diversity techniques. Antenna diversity can again be divided into three cases where the antenna separation λ_a is either much greater than, approximately equal to or less than the carrier wavelength λ_c. In the first case the signals are uncorrelated and experience different propagation path loss and shadowing conditions. In the second case the signals are approximately uncorrelated and in the third case the signals are correlated. With this form of diversity there is no increase is system bandwidth or total transmitted power. Angle diversity resolves and combines signals with different angles of arrival. Polarization diversity combines signals with two different, generally orthogonal, polarizations.

In terms of combining the replicas of the transmitted signal, a number of diversity combining techniques exist. These include scanning, selection, maximal ratio and equal gain combining, where maximal ratio combining achieves the best performance.

1.2.6 Antenna diversity

In a power limited and bandwidth limited wireless communication system, many of the previously mentioned performance enhancing techniques are not suitable. Diversity is the key to reliable communication but time and frequency diversity result in bandwidth expansion. Receive antenna diversity where a single transmit and multiple receive antennas are employed has been well studied and is used in many communication systems such as at the base-station in cellular systems to improve the uplink[1] performance. This method does not require any increase in system power or bandwidth and is effective in improving the system performance.

Mobile terminals, such as those used in cellular systems, are required to be small and

---

[1]Link from mobile terminal to base station.

lightweight and have low power consumption. Employing receive diversity at the mobile terminal increases its cost, size and power consumption due to multiple antennas and radio frequency down conversion chains. Furthermore the multiple antennas are very close together and signals arriving at each antenna are highly correlated which reduces the diversity gain. Thus receive antenna diversity at the mobile terminal is not a practical or effective solution to improve the downlink[2] performance of cellular systems.

Transmit diversity, where multiple transmit antennas are used, improves system performance when receive diversity is not available. Multiple antennas employed at the base station can be sufficiently separated to ensure spatially uncorrelated fading and the extra processing burden is placed on the base station and not on the mobile terminal.

When multiple antennas can be employed at both the transmitter and receiver such as in wireless LANs or point to point communication systems, advantage can be taken of both transmit and receive diversity. Large capacity improvements of such a system can be obtained and this improvement cannot be achieved by receive diversity alone. This was shown from a theoretical view point in [16, 17, 18].

Thus the use of transmit diversity is two fold. It improves the system performance and/or capacity when receive diversity is not available and enhances the performance and/or capacity of receive diversity systems. In both cases the performance gain comes at no increase in system power or bandwidth.

1.2.7   Space-time trellis codes

Information theory has indicated the considerable gains in capacity achievable by multi-antenna systems. The next step was to design coding schemes suitable for multi-antenna transmission which perform close to the theoretical capacity. A number of different approaches have been proposed. These are layered space-time codes [19, 20] and space-time codes (STCs) which can be classified as space-time trellis codes (STTCs) [21] and space-time block codes (STBCs) [22]. These schemes are described in more detail in section 2.4.

---

[2]Link from base station to mobile terminal

They combine spatial and temporal diversity techniques and exploit the benefits of both.

It is well known that the STTCs achieve higher coding gains than STBCs [23] and both achieve maximum diversity gain. In [24] STTCs were shown to outperform layered space-time codes. Therefore STTCs offer a good trade off between performance and complexity. Unlike TCM where coding gain is achieved through signal set expansion, STTCs achieve coding gain through expansion in antenna space.

Much work has been done in the field of STTCs. A number of different channel models have been considered. New codes achieving higher coding gains have been proposed. The performance of STTCs with and without channel state information has been investigated. A few analytical techniques have been presented but these did not clearly explain all aspects of the analysis. A number of simple concatenated schemes using STTCs and convolutional codes as constituent codes have been proposed to increase the coding gain of STTCs.

The good performance of STTCs in terms of coding and diversity gain and their high bandwidth and power efficiency, make them an excellent choice for 3G systems.

1.3 Motivation for research

The rapid growth of wireless subscribers and internet services suggests that wireless internet access will increase rapidly over the next few years. This will require the provision of high data rate as well as reliable wireless communication systems. With a limited and expensive radio spectrum and the limitation on size, cost and power consumption of the mobile terminals, these systems must be power and bandwidth efficient.

The main impairment to wireless transmission is time-varying multipath fading. It is this impairment which makes cellular communication challenging compared to other communication systems. To overcome this problem without increasing the system bandwidth or transmitter power is very challenging.

Diversity is a promising approach, but time and frequency diversity techniques expand

the system bandwidth which is not desired. Antenna diversity is practical and effective as it successfully mitigates the effects of multipath fading at no increase in system power or bandwidth. Conventional approaches employ receive antenna diversity which has been successfully applied to many systems such as the uplink in cellular systems.

However when the receive terminal is limited in terms of cost, size and power consumption such as a mobile unit in a cellular system, receive diversity is not practical or effective. In this situation, transmit antenna diversity is used to effectively combat the effects of multipath fading at no increase in system power or bandwidth and without sacrificing the limitations placed on the mobile terminal. Transmit diversity can also be used to increase the capacity of systems employing receive diversity.

By merging transmit antenna diversity with appropriate channel coding, further performance gains are possible. Space-time trellis codes are one such approach and have received much attention in recent years. The analysis of STTCs has not been well covered and the analysis of concatenated STTCs has only been addressed in quasi-static fading channels. Furthermore only simple concatenated STTC structures have been considered.

This research focuses on the use of coded transmit diversity in single user and multiple user wireless systems. A unique mathematical analysis for STTCs and concatenated STTCs is proposed. A novel double concatenated STTC system is proposed to further improve the coding gain of conventional STTCs. For wireless multiple access systems, a turbo transmit diversity DS/SFH CDMA scheme is considered and its performance is enhanced by employing side information in the turbo decoder.

1.4 System realisability

Any system enhancement comes at some cost being either increased system bandwidth, increased power or the requirement of extra processing power. In all cases this cost must be realisable in order for the system to be practically implemented. In the case of STTCs system performance is enhanced at no cost in transmit power or system bandwidth. However increased processing power, relative to the uncoded system, is required. The concatenated

STTC systems proposed improve system performance at the cost of further processing power.

The processing cost of the proposed systems depends on the hardware on which the system is implemented as well as the efficiency of their implementation. Because no such implementation was done, the processing cost cannot be accurately determined. However an approximate cost analysis can be done. The MAP decoding algorithm used in these systems is approximately 4 times the complexity of the Viterbi algorithm. The Viterbi algorithm is used in many of todays communication systems to decode convolutional codes. Let C denote the computational cost which is calculated as follows.

$$C = 4 \times CV \times NC \times NI \tag{1.1}$$

Here CV is the computational cost of the Viterbi algorithm, NC is the number of constituent decoders and NI is the number of decoding iterations.

Digital signal processors (DSPs), microprocessors and field programmable gate arrays (FPGAs) are constantly being developed to provide increased processing power and more memory. It is thus plausible that many complex systems could be realised in the not too distant future.

1.5 Dissertation overview

This dissertation is divided into six chapters. Chapter 1 gave an overview of 3G cellular systems describing their necessity and requirements. A basic communication system was described and various coding, modulation and diversity techniques to improve system performance were outlined. Antenna diversity and finally space-time trellis codes which merge antenna diversity and channel coding were discussed. Motivation for the work done in this dissertation was then given.

Chapter 2 is a literature survey on multi-antenna transmission systems employing error control coding. A generalised system model employing multiple transmit and receive antennas is presented. The outage capacity and theoretical limits on the performance of

these systems is then described and results are given. Coding schemes for multi-antenna systems which aim to approach these theoretical limits are reviewed. Space-time trellis codes offer the best tradeoff between complexity and performance and are discussed in detail in this chapter. Recent work in this field is reviewed, the STTC system architecture is described and performance results are presented.

In chapter 3 a novel mathematical analysis is proposed to calculate the performance of STTCs in quasi-static and rapid Rayleigh fading channels. This is useful in observing the behaviour of STTCs at high SNRs and is the basis of the analysis proposed in chapter 4 for concatenated STTCs. The analysis draws on some existing techniques but is unique in its application to STTCs. Existing analytical methods are reviewed and the calculation of the pairwise error probability is discussed. The proposed analytical method is fully explained and is compared to simulation results to assess its accuracy.

Concatenated codes using convolutional codes and STTCs as constituent codes are considered in chapter 4 in order to increase the coding gain of STTCs. A review of concatenated convolutional codes and concatenated STTCs is given. Two novel double concatenated STTC structures are proposed where the encoding and decoding of each is described. A new analytical model is then presented for concatenated and double concatenated STTCs in rapid Rayleigh fading channels. Simulation results are given to assess the performance of the proposed system and to verify the accuracy of the proposed analysis.

Chapter 5 focuses on the performance of CDMA systems using transmit antenna diversity. A turbo transmit diversity, direct-sequence/slow-frequency-hopped (DS/SFH) CDMA system is presented and its performance is enhanced by utilising side information (SI) in the turbo decoder. A more realistic channel model is considered with correlated Rayleigh fading in time and partial-band jamming. An overview of CDMA systems, space-time transmit antenna diversity and turbo decoding with SI is given. The system model is described and the modifications to the turbo decoder to incorporate SI are explained. System performance is evaluated by simulation where the effects of SI, diversity and the encoder parameters are investigated.

The results presented in chapters 2 through 5, were generated using custom built software

simulation environments which were developed by the author using the C++ programming language. A general description of the simulation procedure used is presented in appendix D.

Lastly, chapter 6 presents the conclusions drawn in this dissertation.

1.6 Original contributions in this dissertation

The original contributions of this dissertation include:

1. A mathematical analysis for STTCs in rapid and quasi-static fading channels is proposed.

2. Two novel double concatenated STTC structures are proposed.

3. A new analytical model for concatenated and double concatenated STTCs is proposed for rapid fading channels.

4. A turbo transmit diversity DS/SFH CDMA system is modified to incorporate three forms of side information in the turbo decoder.

Parts of this work presented in this dissertation have been presented or submitted by the author to the following local and international conferences:

1. G. Byers, H. Xu and F. Takawira, "Turbo coded diversity scheme with side information for hybrid DS/SFH CDMA systems," *Proceedings of IEEE Communications and Signal Processing Conference (COMSIG 2000)*, Cape Town, South Africa, Sep. 2000.

2. G. Byers and F. Takawira, "Analysis of space-time trellis codes on block and rapid Rayleigh fading channels," *Proceedings of South African Telecommunications Networks and Applications Conference (SATNAC 2001)*, Wild Coast Sun, South Africa, Sep. 2001.

3. G. Byers and F. Takawira, "Double concatenated space-time trellis codes," *Submitted to IEEE International Conference on Communications (ICC 2002)*, New York, USA, April 2002.

Chapter 2

Coding for Multi-Antenna Transmission Systems

2.1 Introduction

This chapter is a literature survey on systems employing error control coding and multiple transmit and receive antennas or multi-element arrays (MEAs). These systems are able to take advantage of diversity in both the spatial and temporal dimensions.

In section 2.2 the system model for a generalised MEA system is presented. Theoretical limits on the capacity and performance of MEA systems in quasi-static fading channels are investigated in section 2.3. An overview of various coding schemes for MEA systems, which attempt to achieve this theoretical capacity, is given in section 2.4. Section 2.5 focuses on space-time trellis codes where the system architecture is described, current literature is reviewed and performance results are given.

2.2   Multi-antenna system model

In this section a basic model of a MEA system is presented. The system model is shown in Fig. 2.1 and is based on the model described in [18, 21]. The choice of channel parameters is done in accordance with [21]. The model describes a single point–to–point wireless communications system with n_T transmit and n_R receive antennas. In this system the overall transmitted power and channel bandwidth are constrained and the channel model is presented in complex baseband form.
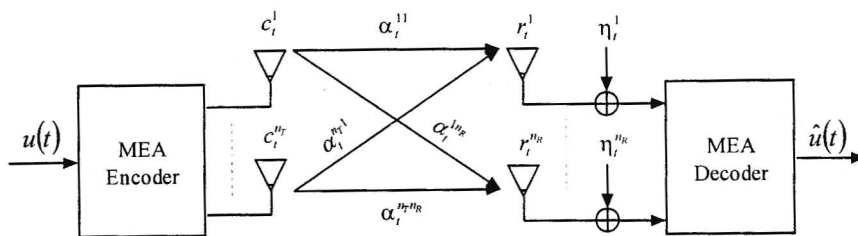
Figure 2.1: A multi-antenna system.

The input data $u(t)$ is encoded by the MEA encoder to produce n_T output symbols c_t^i where $i = \{1, \ldots, n_T\}$. Each of these symbols are then individually modulated to produce signals $\sqrt{E_s}c_t^i$ which are simultaneously transmitted over the n_T transmit antennas. The symbols c_t^i are normalised in magnitude and E_s is chosen so that the average energy of the constellation is 1.

The signal received after matched filtering on receive antenna $j = \{1, \ldots, n_R\}$ is a noisy superposition of the n_T transmitted signals and can be expressed as follows.

$$r_t^j = \sqrt{E_s} \sum_{i=1}^{n_T} c_t^i \alpha_t^{ij} + \eta_t^j \tag{2.1}$$

The Rayleigh fading process is assumed to be frequency flat as the total system bandwidth is narrow. The complex path gain from transmit antenna i to receive antenna j is denoted α_t^{ij}. This is modeled as a zero-mean complex Gaussian random sequence with variance 0.5 per dimension. The antenna elements are assumed to be sufficiently separated to ensure spatially uncorrelated fading i.e. the path gains are independent. This assumption is appropriate if the antenna elements are separated by more than half a wavelength [18].

The noise introduced at receive antenna j is denoted by η_t^j and is also a zero-mean complex Gaussian random sequence with variance $N_0/2$ per dimension, where $N_0/2$ is the two-sided noise power spectral density. The MEA decoder then reconstructs an estimate of the original input data to produce decoded bit stream $\hat{u}(t)$.

In general data is transmitted on a frame by frame basis. In this dissertation both quasi-static and rapid Rayleigh fading channel models are considered. In both channels the transmitted signals are uncorrelated in space. In a quasi-static fading channel the path gains remain constant for the entire frame duration but are independent from one frame to the next. In a rapid fading channel the path gains are uncorrelated in time but are assumed to remain constant for the symbol duration.

The availability of channel state information (CSI) or knowledge of the path gains between each transmit and receive antenna pair affects the performance of the MEA system. In [25] various cases of CSI or no CSI at the transmitter and/or receiver were discussed. These include the cases of no CSI at transmitter or receiver (blind schemes), CSI at the receiver (feedforward schemes) and CSI at both transmitter and receiver (feedback schemes). The CSI is generally estimated using pilot symbols. This chapter as well the rest of this dissertation will focus on schemes where perfect CSI at the receiver can be assumed.

2.3 Channel capacity

Channel capacity is the theoretical limit to error free transmission provided by information theory. In theory no system can perform better than this limit but merely attempt to approach it by using advanced signal processing techniques.

Fundamental limits for MEA systems were presented in [16] for an AWGN channel and in [17] for a quasi-static fading channel with no CSI at transmitter or receiver. Fundamental limits for the most commonly studied case of no CSI at the transmitter and perfect CSI at the receiver were derived in [18] for a quasi-static Rayleigh fading channel.

In this section the information theoretic results from [18] are presented for the capacity of

a MEA system in a quasi-static Rayleigh fading channel in units bps/Hz. It is shown that transmit or receive diversity alone cannot achieve the capacities possible when multiple antennas are used at both the transmitter and receiver.

2.3.1   Background to channel capacity

In [2, Chap. 3] the concept of mutual information $I(x_i; y_j)$ between the events x_i being transmitted and y_j being received was introduced. The average mutual information $I(X; Y)$ given by the output Y about the input X was also discussed for both discrete and continuous random variables. Channel capacity [2, Chap. 7] is the quantity $I(X; Y)$ maximised over the input probabilities $P(x_i)$ and is denoted by $\tilde{C}$ with units bits per input symbol when $I(X; Y)$ is calculated using log to the base 2. This quantity is expressed in (2.2) and is only dependent on the characteristics of the channel, not on the characteristics of the information source.

$$\tilde{C} = \max_{P(x_i)} I(X; Y) \tag{2.2}$$

For a bandlimited AWGN waveform channel with bandwidth W, noise power spectral density N_0 and signal power P_{av}, the channel capacity is given below.

$$\tilde{C} = W \log_2 \left(1 + \frac{P_{av}}{N_0 W} \right) \quad \text{bps} \tag{2.3}$$

The rato $\tilde{C}/W$ is referred to as the normalised channel capacity and will be denoted by C.

The *noisy channel coding theorem* due to Shannon which is sometimes referred to as Shannon's end theorem or the fundamental theorem of information theory, states the following: There exist channel codes (and decoders) that make it possible to achieve reliable communication, with as small an error probability as desired, if the transmission rate $R < C$, where C is the channel capacity. If $R > C$, it is not possible to make the probability of error tend toward zero with any code.

Thus channel capacity C specifies the fundamental limit on the rate R at which information can be transmitted reliably over the communications channel.

2.3.2 Capacity of multi-antenna systems

Consider the MEA system of Fig. 2.1. Let $\boldsymbol{\alpha}$ be the matrix of path gains α_{ij} which describes the fading channel between the transmitter and the receiver. Because one is dealing with a quasi-static fading channel the time dependence of $\boldsymbol{\alpha}$ can be dropped. Capacity can be dealt with probabilistically as $\boldsymbol{\alpha}$ is a matrix of random variables.

In [18] a general expression for the normalised capacity of the MEA system described in section 2.2 was derived and is given in (2.4) below. This assumes that the transmitted signal is composed of n_T statistically independent components of equal power, each having a Gaussian distribution.

$$C = \log_2 \det \left(\boldsymbol{I}_{n_R} + \frac{\rho}{n_T} \boldsymbol{\alpha}^\dagger \boldsymbol{\alpha} \right) \text{ bps/Hz} \tag{2.4}$$

Here $\dagger$ is the transpose conjugate and det is the matrix determinant. $\boldsymbol{I}_{n_R}$ is the $n_R \times n_R$ identity matrix, $\boldsymbol{\alpha}$ is the $n_T \times n_R$ matrix of complex path gains α_{ij} and ρ is the average SNR at each receive antenna.

As can be seen, the system capacity depends on the channel realisation $\boldsymbol{\alpha}$. Capacity is generally treated as a random variable where the aim is to calculate the Complementary Cumulative Distribution Function (CCDF). This is done by Monte-Carlo methods whereby the channel matrix $\boldsymbol{\alpha}$ is generated many times, according to its probability distribution. For each channel realisation, the capacity is calculated using (2.4) and the CCDF is updated. In general 10,000 channel realisations are used in the capacity plots shown in this section.

In Fig. 2.2 a plot of the CCDF for an MEA system is shown for the cases of 1 and 2 transmit and receive antennas. The x-axis gives the capacity C and the corresponding entry on the y-axis gives the probability that the system will exceed this capacity. Thus at the 98% level, 98% of all channel realisations achieve at least the corresponding capacity. Let n_{TR} refer to the case of equal transmit and receive antennas i.e. $n_T = n_R = n_{TR}$. It can be clearly seen that there is a large improvement in the capacity achieved by the $n_{TR} = 2$ system over the $n_{TR} = 1$ system which is more pronounced at higher SNRs. At the 98% level on the CCDF the capacity of the $n_{TR} = 2$ system exceeds that of the
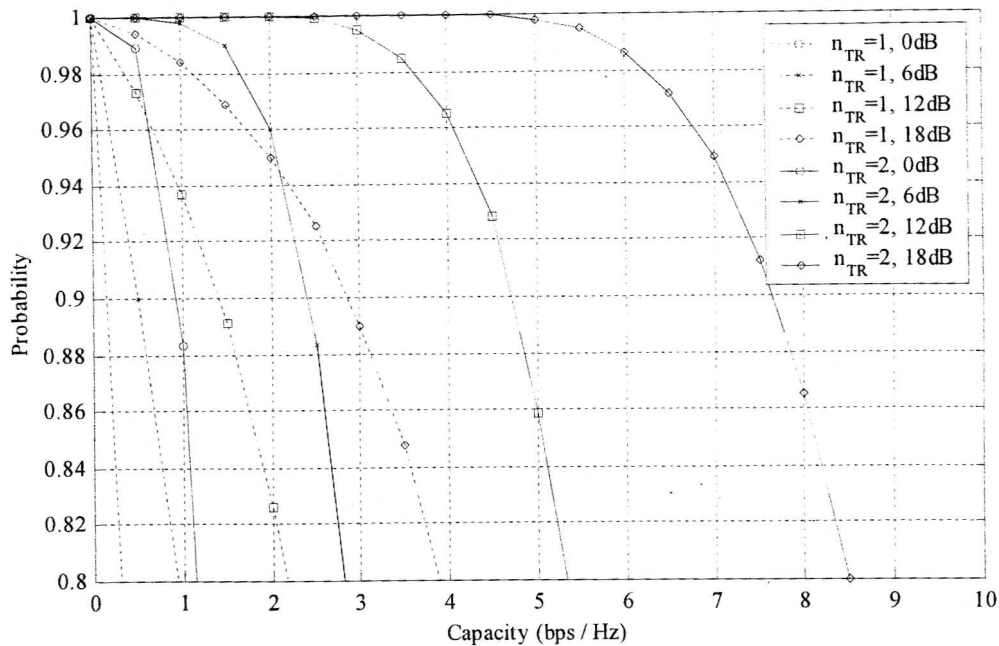
Figure 2.2: Complementary Cumulative Distribution Functions (CCDFs).

$n_{TR} = 1$ system by approximately 3 bps/Hz at 12dB and 5 bps/Hz at 18dB.

The outage capacity of a system is closely related to the CCDF. For example at the 99% level on the CCDF, 99% of all possible channels will achieve or exceed the corresponding capacity. This corresponds to 1% of all channels not achieving this capacity which is referred to as the channel being out. Therefore an outage probability P_{out} of 1% means that 1% of all possible channels will not achieve the corresponding capacity which is called the outage capacity C_{out} of the channel.

It is interesting to observe the dependence of the outage capacity on the number of transmit and receive antennas. In Fig. 2.3 and Fig. 2.4 the capacity is given at a 1% outage probability. In Fig. 2.3 capacity is plotted against the number of receive antennas for a SNR of 5dB where the number of transmit antennas is varied. It can be clearly seen that the capacity saturates if the number of transmit antennas is not increased. Thus transmit diversity is essential if large system capacities are desired. In Fig. 2.4 capacity is plotted for an equal number of transmit and receive antennas n_{TR} where the SNR is varied. Capacity is seen to increase linearly with n_{TR} and at high SNRs a 3dB increase
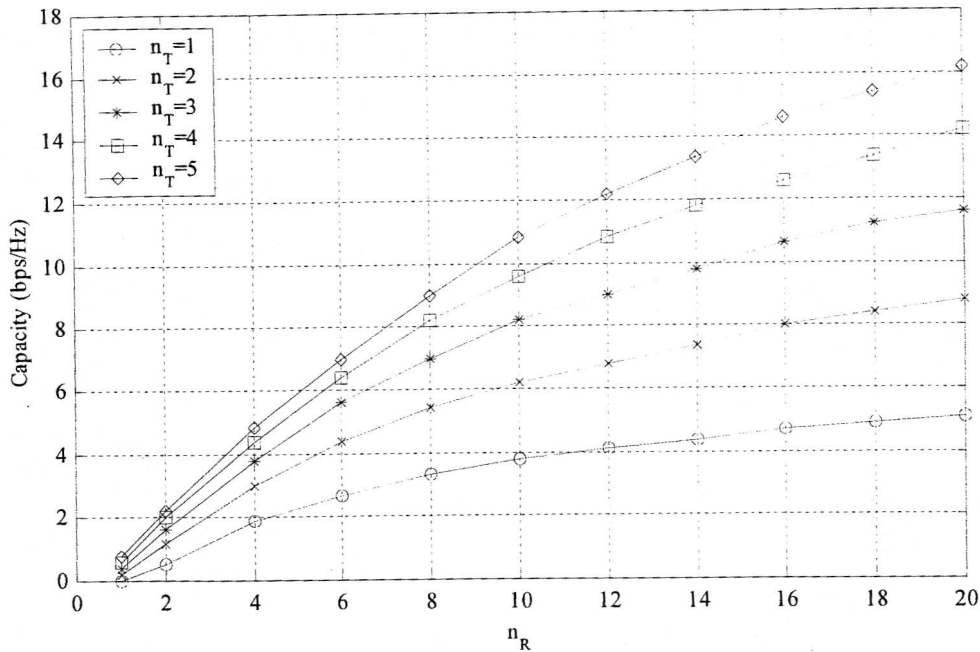
Figure 2.3: Capacity dependence on n_R for varying n_T with SNR = 5dB and at 1% outage probability.

in the SNR corresponds approximately to a n_{TR} bps/Hz increase in capacity.

2.3.3 Frame error rate of multi-antenna systems

The calculation of the FER from the outage capacity was explained in [26]. If a frame is transmitted at a rate R bps/Hz equal to the outage capacity, the FER is simply the probability that a channel outage occurs. For example if a frame is transmitted at $R = C_{out} = 2$ bps/Hz and $P_{out} = 1\%$ then the FER is 10^{-2}.

In Fig. 2.5 the FERs of various MEA systems are shown where the tranmission rate is $R = 2$ bps/Hz in all cases. The notation (n_T, n_R) is used to describe an MEA system with n_T transmit and n_R receive antennas. Comparing the (2,1) case to the (1,2) case it is noted that receive diversity outperforms transmit diversity by 3dB. This is due to the total transmit power being distributed over the 2 transmit antennas. The diversity gains given by the slope of the curve at medium to high SNRs are of interest. A slope of 1
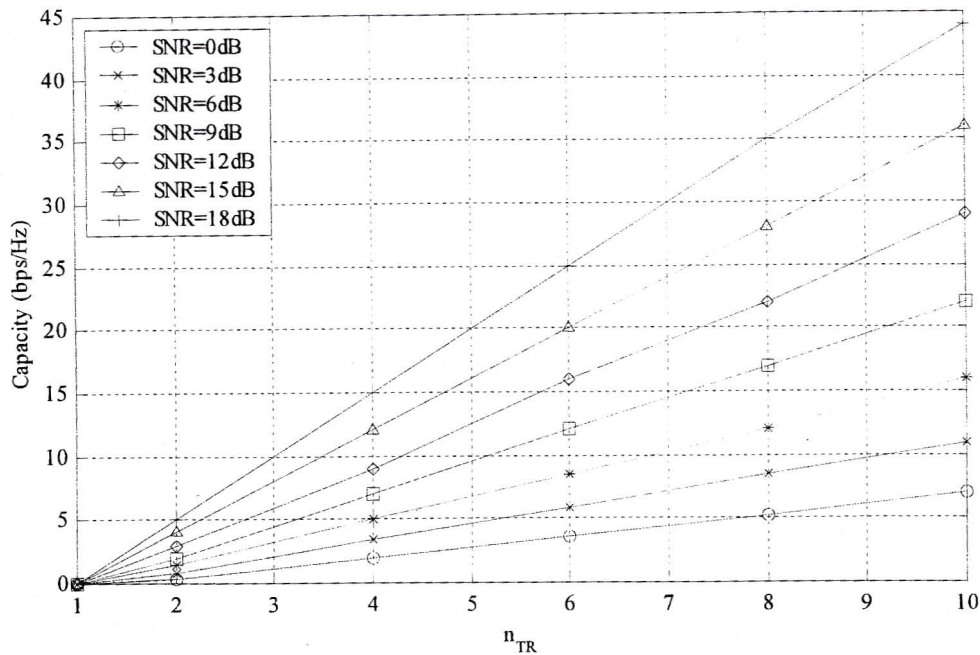
Figure 2.4: Capacity dependence on n_{TR} for varying SNR at 1% outage probability.

dB/dB is achieved for the (1,1) case, 2 dB/dB for the (1,2) and (2,1) cases and 4 dB/dB for the (2,2), (4,1) and (1,4) cases. Thus full spatial diversity is achieved in all cases.

2.4   Coding schemes for multi-antenna systems

Theoretical gains of multi-antenna systems are considerable as shown in the previous section. Motivated by this, a number of systems have been proposed in the literature which aim to approach this capacity limit. Three main approaches have been considered; bit-interleaved space-time codes, layered space-time codes and space-time codes. In this section a review of these approaches is given.

2.4.1   Bit-interleaved space-time codes

Bit-interleaved coded modulation (BICM) was originally proposed in [27] for single-antenna systems and performed well in AWGN and Rayleigh fading channels. This scheme sepa-
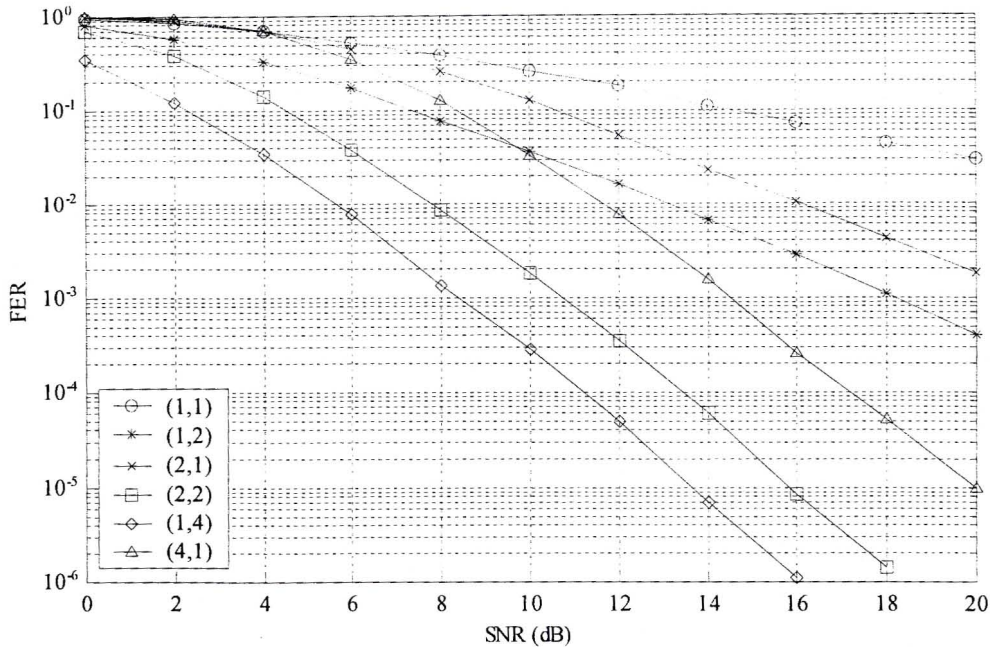
Figure 2.5: FER for various MEA systems at $R = 2$ bps/Hz.

rates the encoding from the modulation stages which makes the system easier to design. For this reason the performance of BICM over a multi-antenna channel was considered. A turbo coded modulation system [28] which interleaved the output bits of a turbo encoder and mapped these bits to the n_T transmit antennas was shown to perform better than space-time block and space-time trellis codes in quasi-static and rapid Rayleigh fading channels. This scheme however did not guarantee maximum diversity and various concatenated space-time trellis coded systems, discussed in chapter 4, should be compared to this system to obtain a "fair" comparison.

2.4.2   Layered space-time codes

Large spectral efficiencies can be achieved by a wireless channel if the number of transmit and receive antennas is large. However as n_T and n_R increase, the complexity of the maximum likelihood detection for space-time codes becomes computationally intensive. For this reason suboptimal space-time architectures which achieve spectral efficiencies similar to ST codes and lower decoding complexities have been investigated.

To achieve this an architecture named BLAST (Bell Laboratories Layered Space Time) was proposed in [19]. The system is based on a layered architecture and is designed such that capacity increases linearly with n_{TR}. The information stream is demultiplexed into n_T equal rate streams which are then separately encoded. The encoded streams are diagonally interleaved whereby each stream is periodically cycled over the n_T transmit antennas such that all streams are transmitted from a different antenna for a fixed duration. In this way each subchannel has the same capacity and none of the encoded streams experiences a deep fade for a long duration. The receiver uses a reduced-complexity suboptimal detector which performs the operations of nulling and cancelation to create independent virtual subchannels.

The BLAST architecture later called D-BLAST (Diagonally Layered BLAST) has some implementation complexities. D-BLAST requires advanced coding techniques to encode the symbols along the space-time diagonals and the diagonal layering structure results in some space-time being wasted at the start and end of the frame. Furthermore the avoidance of catastrophic error propagation is a problem. For these reasons V-BLAST (Vertical BLAST) was proposed in [20] and was later discussed in [29]. This architecture uses no coding and is hence simpler to implement but this comes at the price of some performance degradation over D-BLAST.

2.4.3 Space-time codes

Space-time codes focus on merging antenna diversity with appropriate channel coding to exploit the benefits of both spatial and temporal diversity. In a similar way to TCM where performance gain is achieved through signal set expansion and appropriate coding, ST codes achieve improved performance by antenna expansion combined with appropriate channel coding. There are two classes of ST codes, namely space-time block codes (STBCs) and space-time trellis codes (STTCs). A major difference between ST codes and BLAST is with ST codes there exists a relationship between signals on the different transmit antennas. Unlike bit-interleaved ST codes, where full diversity is not always guaranteed ST codes are designed to achieve maximum diversity gain.

STTCs were originally proposed in [21] where codes were developed for two transmit antennas and various signal constellations. The STTC architecture will be discussed in more detail in the next section. The input data stream is encoded by the STTC encoder to produce n_T streams which are simultaneously transmitted over the n_T transmit antennas. Maximum-likelihood detection along with maximum likelihood decoding is used at the receiver to estimate the original data stream. STTCs achieve maximum diversity gain and good coding gain but unfortunately decoding complexity increases with the number of encoder states.

STBCs were developed to achieve lower decoding complexity than STTCs. STBCs achieve maximum diversity gain but limited coding gain compared with STTCs. A simple STBC for two transmit antennas was initially proposed in [30] which was the basis for the work done in [22] which designed STBCs for any number of transmit antennas. The performance of STBCs was investigated in [31]. With this system the input data is encoded by the STBC encoder to produce n_T streams which are simultaneously transmitted over the n_T transmit antennas. At the receiver, the signals transmitted from the different antennas are decoupled using the orthogonal structure of the STBC. Maximum-likelihood decoding based on linear processing is then used to estimate the original data stream.

For both STTCs and STBCs, decoding requires knowledge or an estimate of the CSI. The case of no CSI at the receiver was investigated in [32] where a unitary space-time modulation scheme was proposed. This scheme does not require the use of training symbols because information is carried on the subspace spanned by orthonormal signals which are sent to each transmit antenna. Differential unitary space-time modulation was proposed in [33] and a differential detection scheme was proposed in [34].

2.5 Space-time trellis codes

Space-time trellis codes combine spatial and temporal diversity techniques and exploit the benefits of both. They are designed to achieve maximum diversity gain and good coding gain and provide the best tradeoff between constellation size, data rate, diversity

advantage and trellis complexity. It is well known that the STTCs achieve greater coding gains than STBCs [23]. In [24] STTCs were shown to outperform layered space-time codes.

This section focuses on STTCs where perfect CSI is available to the receiver. A review of some of the current literature in this field is given. The system architecture is then described and simulation results for various STTCs in quasi-static and rapid Rayleigh fading channels are presented.

2.5.1 Current literature

The field of STTCs with perfect receiver CSI has been one of great interest. Major areas of research include finding optimum codes, performance in different channels, analytical techniques and concatenated coding schemes. The latter two areas will be discussed in chapters 3 and 4 respectively.

Research into finding codes that achieve higher coding gain has been done by a number of authors. STTCs using PSK modulation constructed from known convolutional codes that achieve optimal free distance were proposed in [35]. In [36] a systematic code search was used to find codes achieving maximum diversity gain and improved coding gain over the Tarokh STTCs [21]. Work done in [37] searched for all codes giving maximum diversity gain and for these codes calculated the coding gain. The codes with the highest coding gain were compared using a new performance estimate and the code with the best performance was then selected. Simulation results in quasi-static fading channels showed that the proposed optimal codes resulted in a lower FER than [21, 36] and in some cases [35].

The performance of STTCs in channels other than a spatially uncorrelated Rayleigh fading channel has been investigated. The performance of STTCs in spatially correlated and uncorrelated Nakagami fading channels was investigated in [38]. The STTCs proposed in [21] were shown to be optimal for this channel and were shown to perform well with spatial correlation between the transmit antennas. However some performance degradation over the uncorrelated case was observed.

2.5.2 Encoder architecture

A space-time trellis encoder operates in a similar way to a convolutional encoder except that the connection weights and output symbols form part of an M−ary alphabet. The system is best described in discrete time using the feedforward implementation of the STTC encoder.

The STTC encoder can be described in terms of the number of input bits k at each time instance, the memory m, the constellation size M and the number of transmit antennas n_T. At each time instance t, k bits $(u_t^1, \ldots, u_t^k)$ are shifted into the STTC encoder. Each M-ary output symbol c_t^i for each transmit antenna i, is generated by multiplying each of the k input bits along with the m state bits $(u_t^1, \ldots, u_t^k, s_1, \ldots s_m)$ by their corresponding weights and then adding the products using modulo-M arithmetic.

For example, the Tarokh STTC [21, Fig. 4] with $k = 2$, $m = 2$ (4-state), $M = 4$ (4-PSK) and $n_T = 2$ is shown in Fig. 2.6. At each time instance t, the number of input bits is 2 and the number of output symbols per antenna is 1 which translates to a bandwidth efficiency of 2 bps/Hz.
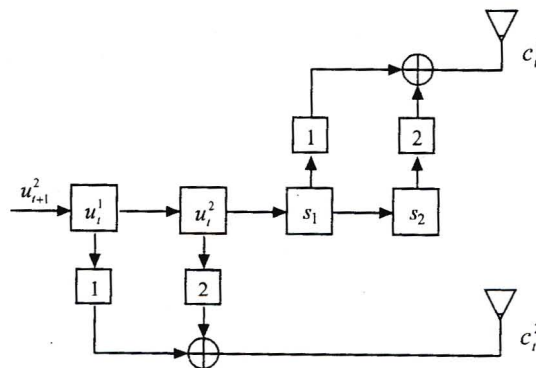
Figure 2.6: Encoder for Tarokh STTC ($k = 2, m = 2, M = 4, n_T = 2$).

A trellis diagram can be used to fully describe a STTC. In Fig. 2.7 the corresponding trellis diagram for the STTC encoder in Fig. 2.6 is given. The rows of the matrix correspond to the current encoder state given by $s_1 + 2s_2$. Each entry in the matrix gives the transmitted symbols c_t^1 and c_t^2 for the current encoder state and input bits u_t^2, u_t^1. The 4-PSK signal constellation used is also shown. The transitions in the trellis diagram from top to bottom

correspond to the matrix entries from left to right.
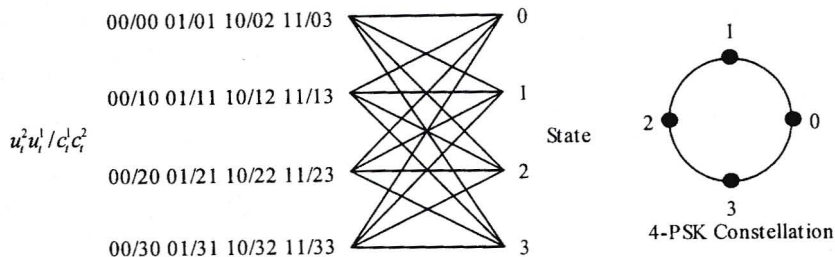
Figure 2.7: Trellis diagram for Tarokh STTC ($k = 2, m = 2, M = 4, n_T = 2$).

2.5.3 Decoder architecture

The channel over which the symbols are transmitted is identical to that described in section 2.2 and the received signal on receive antenna j at time t, r_t^j is given by (2.1). As mentioned previously, decoding requires knowledge of the CSI or α_t^{ij}'s. The Viterbi algorithm can be used to estimate the most likely information stream using the following branch metric for the state transition with output symbols $g_t^1 \ldots g_t^{n_T}$.

$$\sum_{j=1}^{n_R} \left| r_t^j - \sum_{i=1}^{n_T} \alpha_t^{ij} g_t^{n_T} \right|^2 \tag{2.5}$$

It is important to understand that n_T signals are transmitted at each time instance t. These signals are subjected to independent fading and at each receive antenna a composite of these signals corrupted by fading and noise is observed. This is simply a new signal with a different amplitude and phase to either of the transmitted signals. The decoder is required to estimate the likelihood of the received signal by calculating the Euclidean distance between this signal and M^{n_T} possible signals using (2.5).

For the Tarokh STTC, described previously, there are 16 possible composite signals as shown by the markers labeled (a-p) in Fig. 2.8. The actual received signal corrupted by noise is indicated by the stars while the estimate of the received signal is indicated by the triangles. These estimates are then fed to the STTC decoder whereby the most likely orginal bit sequence is estimated. In both figures, the complex fading gains α_t^{11} and α_t^{21}

are set to a constant value. The complex noise η_t^1 is of the order 10^{-2} for high SNR and 10^{-1} for low SNR.
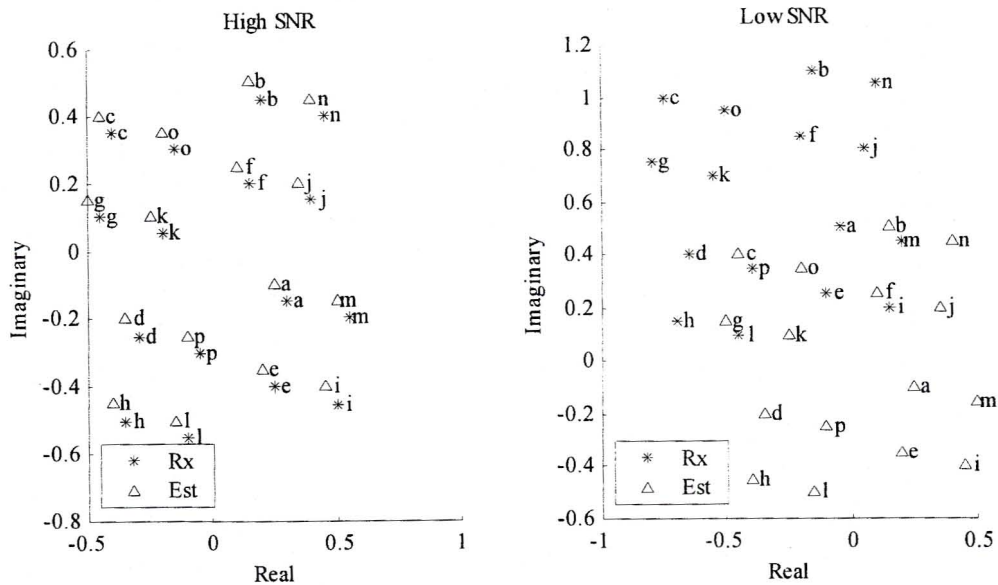
Figure 2.8: Signal space at receiver for high SNR and low SNR.

For high SNRs, the corresponding markers are close together and it is likely that the correct symbol will be chosen. At low SNRs, the corresponding markers are far apart and incorrect decisions are more likely. For example, if 'l' is transmitted then 'l' is the most likely signal at high SNRs while 'g' is most signal likely at low SNRs. It should be noted that if the most likely symbol is not correctly estimated, the STTC decoder may correct this error due to correct estimates of the neighbouring symbols.

2.5.4 Simulation results

In this section the FER performance of various 2 bps/Hz Tarokh STTCs [21] is investigated for both quasi-static and rapid Rayleigh fading channels. These STTCs have $k = 2$ input bits, $n_T = 2$ transmit antennas and use 4-PSK modulation. Simulation results are presented for 4, 8 and 16 state codes corresponding to $m = 2, 3, 4$ and for $n_R = 1$ and $n_R = 2$ receive antennas. The frame size is set to 256 bits in all cases. The trellis diagrams for these codes is given in appendix C.
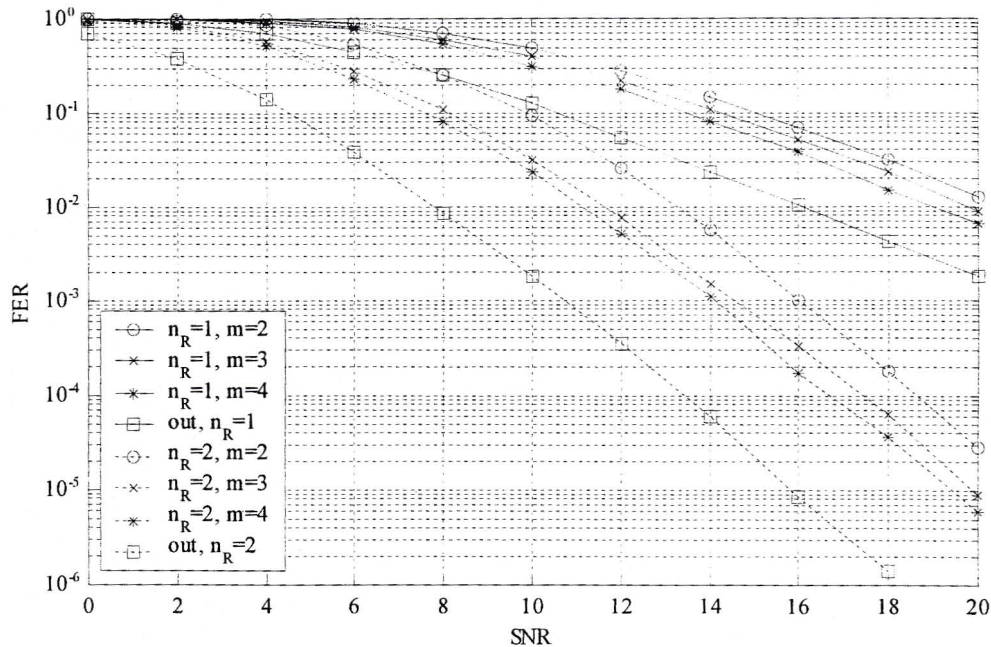
Figure 2.9: FER for Tarokh STTC ($n_T = 2, k = 2, M = 4$) in quasi-static fading.

In Fig. 2.9 the performance of various STTCs in a quasi-static fading channel is shown. It can be seen that the diversity gain determines the slope of the curve and coding gain determines the horizontal offset of the curve. It is clear that system performance is improved by increasing the encoder memory m and by increasing the number of receive antennas. The notation (out, n_R) is used to indicate the outage capacity for n_R receive antennas. This is the probability that the rate $R = 2$ bps/Hz is not supported by the channel as discussed in section 2.3. The outage capacity indicates that the STTCs achieve full diversity gain as indicated by the slope of the curves but do not achieve maximum coding gain.

In Fig. 2.10 the performance of various STTCs is investigated in rapid fading channels. An increase in encoder memory results in a greater improvement in FER performance than in quasi-static fading channels. Again it is clear that increasing the number of receive antennas improves the system performance.
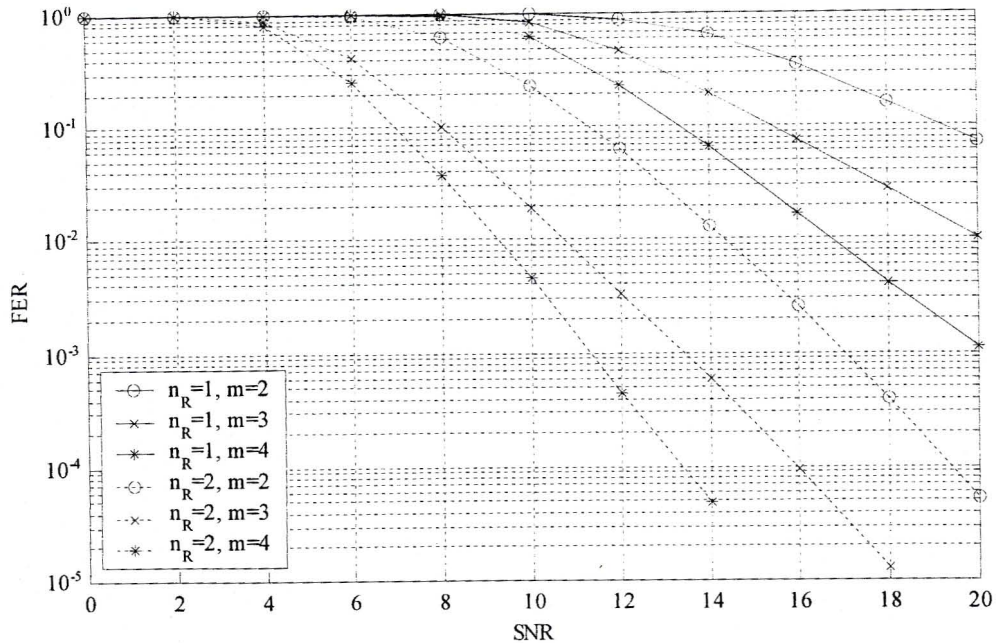
Figure 2.10: FER for Tarokh STTC ($n_T = 2, k = 2, M = 4$) in rapid fading.

2.6 Summary

In this chapter the system model for a generalised MEA system employing multiple transmit and receive antennas was presented. The concept of channel capacity was introduced and the outage capacity of MEA systems was discussed. Theoretical results for the capacity of MEA systems were given for various combinations of multiple transmit and receive antennas. It was shown that transmit diversity is necessary to achieve high system capacity and this cannot be achieved by receive diversity alone. The outage capacity was then used to calculate the FER of various MEA systems. Different coding schemes for MEA systems which attempt to approach the theoretical limits from information theory were discussed. These were bit-interleaved ST codes, layered ST codes and ST codes. STTCs fall into the category of ST codes and offer a good tradeoff between complexity and performance. Current research within this field was reviewed and the encoder architecture was described. Simulation results for 4, 8 and 16 state STTCs in quasi-static and rapid Rayleigh fading channels were presented. It was shown that STTCs achieve maximum diversity gain, but do not achieve the coding gain promised by information theory.

Chapter 3

Analysis of Space-Time Trellis Codes

3.1 Introduction

The performance of any error correcting code can be accurately determined by simulation in the low SNR region. However in the high SNR region generating simulation results is extremely time intensive and in this region analytical upper bounds, calculated mathematically, are used to quickly and accurately determine a code's performance.

The probability of a single error event is called the pairwise error probability (PWEP) which is the probability of transmitting codeword c and incorrectly decoding it at the receiver as valid codeword e. A codeword consists of a number of symbols which can form part of a binary or M-ary alphabet. Ideally the performance of a code should be analysed by calculating the probability of the union of all possible error events but in practice this is difficult to calculate and for this reason is bounded using the union bound.

A few analyses for STTCs have been proposed in the literature but these do not describe how the error events were enumerated and in most cases were not directly extendable to analysis of concatenated STTCs. In this chapter a novel method is proposed to analyse the

performance of STTCs in quasi-static and rapid Rayleigh fading channels. This method draws on some existing techniques, but is unique in its application to STTCs. The analysis is formulated in such a way that it can be used as a building block for the performance analysis of concatenated STTCs discussed in chapter 4.

Section 3.2 gives an overview of existing analytical methods for STTCs and describes in more detail the work which is done in this chapter. The upper bound on the PWEP of STTCs from [21] and a tighter upper bound from [39] is discussed in section 3.3. The application of the union bound using error events to the analysis of error correcting codes is described in section 3.4. A modification to the state transition matrix method [40, 41] is proposed in section 3.5 to efficiently enumerate error events with many parameters. The classification of the error events of STTCs in terms of parameters and the calculation of the bound on the BER and FER using the union bound and the numerical bound [42] is proposed in section 3.6. In order to assess the accuracy of the proposed analysis, these results are compared with simulation results in section 3.7 for a number of STTCs.

3.2 Overview of existing analytical methods for STTCs

A number of methods have been proposed in the literature to analyse the performance of STTCs in Rayleigh fading channels. In general the proposed methods analysed the FER or BER performance of STTCs in quasi-static or rapid Rayleigh fading channels. The union bound was generally used to analyse the code's performance which requires the enumeration of the code's error events. A number of different enumeration methods and bounds on the PWEP of each error event have been proposed. The performance of these analyses can be described in terms of tightness of the bound or how accurately the analysis describes the simulation results and computational efficiency of the bound calculation.

In [43] the FER and BER performance of STTCs was calculated for quasi-static fading channels. An approximation to the union bound on the code's performance was calculated using the distance spectrum of the code. The distance spectrum of a given code is the enumeration of the product measures of important or significant pairwise error events.

Error state reduction techniques were used to reduce the trellis complexity and an efficient algorithm was proposed to enumerate the error events. The new bound proposed in [39] was used to calculate the PWEP of each error event. Although this analysis provided good insight into the code's performance, the bounds were loose and did not converge as more error events were considered even at high SNRs.

The generating function technique was modified in [44] to analyse the BER performance of STTCs in rapid Rayleigh fading channels. The generating function was calculated from the modified state diagram of the code where each branch was labeled using the Chernoff bound on the PWEP from [21]. This method calculated the bound efficiently but the analysis and simulation results differed by approximately 2dB.

The FER performance of STTCs was evaluated in quasi-static and rapid Rayleigh fading channels in [45]. The union bound was used to evaluate the code's performance and error events were enumerated using the "General algorithm" [46]. The new bound was used to calculate the PWEP of each error event. It was shown that the union bound was tight at medium to high SNRs when applied to rapid fading channels but was very loose for quasi-static fading channels. The numerical bound [42] was used to obtain a tight bound for quasi-static fading channels whereby a limited union bound was averaged over the fading distribution using numerical integration.

The analytical bounds in [45] were tighter than those in [43, 44] for both quasi-static and rapid Rayleigh fading channels. However no BER analysis was derived and the modification of the general algorithm to enumerate the error events of the STTC was not described. Previously the general algorithm was used for the analysis of convolutional codes and trellis coded modulation.

In this chapter a novel analytical method is proposed to calculate the FER and BER performance of various STTCs in quasi-static and rapid Rayleigh fading channels. The proposed analysis is based on the work in [45] but a simpler method for enumerating the error events is proposed and is described in detail. This enumeration method is a modification of the state-transition matrix method [40, 41]. The analytical results are compared with simulation results where the tightness of the new bound proposed in [39]

is compared to the Chernoff bound [21] and the necessity for a numerical bound is shown.

3.3 Pairwise error probability for STTCs

This section describes the calculation of the bound on the pairwise error probability for STTCs derived in [21] and a new bound derived in [39].

For a STTC encoder, let a valid transmitted codeword of length L symbols be $c = [\underline{c}_1, \ldots, \underline{c}_L]$ with complex symbol vectors $\underline{c}_t = [c_t^1, \ldots, c_t^{n_T}]$ where each element of $\underline{c}_t$ corresponds to the signal transmitted from antenna i at time t. Equivalently let a valid, but incorrectly decoded codeword be $e = [\underline{e}_1, \ldots, \underline{e}_L]$ with complex symbol vectors $\underline{e}_t = [e_t^1, \ldots, e_t^{n_T}]$.

The conditional pairwise error probability from [21] of transmitting a codeword c and incorrectly decoding it at the receiver as a valid codeword e is given by (3.1) and its exponential upper bound by (3.2).

$$P(c \to e | \alpha) = \frac{1}{2}\text{erfc}\left(\sqrt{d^2(c,e)\frac{E_s}{4N_0}}\right) \tag{3.1}$$

$$\leq \exp\left(-d^2(c,e)\frac{E_s}{4N_0}\right) \tag{3.2}$$

Here $d^2(c,e)$ is calculated as follows.

$$d^2(c,e) = \sum_{t=1}^{L} \|\alpha_t(\underline{c}_t - \underline{e}_t)\|^2 \tag{3.3}$$

In [21] the Chernoff bound was used where the conditional PWEP was averaged over the Rayleigh fading distribution α to give the PWEP which is denoted $P(c \to e)$. In [39] a new bound was proposed which is asymptotically tight at high SNRs and uniformly tighter than the Chernoff bound. The new bound and Chernoff bound are expressed below in (3.4) and (3.5) respectively.

$$P(c \to e) \leq \binom{2rn_R - 1}{rn_R - 1}\left(\frac{E_s}{N_0}\right)^{-rn_R}\left(\prod_{i=1}^{r}\lambda_i\right)^{-n_R} \tag{3.4}$$

$$\leq \left(\frac{E_s}{4N_0}\right)^{-rn_R}\left(\prod_{i=1}^{r}\lambda_i\right)^{-n_R} \tag{3.5}$$

Here λ_i is a nonzero eigenvalue and r the rank of the codeword difference covariance matrix (CDCM) [39, 43, 45]. In this chapter the analysis is simplified by setting $E_s = 1$ and taking the number of transmit antennas into account in the calculation of E_s/N_0 from the SNR in dB.

$$\frac{E_s}{N_0} = \frac{1}{n_T} 10^{\text{SNR}/10} \tag{3.6}$$

In order to generalise the analysis to use either the Chernoff bound or the new bound, the following general expression is used to express the PWEP.

$$P(c \to e) = \left(\prod_{i=1}^{r} \lambda_i \right)^{-n_R} \cdot \gamma(r, n_R) \tag{3.7}$$

For the new bound,

$$\gamma(r, n_R) = \binom{2rn_R - 1}{rn_R - 1} \left(\frac{E_s}{N_0} \right)^{-rn_R} \tag{3.8}$$

and for the Chernoff bound.

$$\gamma(r, n_R) = \left(\frac{E_s}{4N_0} \right)^{-rn_R} \tag{3.9}$$

3.3.1 PWEP in rapid fading channels

In rapid fading channels the α_t^{ij}'s are uncorrelated in time and space. The expression for the eigenvalues in [45] is equivalent to that derived in [21] and is expressed below where i corresponds to the time instances for which $\underline{c}_t \neq \underline{e}_t$.

$$\lambda_i = |\underline{c}_i - \underline{e}_i|^2 \tag{3.10}$$

In this case the rank r of the CDCM is the number of time instances that $\underline{c}_t \neq \underline{e}_t$. The upper bound on the PWEP in rapid fading can now be calculated by substituting the eigenvalues λ_i and rank r into (3.7). A diversity gain of rn_R and coding gain proportional to $\prod \lambda_i$ is achieved.

3.3.2 PWEP in quasi-static fading channels

In quasi-static fading channels, the α_t^{ij}'s are spatially uncorrelated only. As shown in [45] the eigenvalues of the CDCM are equivalent to eigenvalues of the Hermitian matrix

$H(c, e)$ derived in [21]. $H(c, e)$ is the $n_T \times n_T$ matrix with elements H_{pq} and is given in (3.11) below where $\bar{x}$ denotes the complex conjugate of x.

$$H_{pq} = \sum_{t=1}^{L} (c_t^p - e_t^p) \overline{(c_t^q - e_t^q)} \tag{3.11}$$

The non-zero eigenvalues λ_i and rank r of $H(c, e)$ can be substituted into (3.7) to obtain an upper bound on the PWEP. Here a diversity gain of rn_R and coding gain of $(\prod \lambda_i)^{1/r}$ is achieved.

3.4 The union bound

This section briefly discusses the use of the union bound in analysing the performance of coded systems. A number of approximations to the union bound are described to decrease the computational complexity of the calculation and the concept of error events is introduced.

In general the performance of a given code is upper bounded using the union bound. The union bound states that the probability of the union of n_E error events E_i is less than or equal to the sum of the individual probabilities of each error event. This is shown mathematically below.

$$P \left(\bigcup_{i=1}^{n_E} E_i \right) \leq \sum_{i=1}^{n_E} P(E_i) \tag{3.12}$$

From (3.12) it is clear that the union bound will always give an upper bound on the code's performance, in other words the worst case scenario.

For a given code consisting of L symbols the FER (P_f) and BER (P_b) are calculated as follows where $w_{c,e}$ is the number of erroneous information bits when codeword c is transmitted and e is decoded.

$$P_f \leq \sum_{c} \sum_{c \neq e} P(c) P(c \to e) \tag{3.13}$$

$$P_b \leq \sum_{c} \sum_{c \neq e} \frac{w_{c,e}}{kL} P(c) P(c \to e) \tag{3.14}$$

This calculation is computationally expensive and can be simplified using the following two approximations. In the case of geometrically uniform codes [47], the summation over

c can be dropped and one need only consider the all zero codeword sequence c_0. Edge effects are generally small for reasonable frame sizes and only codewords which start and end in the all zero-state of the encoder trellis need to be considered.

Error events resulting in the same PWEP can be grouped together to reduce the number of times the PWEP is calculated. The number of error events classified by the parameters i and $\underline{d}$ is called the error event multiplicity and is denoted by $n(i, \underline{d})$. This is the number of error events of length L, with input Hamming weight i and output error event $\underline{d}$ starting and ending in the all-zero state. The error event $\underline{d}$ is a vector of parameters characterising the erroneous codeword $e(\underline{d})$. The FER and BER can now be calculated as shown below where $P_2(\underline{d})$ is the PWEP $P(c_0 \rightarrow e(\underline{d}))$ as shown in section 3.3.

$$P_f \;\leq\; \sum_{i,\underline{d}} n(i,\underline{d})P_2(\underline{d}) \tag{3.15}$$

$$P_b \;\leq\; \sum_{i,\underline{d}} \frac{i}{kL} n(i,\underline{d})P_2(\underline{d}) \tag{3.16}$$

For large frame sizes it is computationally expensive to consider all possible error events. Many error events have a negligible contribution to the union bound and for this reason can be discarded. Thus by considering only dominant error events, a simple approximation to the union bound is obtained.

A method is required to accumulate common error events as well as their multiplicities and also discard error events that do not contribute significantly to the bound. This is called error event enumeration. In the next section a simple method is proposed which modifies the state transition matrix method [41] for error event enumeration.

3.5 Error event enumeration

In this section error event enumeration is considered. Some existing methods are discussed, these being the state transition matrix method [41] and a modified version of this method [40]. A further generalisation of this method is proposed here which allows for error events represented by many parameters to be enumerated.

3.5.1 State transition matrix method

In the case of convolutional codes an error event is represented by a single parameter d which is the Hamming weight of the codeword. The error event multiplicity has the form $n(i, d)$ which is the number of paths of input weight i and output weight d starting and ending in the all-zero state. These error events can be enumerated using the state transition matrix method [41].

Let $n_s = 2^m$ be the number of encoder states. In [41] an $n_s \times n_s$ state transition matrix $A(L, I, D)$ was considered to analyse the performance of convolutional codes. Each element of the matrix is denoted $A_{sf}(L, I, D)$ and is a 3 dimensional monomial of the form $L^l I^i D^d$ which describes a transition from initial state s to final state f in the state diagram. Here l is the path length, i is the Hamming weight of the input bits and d the Hamming weight of the output bits for this transition. An efficient recursive algorithm was used to enumerate the error events. This method is computationally efficient but initially involves the algebraic inversion of $A(L, I, D)$ which becomes complex for large n_s and for error events with many parameters. Once the matrix is inverted, element (0,0) is considered and is manipulated by hand to obtain a recursive formula. This is not desirable if this method is to be applied to many different codes. Finally the recursive version also requires the error event parameters to be whole numbers.

A generalised version of this method was proposed in [40] whereby the matrix was initialised in the same way as described above except the L term was dropped and $A(I, D)$ was considered. It was noted that the all error event multiplicities $n(i, d)$ were found in the element (0,0) of the matrix $A(I, D)^L$. This version is more general than the recursive version because it avoids the complicated inversion of $A(L, I, D)$, no hand manipulation is required and there is no restriction on the error event parameters.

3.5.2 Modified state transition matrix method

With STTCs many parameters are used to describe an error event, where $2n_T n_T$ parameters are needed in quasi-static fading. Furthermore these parameters are real valued. For

these reasons the recursive version of the state transition matrix method is not used and the generalised version described in [40] is used instead. A simple modification of this method allows for the analysis of STTCs where a single error event described by parameter D is replaced by a vector of error event parameters $\underline{D}$ and hence the initial matrix is denoted $A(I, \underline{D})$.

The proposed modification of the state transition matrix method is now described in detail as well as various optimisations to reduce the computational complexity of the calculation.

Description

Consider a $n_s \times n_s$ state transition matrix $A(I, \underline{D})$ where $n_s = 2^m$ is the number of encoder states. Initially each element of the state transition matrix $A_{sf}(I, \underline{D})$ represents a transition from initial state s to final state f where $s, f = \{1, \ldots, n_s\}$ in the state diagram of the code. $A_{sf}(I, \underline{D})$ is a monomial of the form $I^i \underline{D}^{\underline{d}}$ where the exponent i is the input Hamming weight and the exponent $\underline{d}$ is a vector of the error event parameters.

By raising $A(I, \underline{D})$ to the L_{th} power and considering element $(0,0)$ denoted by $N(I, \underline{D})$ one obtains all the error events and corresponding multiplicities starting and ending in the all-zero state. This is expressed below where $n(i, \underline{d})$ is the number of error events described by $\underline{d}$ with input Hamming weight i starting and ending in the all-zero state.

$$
\begin{aligned}
N(I, \underline{D}) &= \sum_{i, \underline{d}} n(i, \underline{d}) I^i D^{\underline{d}} \\
\underline{D}^{\underline{d}} &= D_1^{d_1} D_2^{d_2} \ldots
\end{aligned}
\qquad (3.17)
$$

Optimisations

Raising $A(I, \underline{D})$ to the Lth power is computationally expensive requiring $L n_s^3$ polynomial multiplications. If L is a power of 2, one can use the recursive method described in [40] and expressed below where $n = \{1, \ldots, \log_2 L\}$.

$$
A(I, \underline{D})^{2^n} = A(I, \underline{D})^{2^{(n-1)}} \cdot A(I, \underline{D})^{2^{(n-1)}}
\qquad (3.18)
$$

Thus $A^2 = A \cdot A$ is calculated followed by $A^4 = A^2 \cdot A^2$ and so on. This reduces the complexity to $n_s^3 \log_2 L$ polynomial multiplications. Further optimisation is achieved by only calculating the matrix elements in zeroth row and column on recursion $n - 1$ and only element $(0,0)$ on the final recursion n. Thus the overall complexity is reduced to $n_s^3 \log_2(L - 2) + 2n_s^2 + n_s$ polynomial multiplications.

Even with these optimisations, the large number of error events translates to multiplication of high degree polynomials with many terms. To multiply two polynomials with n_p terms each, requires n_p^2 multiplications and a further n_p^2 evaluations to combine terms with common exponents. It is therefore necessary to remove terms which do not contribute significantly to union bound as discussed in section 3.4. To remove insignificant terms, a limiting function $f_{lim}(\underline{d})$ is applied $A_{sf}(I, \underline{D})$ whereby a term is removed if $f_{lim}(\underline{d}) \geq d_{lim}$.

3.6 FER and BER analysis of STTCs

In this section a novel method is proposed to analyse the FER and BER performance of STTCs in rapid and quasi-static Rayleigh fading channels. The error events are classified in terms of parameters so that they can be enumerated by the modified state transition matrix method proposed in section 3.5. The initialisation of the matrix $A(I, \underline{D})$ is described in detail as well as the calculation of the FER and BER from the enumerated polynomial $N(I, \underline{D})$.

The following general notation is used. The Hamming weight of the input bits is i. Let $\underline{c}_{sf} = [c_{sf}^1, \ldots, c_{sf}^{n_T}]$ be the vector of transmitted symbols for a transition from state s to state f in the state transition diagram where each element c_{sf}^j is the symbol transmitted from transmit antenna j.

3.6.1 Union bound for rapid fading

For rapid fading channels, the PWEP given by (3.7) requires the number of epochs r for which $\underline{c}_t \neq \underline{e}_t$ and the product of the eigenvalues λ_i. Thus an error event can be described

by three parameters; an input weight i, an eigenvalue product and the rank. Each λ_i is simply the Euclidean distance between the individual symbol vectors $\underline{c}_i$ and $\underline{e}_i$. This product can be calculated on an epoch by epoch basis but the state transition method accumulates the sum of the error event parameters not the product. If the Euclidean distances between symbol vectors are converted to the log domain, multiplication is now equivalent to addition as shown below.

$$\prod_i a_i = \exp\left(\sum_i \ln a_i\right) \tag{3.19}$$

The state transition matrix takes the form $A(I, P, R)$ with elements $A_{sf}(I, P, R)$ and is initialised as follows. If a transition from state s to state f exists then $A_{sf}(I, P, R)$ is calculated as shown below otherwise it is set to zero.

$$A_{sf}(I, P, R) = I^i P^p R^r \tag{3.20}$$

$$p = \begin{cases} 0 & \text{if } \underline{c}_{00} = \underline{c}_{sf} \\ \ln|\underline{c}_{00} - \underline{c}_{sf}|^2 & \text{otherwise} \end{cases}$$

$$r = \begin{cases} 0 & \text{if } \underline{c}_{00} = \underline{c}_{sf} \\ 1 & \text{otherwise} \end{cases}$$

For the 4-state Tarokh STTC given in appendix C, the initial state transition matrix is given below.

$$A(I, P, R) = \begin{bmatrix} 1 & IP^{\ln 2}R & IP^{\ln 4}R & I^2 P^{\ln 2}R \\ P^{\ln 2}R & IP^{\ln 4}R & IP^{\ln 6}R & I^2 P^{\ln 4}R \\ P^{\ln 4}R & IP^{\ln 6}R & IP^{\ln 8}R & I^2 P^{\ln 6}R \\ P^{\ln 2}R & IP^{\ln 4}R & IP^{\ln 6}R & I^2 P^{\ln 4}R \end{bmatrix} \tag{3.21}$$

After the calculation of $A(I, P, R)^L$ element (0,0) is a polynomial of the form,

$$N(I, P, R) = \sum_{i,p,r} n(i, p, r) I^i P^p R^r \tag{3.22}$$

and the union bound on the FER and BER can be calculated as follows.

$$P_f \leq \sum_{i,p,r} n(i, p, r) \exp(-n_R p) \gamma(r, n_R) \tag{3.23}$$

$$P_b \leq \sum_{i,p,r} \frac{i}{kL} n(i, p, r) \exp(-n_R p) \gamma(r, n_R) \tag{3.24}$$

The exponential term converts the sum of Euclidean distances in the log domain to the desired product of Euclidean distances. The $\gamma(\cdot)$ term is replaced by (3.8) when the new bound on the PWEP is used and by (3.9) when Chernoff bound on the PWEP is used. In order to limit the number of terms in each polynomial, a limiting function is calculated whereby a term is removed if $p \geq p_{lim}$.

An important feature of this bound is that $N(I, P, R)$ is calculated independently of the SNR and the number of receive antennas hence the FER and BER of the STTC can be calculated for any SNR and n_R with only a single $N(I, P, R)$ calculation.

3.6.2 Union bound for quasi-static fading

In quasi-static fading channels the PWEP (3.11) is calculated using the rank r and the non-zero eigenvalues λ_i of the Hermitian matrix $H(\boldsymbol{c}, \boldsymbol{e})$. For convenience this matrix is expressed as $\boldsymbol{h}$ with complex elements h_{pq}. Each element of $\boldsymbol{h}$ is an accumulation of terms over the entire frame where each term can be calculated on an epoch by epoch basis which lends itself to accumulation using the state transition matrix method.

An error event can now be described by an input weight i and a matrix $\boldsymbol{h}$. The state transition matrix takes the form $A(I, \boldsymbol{H})$ and is initialised as follows. If a transition from state s to state f exists, $A_{sf}(I, \boldsymbol{H})$ is calculated as shown below otherwise it is set to zero.

$$A_{sf}(I, \boldsymbol{H}) = I^i H_{11}^{h_{11}}, \ldots, H_{pq}^{h_{pq}}, \ldots, H_{n_T, n_T}^{h_{n_T, n_T}} \tag{3.25}$$

$$h_{pq} = \left(c_{00}^p - c_{sf}^p \right) \overline{\left(c_{00}^q - c_{sf}^q \right)} \tag{3.26}$$

For the 4-state Tarokh STTC given in appendix C, the initial state transition matrix is given below where $j = \sqrt{-1}$.

$$A(I, \boldsymbol{H}) = \tag{3.27}$$

$$\begin{bmatrix} 1 & IH_{22}^2 & IH_{22}^4 & I^2H_{22}^2 \\ H_{11}^2 & H_{11}^2 H_{12}^2 H_{21}^2 H_{22}^2 & IH_{11}^2 H_{12}^{2-2j} H_{21}^{2+2j} H_{22}^4 & I^2 H_{11}^2 H_{12}^{-2j} H_{21}^{2j} H_{22}^2 \\ H_{11}^4 & IH_{11}^4 H_{12}^{2+2j} H_{21}^{2-2j} H_{22}^2 & IH_{11}^4 H_{12}^4 H_{21}^4 H_{22}^4 & I^2 H_{11}^4 H_{12}^{2-2j} H_{21}^{2+2j} H_{22}^2 \\ H_{11}^2 & IH_{11}^2 H_{12}^{2j} H_{21}^{-2j} H_{22}^2 & IH_{11}^2 H_{12}^{2+2j} H_{21}^{2-2j} H_{22}^4 & I^2 H_{11}^2 H_{12}^2 H_{21}^2 H_{22}^2 \end{bmatrix}$$

It is important to note that h_{pq} is complex and hence $A_{sf}(I, \boldsymbol{H})$ is a polynomial of dimension $n_T^2 + 1$ with complex coefficients. This computation can be simplified somewhat by noting that $A_{sf}(I, \boldsymbol{H})$ is equivalent to a polynomial of dimension $2n_T^2 + 1$ with real coefficients where H_{pq} and exponent h_{pq} are divided into their real and imaginary parts.

After calculation of $A(I, \boldsymbol{H})^L$ the polynomial of interest is element $(0,0)$ and is expressed as follows.

$$N(I, \boldsymbol{H}) = \sum_{i, \boldsymbol{h}} I^i H_{11}^{h_{11}} \cdot \ldots \cdot H_{n_T, n_T}^{h_{n_T, n_T}} \tag{3.28}$$

The union bound on the FER and BER can be calculated as shown below where the λ_j's are the non-zero eigenvalues and r the rank of the matrix $\boldsymbol{h}$. This matrix is constructed from the error event parameters $\{h_{11}, \ldots, h_{n_T, n_T}\}$

$$P_f \leq \sum_{i, \boldsymbol{h}} n(i, \boldsymbol{h}) \left(\prod_{j=1}^{r} \lambda_j \right)^{-n_R} \gamma(r, n_R) \tag{3.29}$$

$$P_b \leq \sum_{i, \boldsymbol{h}} \frac{i}{kL} n(i, \boldsymbol{h}) \left(\prod_{j=1}^{r} \lambda_j \right)^{-n_R} \gamma(r, n_R) \tag{3.30}$$

From the above equation it can be seen that the contribution of an error event to the union bound is inversely proportional to the eigenvalue product. For this reason the limiting function is defined as,

$$f(\boldsymbol{h}) = \prod_{j=1}^{r} \lambda_j \tag{3.31}$$

where all terms with $f(\boldsymbol{h}) \geq h_{lim}$ are removed from the polynomial.

Again it is important to note that $N(I, \boldsymbol{H})$ is calculated independently of the SNR and the number of receive antennas therefore the FER and BER of the STTC can be calculated for any SNR and n_R with only a single $N(I, \boldsymbol{H})$ calculation.

3.6.3 Numerical bound for quasi-static fading

In section 3.7, it is shown that the union bound is not appropriate for quasi-static fading channels because the bound is loose and does not converge, even at high SNRs. The reason for this is, there are no dominant error events in quasi-static fading channels. In [45] a

much tighter bound was obtained for STTCs using an adaption of the numerical bound proposed in [42]. The numerical bound calculates a limited union bound conditioned on the channel matrix $\boldsymbol{\alpha}$. This is then averaged over the fading distribution $p(\boldsymbol{\alpha})$ using numerical integration. The PWEP conditioned on $\boldsymbol{\alpha}$ is expressed in (3.1) and can be re-written in terms of the error events calculated previously for quasi-static fading channels as shown below.

$$P(\boldsymbol{h}|\boldsymbol{\alpha}) = \frac{1}{2}\mathrm{erfc}\left(\sqrt{d^2(\boldsymbol{h}|\boldsymbol{\alpha})\frac{E_s}{4N_0}}\right) \qquad (3.32)$$

$$d^2(\boldsymbol{h}|\boldsymbol{\alpha}) = \sum_{j=1}^{n_R}\sum_{p=1}^{n_T}\sum_{q=1}^{n_T}\alpha_{pj}\overline{\alpha_{qj}}h_{pq}$$

The numerical bound on the FER and BER can be calculated as shown below where σ_r^2 is variance per dimension of α_{ij} and the $\min(\cdot,\cdot)$ function simply takes the smallest of the two arguments.

$$P_f \leq \int_{\boldsymbol{\alpha}_{\min}}^{\boldsymbol{\alpha}_{\max}} \min\left(1, \sum_{i,\boldsymbol{h}} n(i,\boldsymbol{h})P(\boldsymbol{h}|\boldsymbol{\alpha})\right) p(\boldsymbol{\alpha})d\boldsymbol{\alpha} \qquad (3.33)$$

$$P_f \leq \int_{\boldsymbol{\alpha}_{\min}}^{\boldsymbol{\alpha}_{\max}} \min\left(0.5, \sum_{i,\boldsymbol{h}} \frac{i}{kL} n(i,\boldsymbol{h})P(\boldsymbol{h}|\boldsymbol{\alpha})\right) p(\boldsymbol{\alpha})d\boldsymbol{\alpha} \qquad (3.34)$$

$$p(\boldsymbol{\alpha}) = \prod_{i=1}^{n_T}\prod_{j=1}^{n_R}\frac{1}{2\pi\sigma_r^2}\exp\left(\frac{-\mathrm{Re}(\alpha_{ij})^2 - \mathrm{Im}(\alpha_{ij})^2}{2\sigma_r^2}\right) \qquad (3.35)$$

The conditional FER is limited to a maximum probability of 1. The conditional BER is limited to 0.5 which has been shown to be true by simulations in practical cases [42]. By limiting the FER and the BER, a much tighter upper bound is obtained. For a given code $N(I, \boldsymbol{H})$ need only be calculated once but the numerical integration must be recalculated if the SNR or number of receive antennas is changed.

The numerical integration was performed using NAG C library routine d01fcc which uses an adaptive subdivision strategy over a hyper-rectangular region and is based on methods described in [48, 49]. The real and complex parts of the fading coefficients must be treated separately, hence the order of the integral is $2n_T n_R$.

3.7 Analytical results

In this section the proposed analytical bounds are compared with simulation results in order to assess their accuracy or tightness. Two 4-PSK, 4-state STTCs with 2 transmit antennas are considered, namely the STTC of Tarokh [21, Fig. 4] and an optimal block fading STTC of Yan [37, Table I]. The trellis diagrams for these two codes are given in appendix C. The rapid and quasi-static Rayleigh fading channel models are consistent with those described in section 2.2. The FER and BER are plotted against the SNR per receive antenna. In all cases the number of input bits is 256 corresponding to $L = 128$ transmissions from each transmit antenna.

In the figures which follow, the labels Simulation, Chernoff, New and Numerical refer to the simulation results, the union bound using the Chernoff bound on the PWEP, the union bound using the new bound on the PWEP and the numerical bound respectively. The number following the bound name is the limiting factor which is p_{lim} in the case of rapid fading and h_{lim} in the case of quasi-static fading as described in section 3.5.2.

In Fig. 3.1 to Fig. 3.5 the Tarokh STTC is considered. In Fig. 3.1 the bound and simulation results for the FER and BER are given for a rapid fading channel with a single receive antenna. The Chernoff and the new bound are compared for two values of p_{lim}. For the FER the Chernoff bound is fairly loose (3 dB) even at high SNRs while the new bound is very tight at high SNRs for both the FER and BER. It should be noted that the bound converges at high SNRs even when more error events are considered i.e. p_{lim} is increased. This indicates that in a rapid fading channel there are dominant error events.

In Fig. 3.2 the number of receive antennas is increased to 2 and good agreement of the new bound and simulation results is noted. In both Fig. 3.1 and Fig. 3.2 divergence of the bound is observed at low SNRs which is consistent with the behaviour of the union bound.

Fig. 3.3 presents results for 1 receive antenna in a quasi-static fading channel. No convergence is observed as the number of error events is increased (increase in h_{lim}), even at high SNRs. This is because there are no dominant error events in a quasi-static fading
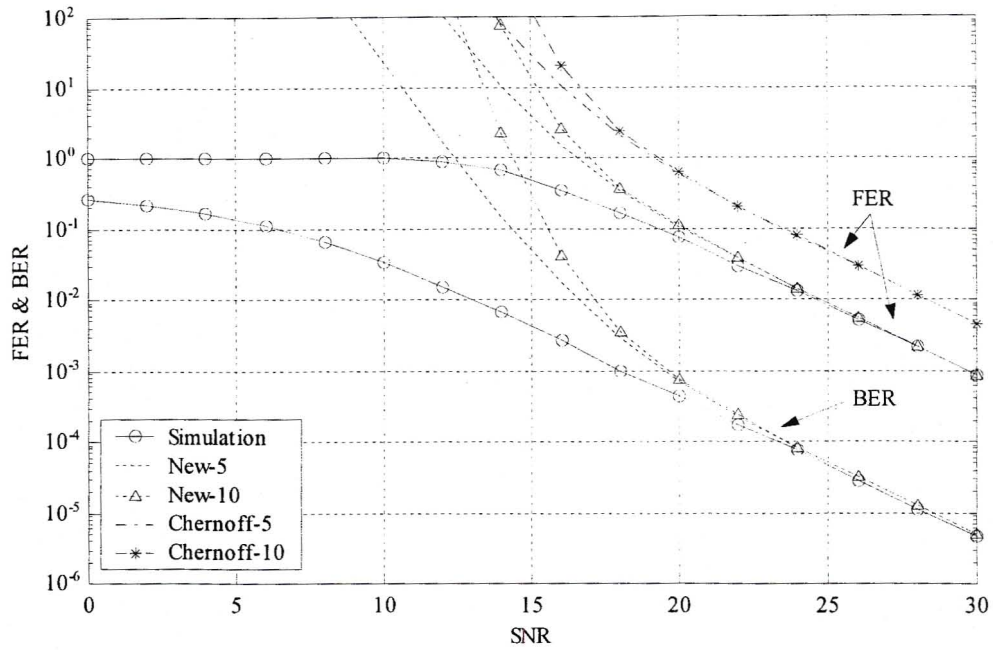
Figure 3.1: Chernoff and new bound for Tarokh STTC in rapid fading with $n_R = 1$.
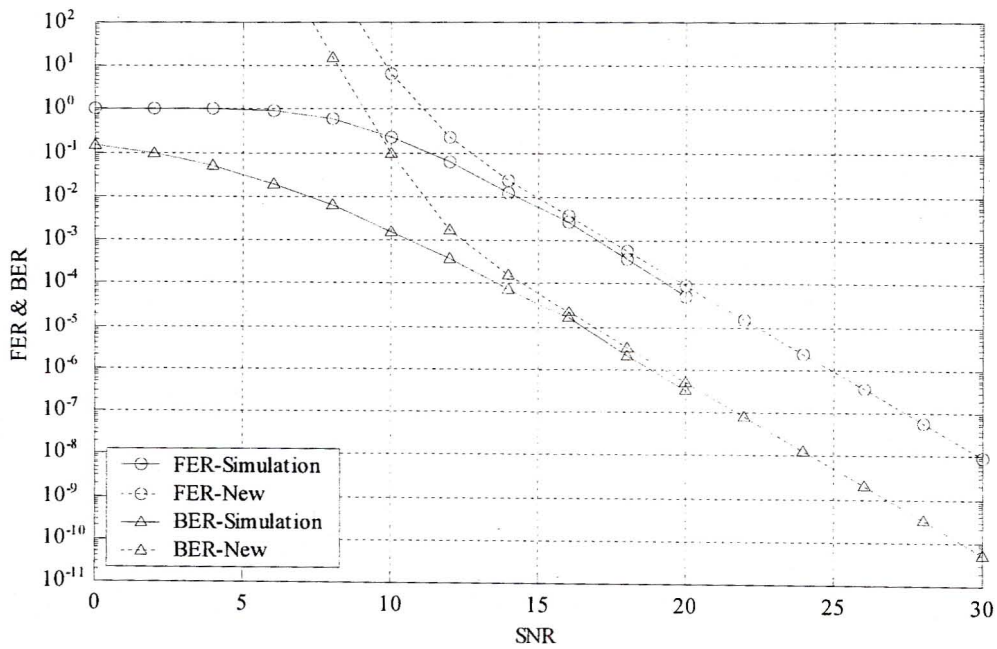
Figure 3.2: Tarokh STTC in rapid fading with $n_R = 2$ using the new bound with $p_{lim} = 10$.
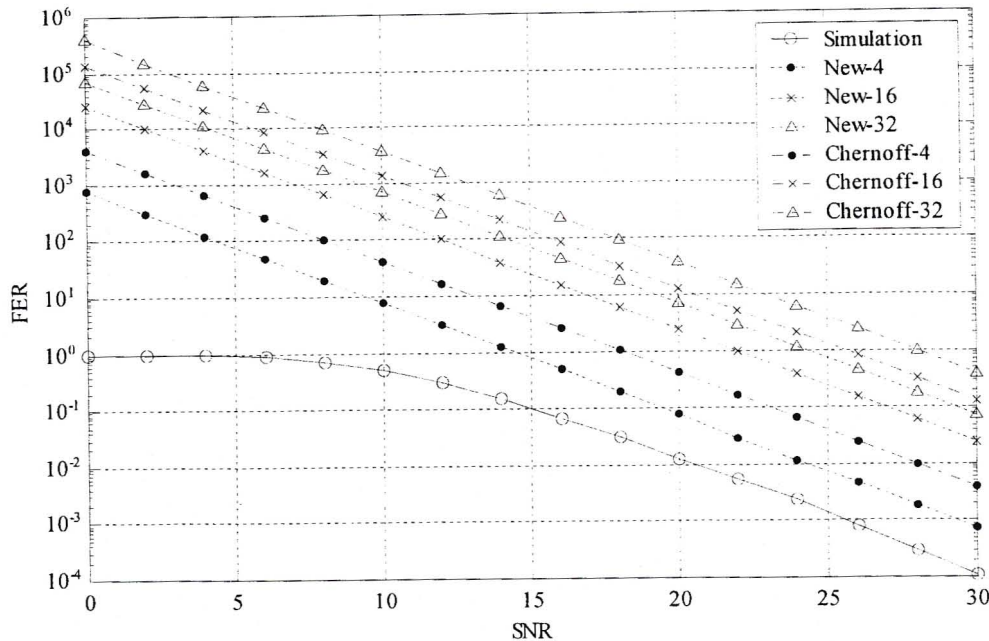
Figure 3.3: Comparison of Chernoff and new bound for Tarokh STTC in quasi-static fading with $n_R = 1$.

channel. Furthermore even for a few error events ($h_{lim} = 4$) the bound is very loose and as more error events are added the discrepancy increases. These two factors clearly indicate the need for the numerical bound.

The numerical bound is shown in Fig. 3.4 and is tight for the FER (0.5 dB) but fairly loose for the BER (3 - 5 dB). This is similar to the behaviour of the numerical bound in [42] where it was applied to convolutional codes in quasi-static Rician fading channels. In Fig. 3.5 the numerical bound is applied to the same system with 2 receive antennas. Again the bound is tight for the FER and fairly loose for the BER although it is slightly tighter than in the single antenna case.

In Fig. 3.4 and Fig. 3.5 one should note that the numerical bound does not diverge at low SNRs as is the case with the union bound in rapid fading channels. Also, the numerical bound does not get tighter at high SNRs which again indicates there are no dominant error events in quasi-static fading channels.
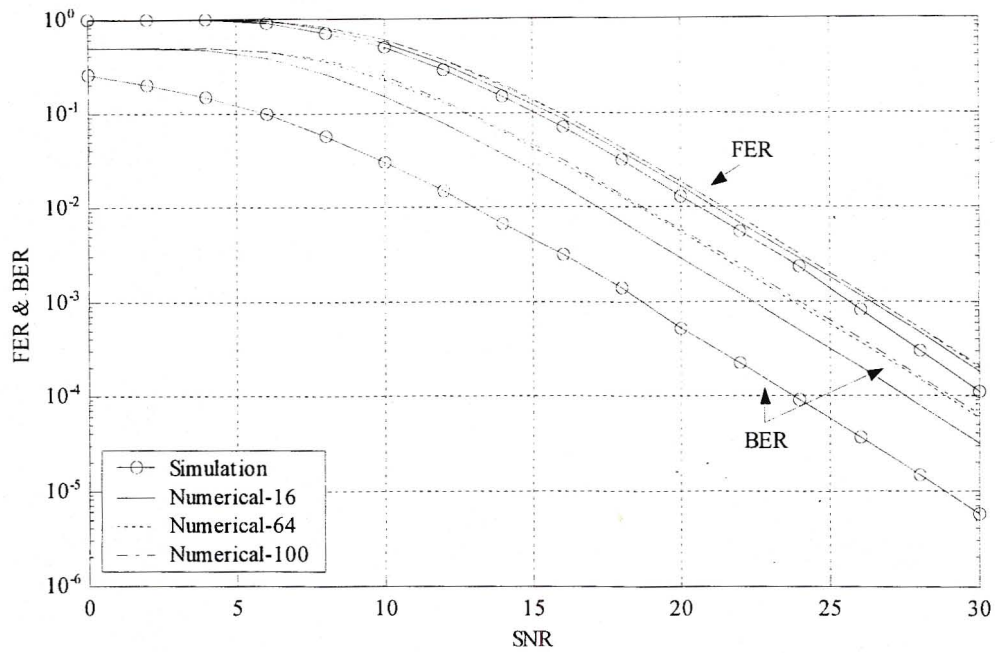
Figure 3.4: Tarokh STTC in quasi-static fading with $n_R = 1$ using the numerical bound.
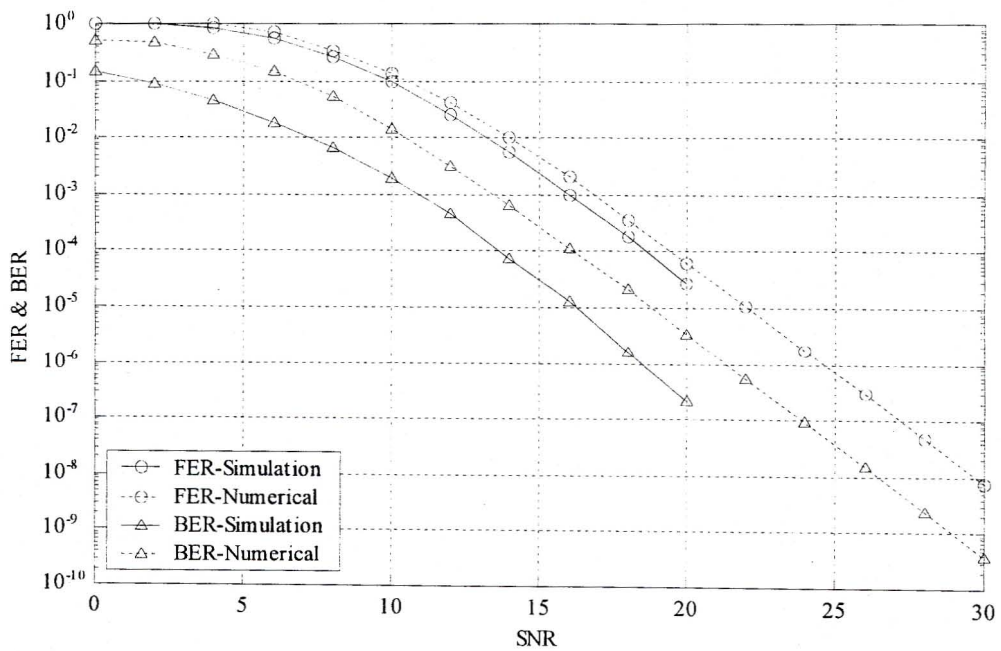
Figure 3.5: Tarokh STTC in quasi-static fading with $n_R = 2$ using the numerical bound with $h_{lim} = 30$.
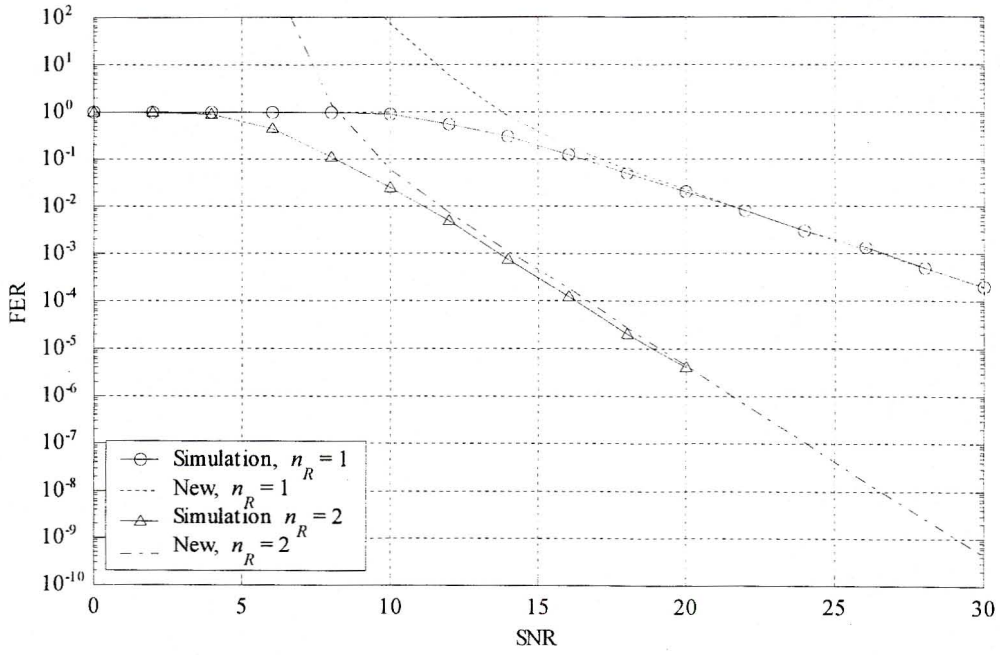
Figure 3.6: Yan STTC in rapid fading using the new bound with $p_{lim} = 10$.
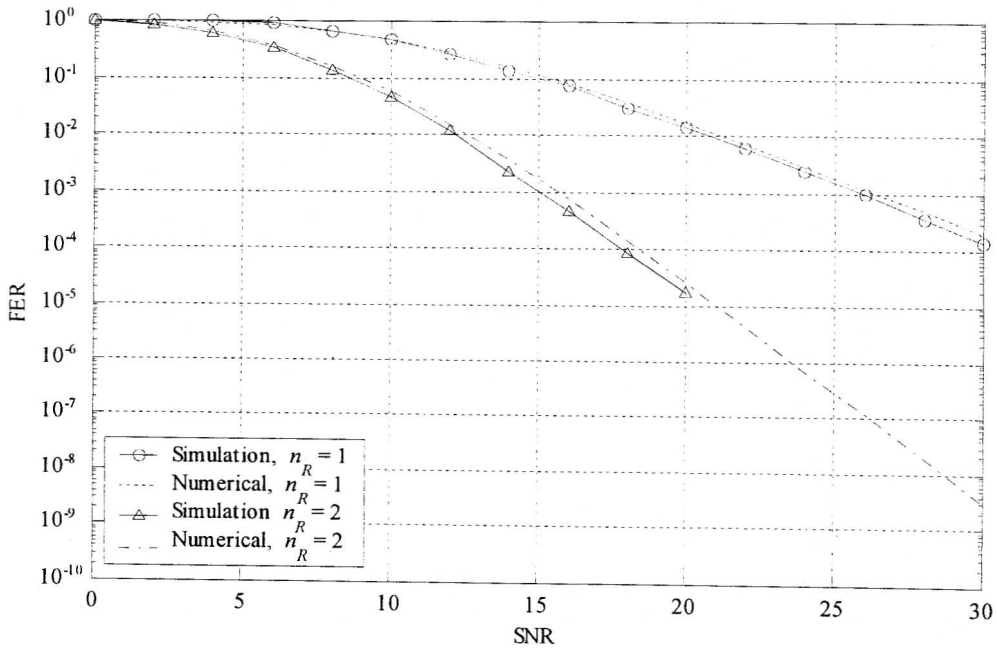
Figure 3.7: Yan STTC in quasi-static fading using the numerical bound with $h_{lim} = 50$.

Fig. 3.6 and Fig. 3.7 present the FER for 1 and 2 receive antennas using the Yan STTC. For rapid fading channels the new bound and simulation results agree as shown in Fig. 3.6. The results for a quasi-static fading channel are shown in Fig. 3.7 where the numerical bound gives a good approximation of the simulation results and is tighter for this code than for the Tarokh STTC.

3.8 Summary

In this chapter a mathematical analysis for STTCs in quasi-static and rapid Rayleigh fading channels was proposed. Current analytical methods were reviewed but in most cases the enumeration of the error events was not well described and the analysis was not easily extendable to the analysis of concatenated STTCs. The original bound on the PWEP from [21] and a new bound from [39] were presented. The application of the union bound to the analysis of coded systems and methods to simplify the complexity of the calculation using error events were discussed.

A novel method for enumerating the error events of STTCs was proposed and described in detail. This method modified the state transition matrix method [40, 41] and introduced a number of optimisation techniques to decrease the complexity of this computation. The classification of the error events in terms of parameters to allow for enumeration using the proposed method was described. The initialisation of the state transition matrix and calculation of the bound on the BER and FER from this matrix raised to the Lth power was fully explained. For rapid fading channels the union bound was used and for quasi-static fading the union and numerical bound were used.

The proposed analysis was compared with simulation results for two different 4-state STTCs in rapid and quasi-static fading channels with one and two receive antennas. The Chernoff bound on the PWEP was compared with the new bound and in all cases the new bound was shown to be tighter. The union bound using the new bound on the PWEP agreed well with simulation results in rapid fading channels for both the FER and BER. In quasi-static fading channels the union bound did not converge and was very loose as

there are no dominant error events in these channels. For this reason a numerical bound, requiring numerical integration, was considered and this bound agreed well with simulation results even at low SNRs. The numerical bound was shown to be tighter for the FER than for the BER and was also tighter for the Yan STTC than for the Tarokh STTC.

Chapter 4

Double Concatenated Space-Time Trellis Codes

4.1 Introduction

Concatenated coding was first proposed by D. Forney [6] in 1966 where an outer Reed Solomon code was serially concatenated with an inner convolutional code. The main reason for using a concatenated code as opposed to a more complex single code was to achieve lower decoding complexity with equivalent error rate performance. In decoding this concatenated code, there was no feedback of information from the outer to the inner decoder. The first concatenated system to make use of iterative decoding was proposed in [7, 8] and was shown to achieve large performance gains over conventional concatenated systems.

Space-time coding combines spatial and temporal diversity to increase both the bandwidth efficiency and reliability of wireless communication systems. Although space-time trellis codes achieve maximum diversity gain, they do not achieve good coding gain. For these reasons the marriage of the fields of concatenated coding using iterative decoding and STTCs was a logical step towards improving the coding gain of STTCs.

This chapter focuses on concatenated systems built from STTCs and convolutional codes (CCs) which can be decoded in an iterative fashion. A number of simple concatenated STTC systems have already been proposed in the literature and have shown an improved coding gain over conventional STTCs. In this chapter two novel double concatenated STTC systems are proposed in order to further improve the coding gain of STTCs. Furthermore an analytical model for concatenated STTCs is developed based on existing analytical techniques for concatenated CCs and the analysis proposed for STTCs in chapter 3.

Firstly, an overview of turbo codes and other concatenated CCs is given describing; existing structures, the encoding and decoding procedures, decoding algorithms and factors affecting their performance. Existing concatenated STTC structures are then reviewed in section 4.3. The system models for the proposed double concatenated STTC structures are presented in section 4.4, where the encoding and decoding procedures are explained. The bitwise additive SISO algorithm is also presented which is used to decode the individual constituent codes. An analysis for simple and double concatenated STTCs is derived in section 4.5. Lastly the system's performance is evaluated by simulation in section 4.6 for quasi-static and rapid Rayleigh fading channels and the analytical bounds are compared with the simulation results in section 4.7 to evaluate the accuracy of the analysis.

4.2 Concatenated convolutional codes

This section presents an overview of concatenated convolutional codes. A high level description of the encoding and iterative decoding of turbo codes is presented. A number of different concatenated coding structures proposed in the literature are then discussed. An overview of the various decoding algorithms appropriate for iterative decoding is given. Finally various factors affecting the performance of concatenated codes are discussed.

4.2.1   Turbo codes

The first concatenated code using an iterative decoding algorithm was proposed in 1993 by Berrou, Glavieux and Thitimajshima [7, 8]. This turbo code or parallel concatenated convolutional code (PCCC) was shown to achieve reliable communications at SNRs close to the Shannon limit in AWGN channels. At first many researchers were dubious as to the validity of the excellent results. However, as more research was done in this field the impressive performance of turbo codes came to be accepted.

A number of tutorial papers [50, 51, 52] describing the fundamental concepts of turbo codes are available. A good summary of key issues and an overview of the recent research is presented in [53].

Initially the BER of turbo codes decreases rapidly with an increase in SNR but at higher SNRs an error floor region is reached where the BER performance curve experiences a reasonable change in slope. This error floor is due to the weakness of the constituent codes and can be lowered in a number of ways, one of which is to use a different concatenated coding structure.

The turbo encoder

A rate 1/3 turbo encoder is shown in Fig. 4.1 which consists of two recursive systematic convolutional codes (RSCs) concatenated in parallel and separated by interleaver π. The uncoded bits u_t are encoded by C_1 which outputs systematic bits u_t and parity bits x_t^1. The order of uncoded bits is permuted by interleaver π and then encoded by C_2 which outputs systematic bits and parity bits x_t^2. The systematic output of C_2 is not used. The 3 bit streams u_t, x_t^1 and x_t^2 are then converted to a single serial bit stream, modulated and transmitted.
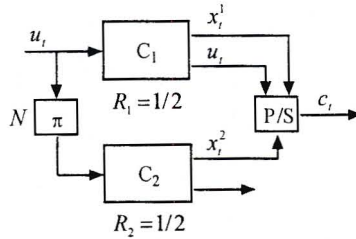
Figure 4.1: Turbo encoder.

The turbo decoder

Turbo decoding is performed in a modular fashion where soft estimates of the uncoded bits are exchanged between the constituent decoders. A block diagram of a turbo decoder is shown in Fig. 4.2 where the subscript of λ describes the type of soft information. The different types of soft information are discussed shortly.
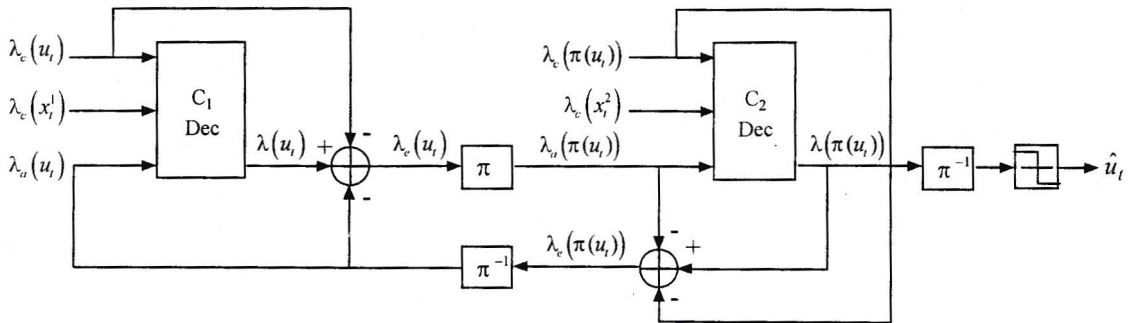
Figure 4.2: Turbo decoder.

Soft information is generally passed between decoders in the form of a log-likelihood ratio (LLR). The LLR of the uncoded bits u_t is given below,

$$\lambda(u_t) = \ln\left(\frac{P(u_t = 1)}{P(u_t = 0)}\right) \tag{4.1}$$

where $u_t = 1$ for a positive LLR and $u_t = 0$ for a negative LLR. The amplitude of the LLR is the likelihood of this decision.

Four types of soft information are present in a concatenated decoder. The channel information (λ_c) is that provided by the soft outputs of the demodulator. The a-priori or intrinsic information (λ_a) is that known before the decoding process starts and does not include

information from the channel or code constraints. The a-posteriori or total information (λ) is that provided by the decoder taking into account all available information sources. Finally the extrinsic information (λ_e) is the a-posteriori information excluding the a-priori information gained from a previous decoder and any channel information which will be used in the next decoder. Generally extrinsic information from the current decoder becomes a-priori information for the next decoder. In concatenated decoding only extrinsic information can be exchanged between decoders.

The decoding process starts with $\lambda_a(u_t)$ set to 0 as no a-priori information is initially available. The soft demodulator outputs $\lambda_c(u_t)$ and $\lambda_c(x_t^1)$ are fed to C_1 and $\lambda_c(x_t^2)$ and an interleaved $\lambda_c(u_t)$ is fed to C_2.

The following process is iterated a number of times. Decoder C_1 calculates the LLR of the uncoded bits $\lambda(u_t)$ using the a-priori and channel information. The a-priori and channel information $\lambda_c(u_t)$ of C_1 are then subtracted from the decoder output to obtain $\lambda_e(u_t)$ which is then interleaved to obtain $\lambda_a(\pi(u_t))$ and fed to C_2. Decoder C_2 then calculates the LLR $\lambda(\pi(u_t))$. The a-priori and channel information $\lambda_c(\pi(u_t))$ of C_2 are then subtracted from the decoder output to obtain $\lambda_e(\pi(u_t))$. This is de-interleaved and fed to C_1 to become a-priori information on the next iteration.

In this way the decoding process can be repeated or iterated a number of times where the estimate of the uncoded bit stream is improved on each iteration. Thus errors not corrected by one decoder may be corrected by the other decoder. On the final iteration a hard decision is made on the output LLR of C_2 which gives an estimate of the uncoded bits.

4.2.2 Other concatenated convolutional codes

This section gives an overview of the different types of concatenated CCs. All codes discussed here can be decoded using an iterative decoding algorithm in a similar way to turbo codes.

In [54, 55] a serially concatenated convolutional code (SCCC) using an iterative decoding

algorithm was described. This structure was similar to that proposed by Forney and consisted of a serial concatenation of an outer and inner convolutional code separated by an interleaver as shown in Fig. 4.3. The uncoded bits u_t are encoded by C_1, interleaved by π and encoded by C_2 to give coded bits c_t. SCCCs were shown to outperform turbo codes at high SNRs but not at low SNRs and reach the error floor region at lower BERs.
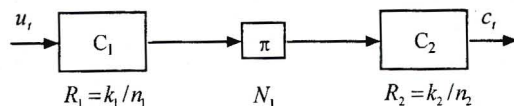
Figure 4.3: Serially concatenated convolutional encoder.

Multiple turbo codes [56, 57] are an extension of turbo codes where multiple constituent encoders are concatenated in parallel. When 3 constituent codes and 2 interleavers are used, the code is referred to as a double parallel concatenated convolutional code (DPCCC). It was shown by simulation that the BERs achieved by DPCCCs are lower than those achieved by turbo codes.

Double serially concatenated convolutional codes (DSCCCs) [58] are an extension of SCCCs to 3 constituent codes and 2 interleavers. The basic structure is a serial concatenation of an outer, middle and inner code with each code separated by an interleaver. Analytical and simulation results indicated a lower error floor for DSCCCs than SCCCs. DSCCCs were shown by simulation in [58] to achieve improved performance over turbo codes, SCCCs and DPCCCs at medium to high SNRs.

Hybrid concatenated convolutional codes (HCCCs) were discussed in [59]. This code is a parallel concatenation of a convolutional code and a SCCC separated by an interleaver. At high SNRs its performance was shown to be similar to SCCCs and superior to turbo codes. At low SNRs this code was shown to outperform both SCCCs and turbo codes.

4.2.3   Decoding algorithms

Concatenated codes can be decoded using maximum likelihood decoding algorithms based on the entire code trellis. For medium to large interleaver sizes, this is far too complex to be implemented in a realistic system. An important feature of concatenated codes is that their decoders can be implemented with realisable complexity using a suboptimal, yet powerful, iterative decoding algorithm whereby the constituent codes are decoded separately and soft information is exchanged between decoders in an iterative fashion.

Decoding algorithms used for iterative decoding of turbo codes can be derived from either the Viterbi algorithm [5] or the maximum a posteriori (MAP) [60] algorithm. The main difference between these two algorithms is that the Viterbi algorithm finds the most likely state sequence and hence minimises the FER while the MAP algorithm finds the most likely individual state and hence minimises the BER.

The soft-output Viterbi algorithm (SOVA) was proposed in [61] and was derived from the Viterbi algorithm. It computes a reliability estimate of each bit which can be improved using the Improved SOVA algorithm [62].

The MAP algorithm or BCJR algorithm, due to the authors initials, was first applied to turbo decoding in [7]. This algorithm is computationally intensive and is sensitive to round-off errors. These issues are resolved by computing the MAP algorithm in the log domain by using either the log-MAP or the max-log-MAP algorithms. A concise summary of the above mentioned decoding algorithms was presented in [63].

The decoding algorithms discussed thus far are only suitable for the decoding of turbo codes or multiple turbo codes because they only give an improved estimate of the uncoded bits. In the decoding of SCCCs and HCCCs, improved estimates of the coded bits and the uncoded bits are required. For this reason the soft-input soft-output (SISO) module was proposed in [55, 64]. This four port module accepts the input LLRs of the coded and uncoded bits and calculates an update of these LLRs based on the code constraints. The SISO algorithm can be implemented in the multiplicative or additive form. The multiplicative SISO is an extension of the MAP algorithm while the additive SISO is an

extension of the log-MAP algorithm. The additive SISO algorithm is described in detail in section 4.4.

4.2.4 Performance parameters

A host of parameters determine the performance of concatenated codes. A comparison of these parameters is presented in [53] for turbo codes and in [65] for SCCCs as well as turbo codes. Many of the papers referenced in this section also compare parameters influencing the performance of concatenated convolutional codes. In this section a brief overview of these parameters is presented.

Constituent decoding algorithm

The decoding algorithm can be chosen by trading increased complexity for improved performance or vice-versa. The computational complexity of the decoding algorithms from most complex to least complex is the MAP followed by the log-MAP, then the max-log-MAP and finally the SOVA. In a concatenated system the performance of the log-MAP algorithm is marginally inferior to that of the MAP algorithm. The max-log-MAP algorithm performs worse than the log-MAP, but better than the SOVA algorithm. The log-MAP algorithm gives a good tradeoff between complexity and performance.

Number of decoding iterations

Increasing the number of decoding iteration results in improved performance but the gain in performance diminishes with each new iteration and eventually a saturation point is reached where no further performance gain is achieved. Concatenated codes using long interleavers require more iterations than short interleavers to reach this saturation point. Stopping criteria to find the optimal number of iterations at which to stop the decoding process is an important area of research and a few of these criteria are discussed in [65, Chap. 6].

Interleavers

The role of the interleaver is two fold. Firstly it generates a long block code from the short constraint length constituent codes and secondly it allows for the application of an iterative decoding algorithm which can exchange soft information between decoders by decorrelating the inputs of the decoders. In other words the interleaver ensures that low weight sequences in the first encoder are mapped to high weight sequences in the second encoder.

At low SNRs the interleaver size has a large influence on the code's performance while the interleaver structure has a negligible effect. At high SNRs the code's performance is dependent on both interleaver size and structure. A longer interleaver results in improved performance and lowers the BER at which the error floor region is reached. A well structured interleaver will map low weight input sequences for the 1st encoder to high weight input sequences in the 2nd encoder. A number of interleaving structures are discussed in [65, Chap. 7] which are divided into 4 categories. These are block, convolutional, random and code matched interleavers.

Constituent codes

The type, constraint length and generator polynomials of the constituent encoders have a large influence on the overall code's performance. In the case of turbo codes recursive rather than non-recursive convolutional codes result in a higher interleaver gain and thus a lower BER for interleavers of reasonable length [66]. Convolutional codes achieving the largest minimum free distance may not result in a minimum free distance concatenated code due to the effect of the interleaver. Increasing the constraint length of the constituent codes improves the overall code's performance at high SNRs but generally degrades its performance at low SNRs. Therefore concatenated codes must be designed considering the joint effect of the interleaver and the constituent codes.

Trellis termination

The performance of a concatenated code can be improved if all or some of the encoders are terminated in a known state which is generally taken to be the all-zero state. Turbo codes can be terminated by calculating tail bits for the first encoder and leaving the second encoder un-terminated. A slight performance gain is observed if both encoders are terminated. SCCCs are easily terminated by adding tail bits to the end of the frame.

4.3   Concatenated space-time trellis codes

Many concatenated ST coding structures have been proposed in the literature and this section presents a brief overview of the recent work done in this field.

Full spatial diversity in quasi-static fading channels is achieved when the rank of the CDCM, discussed in section 3.3, is equal to the number of transmit antennas. Full rate is achieved when the overall bandwidth efficiency of the system is equal to the bandwidth efficiency of the signal constellation. For example BPSK, QPSK and 8-PSK achieve bandwidth efficiencies of 1, 2 and 3 bps/Hz respectively. These bandwidth efficiencies may not be achieved in practice due to non-ideal bandlimiting with practical filters.

A Turbo-TCM code was serially concatenated with a STBC in [67]. This concatenation was shown to improve the performance of STBCs. Feedback of soft information from the STBC decoder to the Turbo-TCM decoder was considered but it was shown that no improvement could be gained.

In [68] a space-time turbo code was proposed which achieved maximum diversity gain and full rate of 1 bps/Hz for both two (punctured) and three transmit antennas using BPSK modulation. This system concatenated two recursive systematic convolutional codes in parallel with suitable interleaving to ensure full spatial diversity. The performance of the proposed space-time turbo code was compared to that of STTCs with similar complexity where it was shown to give small gains in quasi-static fading and large gains in rapid fading channels.

A parallel concatenation of two recursive systematic STTCs using QPSK modulation was proposed in [69] where full rate and full spatial diversity were achieved. The FER performance of this system was considered in quasi-static fading channels and significant performance gains over conventional STTCs were achieved.

A space-time turbo code using QPSK modulation was proposed in [70, 71] which achieved maximum diversity gain and full rate. The outputs of a turbo encoder were punctured, interleaved, multiplexed and transmitted over two antennas. This code achieved a similar performance to a 64-state STTC in quasi-static fading and improved performance in rapid fading channels.

The outputs of a turbo encoder were bit interleaved, QPSK modulated and transmitted over multiple antennas in [28, 72]. Full rate was achieved, but maximum diversity gain was not guaranteed. Simulation results indicated that the proposed code outperforms a 16-state STTC.

A serially concatenated system was proposed in [73] which achieved full rate of 2 bps/Hz using QPSK modulation but did not guarantee full diversity gain. Each output of a STTC was interleaved and serially concatenated with a rate-1 recursive inner code. Simulation results in quasi-static fading channels showed that the proposed system achieved lower FERs than STTCs. This work was extended in [74] to achieve full rate and maximum diversity gain by making all interleavers and RSC codes identical.

In [75, 76] a parallel concatenation of two recursive STTCs as well as a serial concatenation of a RSC code and a recursive STTC was proposed. Maximum diversity gain was achieved for both systems using QPSK modulation. For the parallel concatenated code, full rate of 2 bps/Hz was achieved with suitable interleaving and puncturing. For the serially concatenated code, a bandwidth efficiency of 1 bps/Hz was achieved. Simulation results for quasi-static and rapid Rayleigh fading channels were presented where the proposed systems achieved superior performance to STTCs. It was also concluded that recursive STTCs result in larger performance gains than non-recursive STTCs in a concatenated system.

4.4 System model for the ST-PC and ST-SC systems

Double [58] and hybrid [59] concatenated CCs have been shown to achieve superior performance over simple concatenated CCs such as turbo codes and SCCCs as discussed in section 4.2. The simple concatenated STTCs proposed in the literature have demonstrated improved coding gains over conventional STTCs. Motivated by these two factors two double concatenated STTC systems with 2 interleavers and 3 constituent codes are proposed to further improve the coding gain of STTCs.

Any of the concatenated STTC systems discussed in section 4.3 could be modified to incorporate a third encoder. When selecting a concatenated system to modify, one would ideally choose the system with the best performance. However no results directly comparing the relative performance of these systems could be found in the literature. The serially concatenated structure of [75] was simple and easily modified to incorporate a third encoder. In this section the outer convolutional encoder is replaced by a turbo code or PCCC and a SCCC in the aim of increasing the coding gain of the overall code. These two systems will be referred to as ST-PC and ST-SC respectively.

In this section the encoding and decoding of the proposed ST-PC and ST-SC systems is explained. The bitwise additive SISO algorithm used to decode the constituent STTCs and CCs is also described. In all cases the systems have a bandwidth efficiency of 1 bps/Hz.

4.4.1 ST-PC and ST-SC transmitter

The STTC architecture and channel model is identical to that discussed in chapter 2. There are n_T transmit and n_R receive antennas which are sufficiently separated to ensure spatially uncorrelated fading.

In Fig. 4.4 and Fig. 4.5 the transmitter models for the ST-PC and ST-SC systems are presented. In both systems the input frame $\underline{u}$ of the uncoded bits is encoded by the double concatenated STTC encoder to produce a vector $\underline{c_t}$ of n_T output symbols which are then

simultaneously transmitted over the n_T transmit antennas.

The interleavers are all pseudo random and operate on bits, not symbols. The convolutional encoders are either both recursive systematic convolutional (RSC) or both non-recursive convolutional (NRC) encoders. The STTC encoder is either a non-recursive or a recursive STTC encoder which will be referred to ST and RST respectively.

Encoding of ST-PC

The ST-PC system is shown in Fig. 4.4 where the input bits $\underline{u}$ are encoded by C_1 as well as by C_2 after interleaving by π_p. The block P/S converts the bit streams from C_1 and C_2 into a single serial stream. In the case of NRC codes all the output bits of C_1 and C_2 are converted to a serial bit stream while in the case of RSC codes the systematic and parity bits of C_1 and only the parity bits of C_2 are converted to a serial bit stream. This serial bit stream is then interleaved by π_s and finally ST encoded. All encoders except C_2 are terminated.
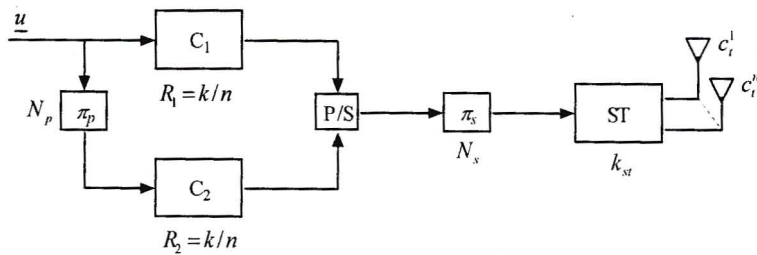
Figure 4.4: Block diagram of the ST-PC encoder.

Encoding of ST-SC

In Fig. 4.5 the ST-SC system is shown. The input bits $\underline{u}$ are encoded by C_1 and interleaved by π_1. These interleaved bits are encoded by C_2 and interleaved by π_2 and lastly ST encoded. In this system all the encoders are terminated.
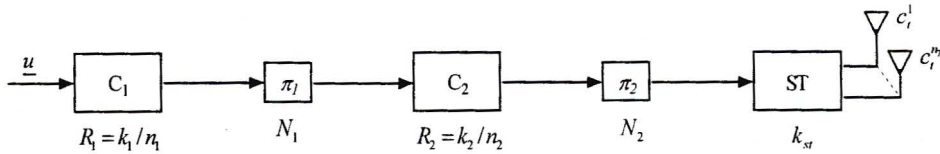
Figure 4.5: Block diagram of the ST-SC encoder.

Puncturing

In order to compare the systems discussed in this section under identical bandwidth efficiencies, puncturing of the output symbol vectors $\underline{c}_t$ is necessary to maintain an overall bandwidth efficiency of 1 bps/Hz. For simplicity the puncturing block is not shown in the encoder and decoder diagrams. At the transmitter the punctured symbol vectors $\underline{c}_t$ are not transmitted and at the receiver the LLRs corresponding to the punctured symbols are set to zero. Although this may limit the diversity gain of the system in quasi-static fading, based on the rank criterion discussed in section 3.3, simulation results in section 4.6 indicate that this effect is negligible.

4.4.2 ST-PC and ST-SC receiver

In this section the bitwise additive SISO algorithm which is used to decode each constituent code, is described. The decoding process of the proposed ST-PC and ST-SC systems is then explained.

The bitwise additive SISO algorithm

The core of the iterative decoding algorithm is the soft-input, soft-output (SISO) module [55]. In this dissertation the algorithm is implemented in its bitwise additive form [77] where soft information is exchanged between decoders in the form of bit logarithmic likelihood ratios (LLRs). This makes the process of interleaving and de-interleaving straightforward as no conversions between bit LLRs and symbol LLRs are required.

Consider a trellis encoder with m memory elements, L input symbols u and L output
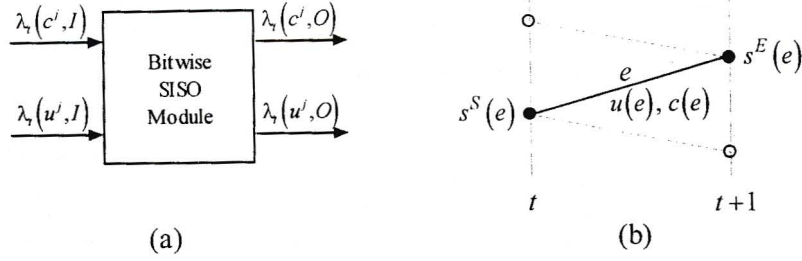
Figure 4.6: (a) SISO module. (b) Trellis section for edge e.

symbols c. The input symbols are drawn from an alphabet of $n_u = 2^k$ symbols each consisting of k bits where $u = \{u^1, \ldots, u^k\}$ and k is the number of encoder input bits at each time instance. For CCs the output symbols are drawn from an alphabet of $n_c = 2^n$ symbols each consisting of n bits where $c = \{c^1, \ldots, c^n\}$ and n is the number of encoder output bits at each time instance. For STTCs the output symbols are drawn from an alphabet of $n_c = M^{n_T}$ symbols each consisting of n_T M-PSK symbols where $c = \{c^1, \ldots, c^{n_T}\}$.

The four port SISO module in Fig. 4.6a accepts the input LLRs of the coded and uncoded bits, $\lambda_t(c^j, I)$ and $\lambda_t(u^j, I)$, and outputs an update of the these LLRs, $\lambda_t(c^j, O)$ and $\lambda_t(u^j, O)$, based upon the code constraints.

The dynamics of a trellis code can be described by a single trellis section which gives all the possible transitions or edges between the encoder states at time t and time $t+1$. A trellis section is described by a set of $n_s = 2^m$ states, where the state of the trellis at time t is $S_t = s$, and a set of $n_e = n_u \cdot n_s$ edges connecting these states. A single trellis section for edge e is given in Fig. 4.6b. An edge e describes the transition from initial state $s^S(e)$ to final state $s^E(e)$ with corresponding input symbol $u(e)$ output symbol $c(e)$.

The input-output relationships of the SISO module are now defined for a frame length of L symbols which corresponds to an input frame size of Lk bits. For $t = \{1, \ldots, L\}$,

$$\lambda_t(c^j, O) = \overset{*}{\underset{e:c^j(e)=1}{\max}} \left\{ \alpha_{t-1}(s^S(e)) + \lambda_t(u(e), I) + \sum_{i=1, i \neq j}^{n} c^i(e)\lambda_t(c^i(e), I) + \beta_t(s^E(e)) \right\} \quad (4.2)$$
$$- \overset{*}{\underset{e:c^j(e)=0}{\max}} \left\{ \alpha_{t-1}(s^S(e)) + \lambda_t(u(e), I) + \sum_{i=1, i \neq j}^{n} c^i(e)\lambda_t(c^i(e), I) + \beta_t(s^E(e)) \right\}$$

$$\lambda_t(u^j, O) = \max_{e:u^j(e)=1}^* \left\{ \alpha_{t-1}(s^S(e)) + \lambda_t(c(e), I) + \sum_{i=1, i \neq j}^{k} u^i(e)\lambda_t(u^i(e), I) + \beta_t(s^E(e)) \right\} (4.3)$$

$$- \max_{e:u^j(e)=0}^* \left\{ \alpha_{t-1}(s^S(e)) + \lambda_t(u(e), I) + \sum_{i=1, i \neq j}^{k} u^i(e)\lambda_t(u^i(e), I) + \beta_t(s^E(e)) \right\}$$

In this algorithm, the output LLRs do not depend on their corresponding simultaneous input. Thus the LLRs $\lambda_t(c^j, O)$ and $\lambda_t(u^j, O)$ are an update of the input LLRs $\lambda_t(c^j, I)$ and $\lambda_t(u^j, I)$.

The forward and backward metrics, $\alpha_t(\cdot)$ and $\beta_t(\cdot)$ are calculated in (4.4) and (4.5) below.

$$\alpha_t(s) = \max_{e:s^E(e)=s}^* \left\{ \alpha_{t-1}(s^S(e)) + \lambda_t(u(e), I) + \lambda_t(c(e), I) \right\} \qquad (4.4)$$

$$\beta_t(s) = \max_{e:s^S(e)=s}^* \left\{ \beta_{t+1}(s^E(e)) + \lambda_{t+1}(u(e), I) + \lambda_{t+1}(c(e), I) \right\} \qquad (4.5)$$

These metrics are initialised as follows:

$$\alpha_0(s) = \begin{cases} 0 & \text{if } s = S_0 \\ -\infty & \text{otherwise} \end{cases}$$

$$\beta_L(s) = \begin{cases} 0 & \text{if terminated and } s = S_0 \\ 1/n_s & \text{if non-terminated} \\ -\infty & \text{otherwise} \end{cases}$$

The max* operator performs addition in the log domain and is calculated recursively. To calculate $\max_j^*(a_j)$, (4.6) is evaluated recursively where δ_1 is initialised to a_1 and $\max(\cdot)$ takes the maximum of the two arguments. For $j = \{2, \ldots, J\}$,

$$\delta_j = \max(\delta_j, \delta_{j-1}) + \ln\left[1 + \exp(|\delta_j - \delta_{j-1}|)\right] \qquad (4.6)$$

On the final iteration J,

$$\max_j^*(a_j) = \delta_J \qquad (4.7)$$

For both CCs and STTCs the input symbol LLRs of the uncoded bits $\lambda_t(u, I)$ are calculated as follows where $l = \{1, \ldots, n_u\}$.

$$\lambda_t(u = u_l, I) = \sum_{i=1}^{k} u_l^i \lambda_t(u^i, I) \qquad (4.8)$$

For CCs the input LLRs of the coded bits are always received from other SISO modules and not from the demodulator and can be calculated as shown below where $l = \{1, \ldots, n_c\}$.

$$\lambda_t(c = c_l, I) = \sum_{i=1}^{n} c_l^i \lambda_t(c^i, I) \tag{4.9}$$

For STTCs, the input LLRs of the coded M-PSK symbols are only received from the soft outputs of the demodulator and are calculated as shown (4.10). The received signal r_t^j at time t on receive antenna j after matched filtering is given by (2.1). Let $\underline{g}_l$ be one of the possible output symbol vectors of the STTC encoder where $l = \{1, \ldots, n_c\}$. Let $\underline{g}_1$ be the reference symbol vector.

$$
\begin{aligned}
\lambda_t(c = \underline{g}_l, I) &= \hat{\lambda}_t(c = \underline{g}_l, I) - \hat{\lambda}_t(c = \underline{g}_1, I) \\
\hat{\lambda}_t(c = \underline{g}_l, I) &= -\frac{1}{2\sigma_r^2} \sum_{j=1}^{n_R} |r_t^j - \sum_{i=1}^{n_T} \alpha_{ij}^t g_l^i|^2
\end{aligned}
\tag{4.10}
$$

Decoding of ST-PC

A simplified diagram of the ST-PC decoder is shown in Fig. 4.7. In describing the following systems the subscript t of λ and the superscript j of c and u will be dropped for simplification purposes. The subscript of the c or u specifies the decoder where st is used for the ST encoder, 1 for the convolutional encoder C1 and 2 for convolutional encoder C2

On the first iteration the SISO module inputs $\lambda(u_{st}, I)$ and $\lambda(u_1, I)$ are set to zero since no a-priori information is available and $\lambda(c_{st}, I)$ is calculated using equation 4.10. The following process can now be iterated.

The LLR $\lambda(u_{st}, O)$ is calculated by the ST SISO module and is passed through the inverse interleaver π_s^{-1}. The information pertaining to the coded bits of C$_1$ and C$_2$, $\lambda(c_1, I)$ and $\lambda(c_2, I)$ respectively, is then extracted. In the case of NRC codes, this information is passed directly to the corresponding decoders. In the case of RSC codes, the LLRs corresponding to systematic and parity bits of C$_1$ are passed to the C$_1$ SISO module while LLRs corresponding to the interleaved (π_p) systematic bits of C$_1$ and the parity bits of C$_2$ are fed to the C$_2$ SISO module.

The C$_1$ SISO module then calculates the output LLRs and passes $\lambda(u_1, O)$ through in-
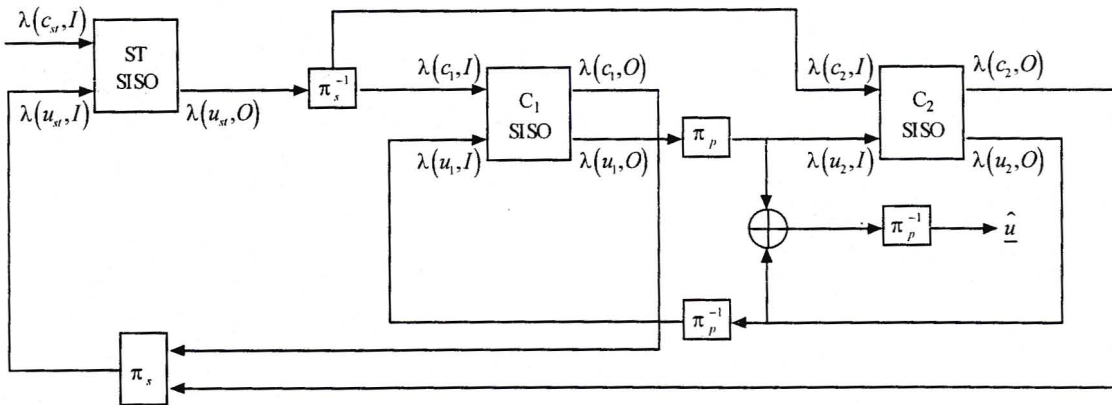
Figure 4.7: Block diagram of the ST-PC decoder.

terleaver π_p to obtain $\lambda(u_2, I)$. In the case of RSC codes, $\lambda(c_1, I)$ contains information pertaining to the uncoded bits and hence this information is subtracted from $\lambda(u_1, O)$ before being fed forward to the C_2 SISO module. This ensures that only extrinsic information is exchanged between the two decoders.

The output LLRs of the C_2 SISO module are then calculated and $\lambda(u_2, O)$ is passed through inverse interleaver π_p^{-1} to obtain $\lambda(u_1, I)$ for the next iteration. Again, in the case of RSC codes $\lambda(c_2, I)$ contains information pertaining to the uncoded bits and hence this information is subtracted from $\lambda(u_2, O)$ before being fed back to the C_1 SISO module.

In the case of NRC codes, a single LLR stream is constructed from $\lambda(c_1, O)$ and $\lambda(c_2, O)$. In the case of RSC codes a single LLR stream is constructed from the parity bits of $\lambda(c_1, O)$ and $\lambda(c_2, O)$ and the systematic bits of $\lambda(c_2, O)$ de-interleaved by π_p^{-1}. Various weighted combinations of the systematic bits from $\lambda(c_1, O)$ and $\lambda(c_2, O)$ were fed back to the ST SISO module but best results were achieved using the method described above. The constructed LLR stream from the SISO modules C_1 and C_2 is then interleaved by π_s to become $\lambda(u_{st}, I)$ on the next iteration.

The above process is then iterated several times. On the final interaction $\lambda(u_2, I)$ and $\lambda(u_2, O)$ are added and passed through inverse interleaver π_p^{-1} to obtain an estimate of the original bit stream $\hat{\underline{u}}$.

Decoding of ST-SC

The decoder of the ST-SC system is shown in Fig. 4.8 where decoding is somewhat simpler than the decoding of the ST-PC system. Assuming equally likely transmitted source symbols, the input $\lambda(u_1, I)$ is always set to zero. On the first iteration $\lambda(u_{st}, I)$ and $\lambda(u_2, I)$ are set to 0 as no a-priori information is available, and $\lambda(c_{st}, I)$ is calculated using equation (4.10).
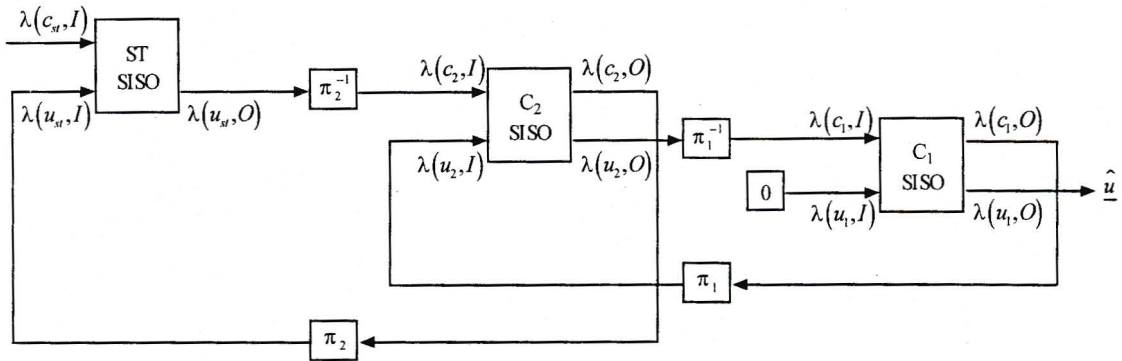
Figure 4.8: Block diagram of the ST-SC decoder.

The ST SISO module calculates $\lambda(u_{st}, O)$ and passes this information through the inverse interleaver π_2^{-1} to obtain $\lambda(c_2, I)$. The output LLRs of SISO module C_2 are then calculated and $\lambda(u_2, O)$ is passed through the inverse interleaver π_1^{-1} to obtain $\lambda(c_1, I)$. The output $\lambda(c_2, O)$ is passed through interleaver π_2 to become $\lambda(u_{st}, I)$ on the next iteration.

The C_2 SISO module then calculates the output LLRs and $\lambda(c_1, O)$ is passed through interleaver π_1 to become $\lambda(u_2, I)$ on the next iteration. On the final iteration $\hat{\underline{u}}$ can be calculated directly from $\lambda(u_1, O)$.

4.5 Analysis of concatenated STTCs

In this section an analysis is derived for the serially concatenated system from [75] which will be denoted ST-CC as well as the proposed double concatenated ST-PC system.

As with ST codes, it is impractical to generate simulation results for concatenated coding

schemes at high SNRs and in this region, analytical bounds are used to evaluate the code's performance. These bounds are useful in determining the code's error floor region which is difficult to determine by simulation. Simulation results and analytical bounds are both necessary to investigate the performance of a concatenated code.

The ST-PC system with NRC codes and the ST-SC system employ puncturing to achieve a bandwidth efficiency of 1 bps/Hz. Puncturing complicates the analysis as the state transition matrix must be expanded to model the effect of puncturing and is very large for the ST-SC system where every 9th transmission is punctured. For this reason only the non-punctured ST-PC system with RSC codes and the ST-CC system are considered.

Some work on the analysis of concatenated STTCs has been presented in the literature. A performance analysis for a parallel concatenated STTC structure was proposed in [26, 78, 79]. In [78] an analytical expression for the BER in an AWGN channels was derived. This work was extended in [26] to quasi-static fading channels. Good agreement of simulation and analytical results were obtained here. An approximate analysis was derived in [79] but the analytical results were loose when compared to simulation results. To the extent of the authors knowledge, no literature has considered the analysis of concatenated STTCs in rapid Rayleigh fading channels.

In this section the necessity of the uniform interleaver for the analysis of convolutional codes is described. Analytical expressions for turbo codes and SCCCs are then presented and the validity of this analysis is discussed. Analytical expressions are then derived for the FER of the ST-CC and the ST-PC systems with RSC codes in rapid Rayleigh fading channels. The proposed analysis is based on analytical methods for concatenated convolutional codes from [55, 66] and the analysis of STTCs proposed in chapter 3.

4.5.1 The uniform interleaver

This section describes the analytical upper bounding of concatenated convolutional codes.

An analytical union bound for turbo codes was first proposed in [80, 81] and was later discussed in more detail in [66]. This bounding technique was also applied to serially

concatenated CCs [55], double serially concatenated CCs [58] and hybrid concatenated CCs [59].

In [66] an exact and an approximate analysis were proposed for turbo codes, the results of which are presented here. Consider the turbo encoder of Fig. 4.1 and let N be the number of bits and L be the number of symbols in each input frame where $L = N$ for this encoder. The first approximation to be made is to perform the analysis on the basis that the all-zero sequence was transmitted. This can be done because the constituent codes are linear and hence the overall concatenated code is also linear.

The proposed analysis in [66] considered a hyper-trellis of the turbo code with states S_{mn} corresponding to state S_m of C$_1$ and S_n of C$_2$. Each branch of the hyper-trellis $S_{mn} \rightarrow S_{pq}$ corresponds to all paths which start in state S_{mn} and end in state S_{pq} of the hyper-trellis after L steps.

The input-redundancy weight enumerating function (IRWEF) of the constituent code C$_x$ is useful for the analysis of turbo codes and is defined as,

$$N_{mp}^x(I, Z) = \sum_{i,z} n_{mp}^x(i, z) I^i Z^z \qquad (4.11)$$

where $n_{mp}^x(i, z)$ is the number of error events with input weight i and output parity weight z, such that the output weight of the codeword is $w + z$, connecting state S_m and state S_p in L steps.

The input-output weight enumerating function (IOWEF) of the equivalent turbo code for the branch label $S_{mn} \rightarrow S_{pq}$ is defined as follows,

$$N_{mn,pq}(I, D) = \sum_{i,d} n_{mn,pq}(i, d) I^i D^d \qquad (4.12)$$

where the error event multiplicity $n_{mn,pq}(i, d)$ is the number codewords with input weight i and output weight d which start in state S_{mn} and end in state S_{pq} of the hyper-trellis after L steps. The calculation of these multiplicities is simplified by the notion of a uniform interleaver.

A uniform interleaver is a probabilistic device of length N that allows the performance of a concatenated code to be averaged over the set of all possible deterministic interleavers. It

maps an input word of weight i into all its distinct permutations $\binom{N}{i}$ with equal probability $1/\binom{N}{i}$. In [66] it was shown that the IOWEF calculated using a uniform interleaver is equivalent to the IOWEF averaged over all possible interleavers. Furthermore there always exists at least one deterministic interleaver with performance equal to or better than the uniform interleaver.

The uniform interleaver allows the IOWEF of the equivalent turbo code to be calculated as the normalised product of IRWEFs of the constituent codes and each multiplicity in (4.12) is calculated as follows.

$$n_{mn,pq}(i,d) = \frac{n_{mp}^1(i,z_1)n_{nq}^2(i,z_2)}{\binom{N}{i}} \tag{4.13}$$
$$d = i + z_1 + z_2$$

The multiplicities $n_{mp}^x(i,z_x)$ can be calculated using standard enumeration techniques for convolutional codes [40, 41, 66]. Once the equivalent IOWEF of the turbo has been calculated, the union bound together with the PWEP of each error event is used to calculate the BER and FER.

For constituent codes with many states and for long interleavers, the analysis becomes extremely complex even though the complexity is only related to that of the constituent codes. A simpler analysis was proposed in [66] which was shown to be accurate for interleavers significantly larger (10 times) than the constraint length of the constituent code. The approximation only considers the branch $S_{00} \rightarrow S_{00}$ joining the all-zero states of the hyper-trellis. Thus only the IOWEF $N_{00,00}(i,d)$ is calculated. From now on all subscripts of the IOWEFs, the IRWEFs and the corresponding multiplicities refer to transitions between the all-zero state and for this reason the subscripts are dropped.

4.5.2 Analysis of turbo codes and SCCCs

This section presents the analytical expressions for the analysis of turbo codes and SCCCs using the approximations discussed in the previous section. This forms the basis for the analysis of concatenated STTC systems which is discussed later in this chapter. The standard union bound for the FER of convolutional codes in AWGN channels with BPSK

modulation using the complementary error function on the PWEP is given below where R_c is the overall code rate.

$$P_f \leq \sum_{i,d} n(i,d)\mathrm{erfc}\left(\sqrt{\frac{dR_cE_b}{N_0}}\right) \tag{4.14}$$

The error event multiplicities $n(i,d)$ of the concatenated code are calculated from the multiplicities of the constituent codes using the notion of the uniform interleaver.

In this dissertation the state transition matrix method in [40] is used to enumerate the multiplicities of the constituent convolutional codes. The initial matrix representing encoder x must be raised to the L_xth power, after which element $(0,0)$ of this matrix is a polynomial of the form,

$$N^x(I,D) = \sum_{i,d} n^x(i,d)I^iD^d \tag{4.15}$$

where $n^x(i,d)$ is the number of error events of length L_x symbols with input weight i and output weight d starting and ending in the all-zero state. In a similar way to enumerating the error events for STTCs, a limiting function is used to limit the number of terms in each polynomial whereby a term is removed if the output weight $d \geq d_{lim}$. The symbols D and d can be substituted for Z and z where only the parity output weight is required as is the case for RSC codes.

For the rate 1/3 turbo code in Fig. 4.1, the interleaver length is N bits. The multiplicities $n(i,d)$ of the concatenated code can be calculated as shown below where the multiplicities $n^1(i,z_1)$ and $n^2(i,z_2)$ of the constituent codes are obtained by enumerating error events of length $L_1 = L_2 = N$.

$$
\begin{aligned}
n(i,d) &= \frac{n^1(i,z_1)n^2(i,z_2)}{\binom{N}{i}} \\
d &= i + z_1 + z_2 \\
R_c &= \frac{1}{3}
\end{aligned}
\tag{4.16}
$$

For the SCCC in Fig. 4.3 the interleaver length is N_1 bits. The multiplicities of the constituent codes $n^1(i,d_1)$ and $n^2(i,d_2)$ are obtained by enumerating error events of length $L_1 = N/k_1$ and $L_2 = N_1/k_2$ respectively. The multiplicities of the concatenated code can

now be calculated as follows.

$$
\begin{aligned}
n(i,d) &= \sum_l \frac{n^1(i,l)n^2(l,d)}{\binom{N_1}{l}} \tag{4.17} \\
N_1 &= N\frac{n_1}{k_1} \\
R_c &= \frac{k_1 k_2}{n_1 n_2}
\end{aligned}
$$

4.5.3 Validity of analysis

In [55] the difficulties and shortcomings of the above analysis for concatenated convolutional codes were described. The analysis uses the union bound which is an upper bound on the error probability as described in section 3.4. Therefore the sum of the PWEPs does not give a true probability and results in the bound diverging at low SNRs. In order to obtain this divergence many error events must be considered and this is computationally intensive to calculate, especially for large frame sizes. For this reason divergence of the bound is sometimes not observed. Another shortcoming is that the bound which is based on maximum-likelihood decoding is not entirely suited to the analysis of codes which use a suboptimal iterative decoding algorithm. Therefore at medium to high SNRs this upper bound on ML decoding may result in a slight lower bound on suboptimal iterative decoding [41, 66].

4.5.4 Analysis of the ST-CC and ST-PC systems

Using the analytical method proposed in chapter 3 for STTCs and the analytical methods discussed thus far for concatenated convolutional codes, an analysis is proposed for the ST-CC and ST-PC systems using RSC codes.

The union bound together with the new bound [39] on the PWEP is used to calculate the FER of concatenated STTCs. In a rapid fading channel, an error event is characterised by a common input weight i, logarithmic eigenvalue product p and rank r. The FER can be calculated using (3.24) which is repeated in here in terms of the new bound and as a

function of E_b/N_0, not E_s/N_0.

$$P_f \leq \sum_{i,p,r} n(i,p,r) \exp(-n_R p) \binom{2rn_R - 1}{rn_R - 1} \left(\frac{R_c E_b}{n_T N_0}\right)^{-rn_R} \tag{4.18}$$

Here R_c is the overall code rate which relates the uncoded bit period T_b to the unmodulated symbol period T_s such that $R_c = T_s/T_b$.

In order to calculate the FER of a concatenated STTC system, the error event multiplicities $n(i,p,r)$ must be calculated considering the contributions of the constituent codes and interleavers. As discussed in section 4.5.1 it is not feasible to calculate the union bound for a specific interleaver and instead a uniform interleaver is used to average over all possible interleavers. In this way the bound can be calculated from the multiplicities of the constituent codes.

Because all constituent codes considered are linear, the entire concatenated code is linear and thus the analysis is considered for transmission of the all-zero codeword sequence. The analysis can also be simplified only by considering error events starting and ending in the all-zero state as discussed in [66] and section 4.5.1.

The next two sections describe the calculation of error event multiplicities $n(i,p,r)$ for the ST-CC and ST-PC systems. The following notation is used. N is the input frame size in bits. For convolutional encoder C_x, the code rate is $R_x = k_x/n_x$ where k_x is the number of input bits and n_x is the number of output bits at each time instance. The error event multiplicities are enumerated as discussed in section 4.5.2. The STTC system has k_{st} input bits, n_T transmit antennas and n_R receive antennas. The error events of the STTC have multiplicities $n^{st}(i,p,r)$ and length L_{st} symbols. Enumeration of these error events is discussed in chapter 3. The length of interleaver π_x in bits is N_x.

Calculation of $n(i, p, r)$ for the ST-CC system

This system consists of a convolutional code serially concatenated with a STTC as shown in Fig. 4.9 below.

Using the concept of the uniform interleaver, $n(i,p,r)$ for the ST-CC system is calculated
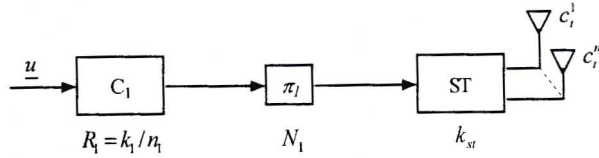
Figure 4.9: Block diagram of the ST-CC encoder.

in a similar way to SCCCs.

$$n(i, p, r) = \sum_{l} \frac{n^1(i, l)n^{st}(l, p, r)}{\binom{N_1}{l}} \tag{4.19}$$

$$N_1 = N\frac{n_1}{k_1}$$

$$R_c = \frac{k_1 k_{st}}{n_1}$$

The multiplicities $n^1(i, d_1)$ and $n^{st}(i, p, r)$ are calculated by enumerating error events of length $L_1 = N/k_1$ and $L_{st} = N_1/k_{st}$ respectively. By substituting (4.19) into (4.18) the FER of the ST-CC system is obtained.

Calculation of $n(i, p, r)$ for the ST-PC system

A block diagram of the ST-PC encoder is shown in Fig. 4.4 where the constituent encoders C_1 and C_2 are assumed to be RSC codes with identical parameters. The error event multiplicities of the concatenated code are calculated by considering the code as a serial concatenation of a turbo code and a STTC.

For the STTC, $n^{st}(i, p, r)$ is calculated by enumerating error events of length $L_{st} = N_s/k_{st}$. For the RSC codes, the parity weights of C_1 and C_2 are considered and the multiplicities $n^1(i, z_1)$ and $n^2(i, z_2)$ are obtained by enumerating error events of length $L_1 = L_2 = N/k$. The calculation of $n(i, p, r)$ for the overall ST-PC encoder is given below.

$$n(i, p, r) = \sum_{\substack{z_1, z_2: \\ i_{st} = i + z_1 + z_2}} \frac{n^1(i, z_1)n^2(i, z_2)n^{st}(i_{st}, p, r)}{\binom{N}{i}\binom{N_s}{i_{st}}} \tag{4.20}$$

$$N_s = N\frac{2n - k}{k}$$

$$R_c = \frac{k k_{st}}{2n - k}$$

The FER of the ST-PC system can now be calculated by substituting (4.20) into (4.18).

4.6   Simulation results

In this section, the performance of the proposed ST-PC and ST-SC systems is evaluated by simulation in quasi-static and rapid Rayleigh fading channels. These results assess the system performance for low to medium SNRs.

The simulation results are generated using Monte-Carlo methods where (4.10) is evaluated to generate the received signal which is then decoded as described in section 4.4.2. The number of bit and frame errors is then recorded.

The results shown are of FER versus (E_b/N_0) which is different from the definition in [21]. This definition takes into account the rate of the code and allows for comparison with systems of different code rates. In all simulations, an input frame size N of 130 bits and 1300 bits is used. The short frame is more suited to voice transmission as it causes a short delay, while the longer frame is more suited to data transmission because it generally results in lower FERs. For all systems, 2 transmit and a single receive antenna are used and the number of decoding iterations is 6.

Two 4-PSK, 4-state STTCs are considered, namely the non-recursive STTC of Tarokh [21, Fig. 4] and the recursive STTC of Tujkovic [75, Fig. 11] which will be referred to as ST and RST respectively. Recursive (RSC) and non-recursive (NRC) rate-2/3, 4-state convolutional codes are considered [55, Table III]. These constituent codes are presented in appendix C. The convolutional codes are either both RSC codes or both NRC codes. In all cases the overall bandwidth efficiency of the system is 1 bps/Hz where puncturing is performed if required. Puncturing was not required for the ST-PC system with RSC codes but was required for the ST-PC system with NRC codes where every 3rd tranmission was punctured and for the ST-SC system where every 9th tranmission was punctured.

Figures 4.10 to 4.13 present simulation results for the ST-PC and ST-SC systems, comparing various combinations of constituent encoders. In Fig. 4.10, results are shown for the ST-PC system in a quasi-static fading channel. The lowest FER is achieved using 2 RSC codes and a ST code for both input frame sizes. In all cases no interleaving gain in terms of FER is achieved by increasing the input frame size.
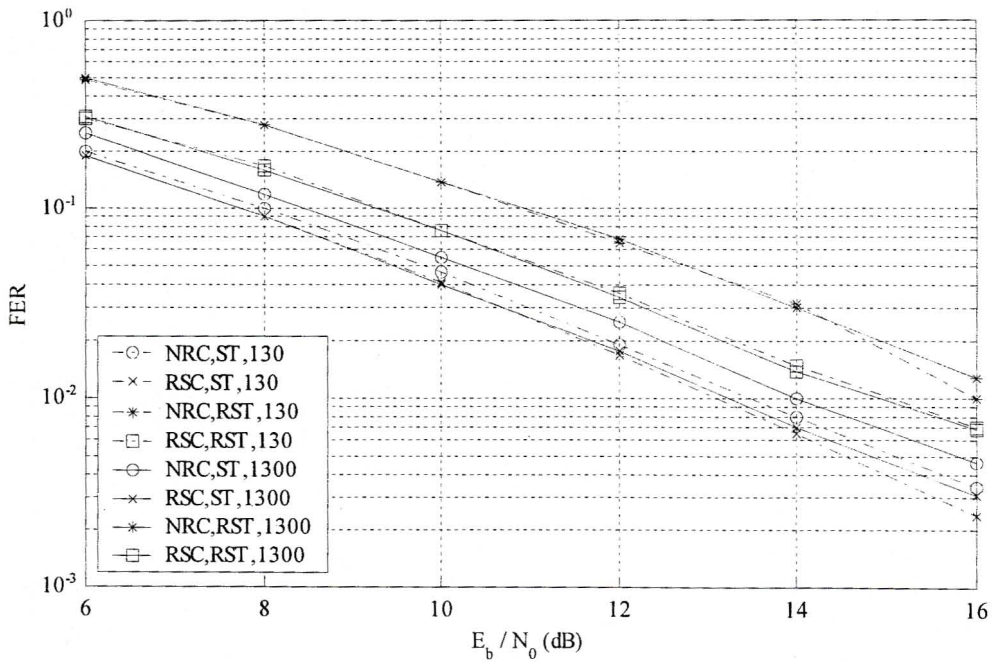
Figure 4.10: Performance of the ST-PC system in quasi-static fading.

The performance of the ST-PC system in a rapid fading channel is shown in Fig. 4.11. It is observed that for $N = 130$, 2 RSC codes and a ST code achieve the lowest FER. For $N = 1300$, 2 RSC codes and a ST code give the best FER performance at low SNRs (< 6dB), while 2 RSC codes with a RST code, judging from the slope of the two curves, achieve a lower FER at higher SNRs (> 7dB). For all encoder combinations, except for the case of 2 NRC codes and a ST code, interleaving gain in terms of FER is achieved. For $N = 1300$ bits, an error floor is present for 2 RSC codes and a ST code but is not observed for the same scheme using a RST code.

In Fig. 4.12, results for the ST-SC system are shown for the case of quasi-static fading. Similar to the ST-PC system, the lowest FER is achieved using 2 RSC codes and a ST code for $N = 130$ and $N = 1300$. Again it is observed that no interleaving gain in terms of FER is achieved.

Simulation results for the ST-SC system in rapid fading are given in Fig. 4.13. The lowest FER is achieved using 2 RSC codes and a ST code for both input frame sizes. By increasing the input frame size, interleaving gain is clearly achieved which is present at
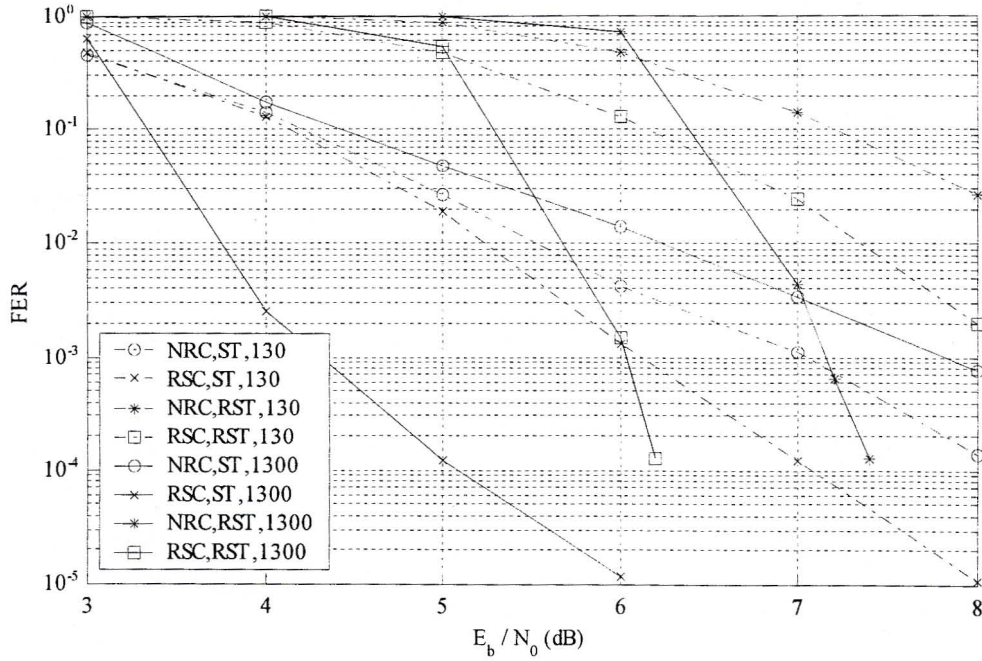
Figure 4.11: Performance of the ST-PC system in rapid fading.
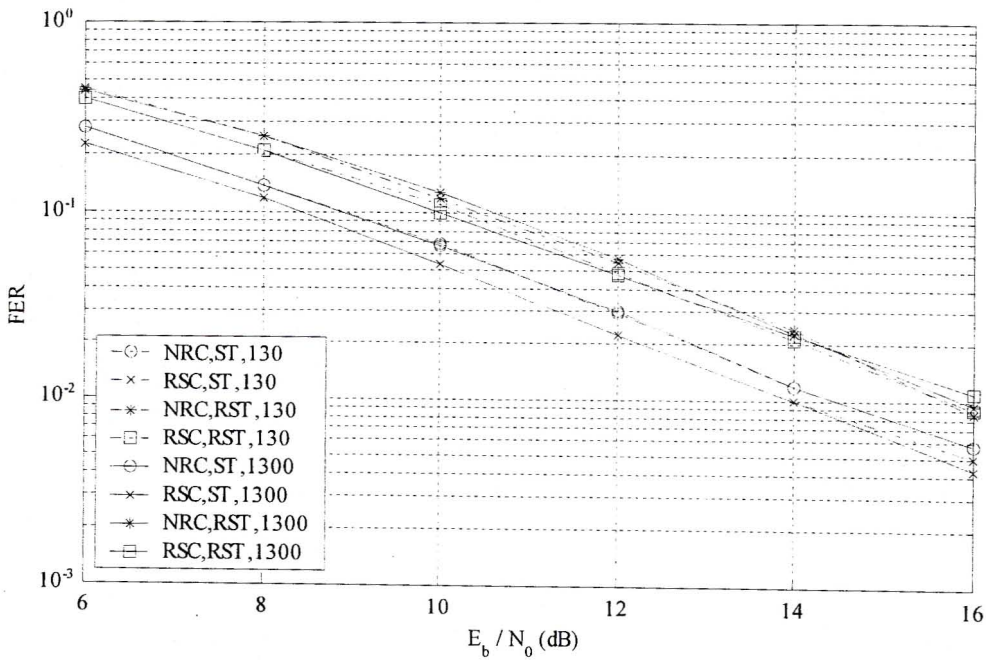
Figure 4.12: Performance of the ST-SC system in quasi-static fading.
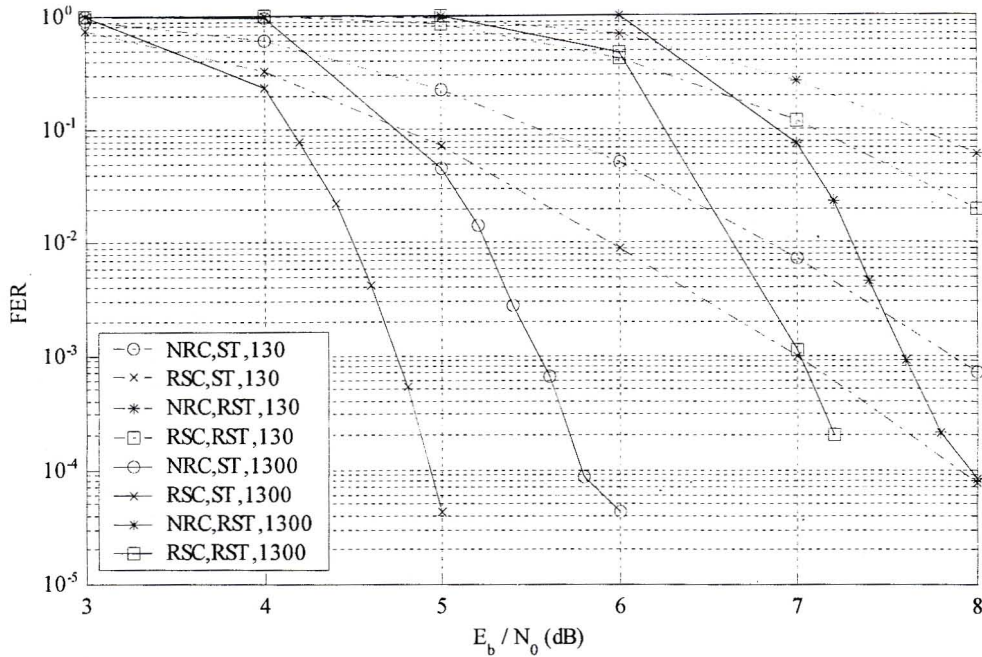
Figure 4.13: Performance of the ST-SC system in rapid fading.

low SNRs for the case of a ST code and at medium SNRs for the case of a RST code.

In figures 4.10 to 4.13 it is observed that in general system performance at low to medium SNRs is improved by using non-recursive ST codes over recursive ST codes and RSC codes over NRC codes. It is also noted that interleaving gain in terms of FER is not achieved in quasi-static fading channels but is present in rapid fading channels. This is due to the iterative decoding algorithm taking advantage of the extra temporal diversity in rapid fading channels. For quasi-static fading channels, the diversity gain or slope of the performance curve is the same for all systems indicating that limited puncturing of the ST code has a negligible effect on the diversity gain.

Figures 4.14 to 4.17 compare the FER and BER performance of the proposed ST-PC and ST-SC systems with the serially concatenated system (ST-CC) proposed in [75], using the optimal combination of encoders. Both proposed systems use 2 RSC codes and a ST code. The ST-CC system uses a rate 1/2, 4-state outer code with the [1, 5/7] generator polynomial with a RST inner code for rapid fading and a ST inner code for quasi-static fading channels.
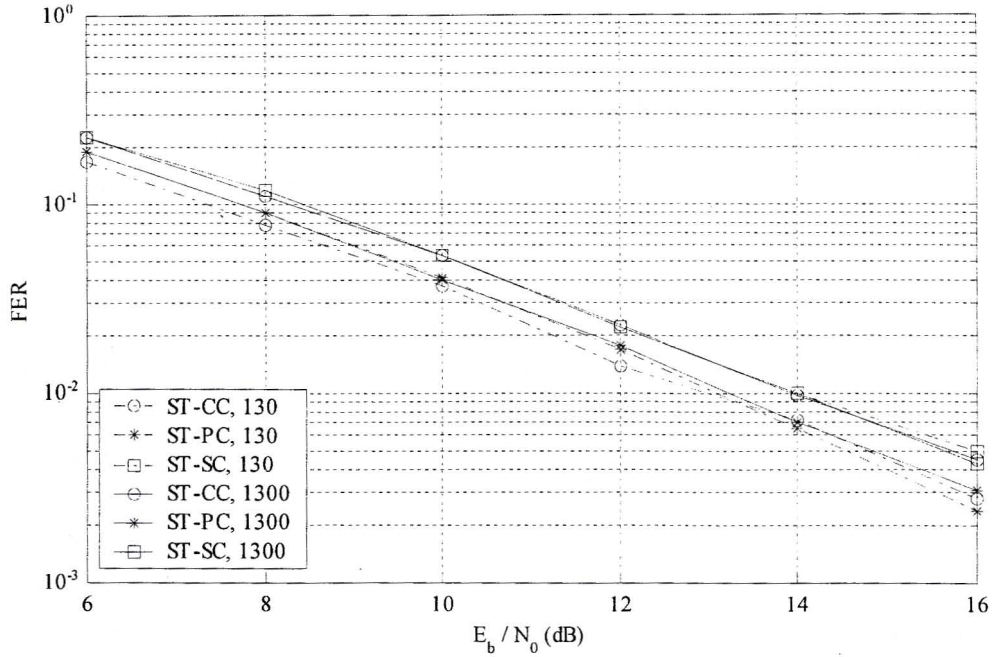
Figure 4.14: FER performance comparison in quasi-static fading channels.

In Fig. 4.14 results are shown for quasi-static fading where the FER performance of the 3 systems is similar. The lowest FER is achieved by the ST-CC and ST-PC system for $N = 130$ and by the ST-PC system for $N = 1300$. Note that the ST-CC system has a higher FER when N is increased while the FER performance of the 2 proposed systems is the same when N is increased. The BER performance in Fig. 4.15 shows similar trends.

A comparison of the 3 systems in rapid fading is shown in Fig. 4.16. For $N = 130$ the ST-PC system has the lowest FER followed by the ST-SC system and then the ST-CC system. For $N = 1300$, the ST-PC system achieves the lowest FER at low SNRs (< 5dB) while the ST-SC system achieves the lowest FER at higher SNRs. The ST-PC system has a coding gain of 1dB at a FER of 10^{-3} for $N = 130$ and 0.8dB at a FER of 10^{-2} for $N = 1300$ over the ST-CC system. The performance of the ST-SC system over the ST-CC system is negligible for both input frame sizes. Similar trends are observed in Fig. 4.17 for the BER performance of these systems.

In the literature the performance of iterative decoding schemes have been shown to converge to the Shannon limit in AWGN channels. However in Rayleigh fading channels the
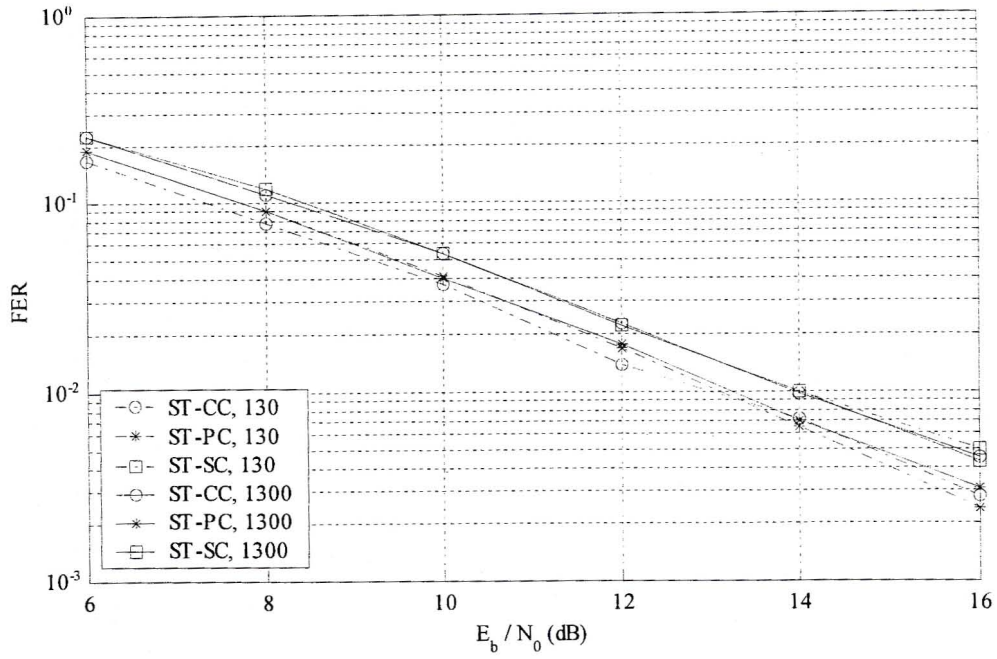
Figure 4.15: BER performance comparison in quasi-static fading channels.
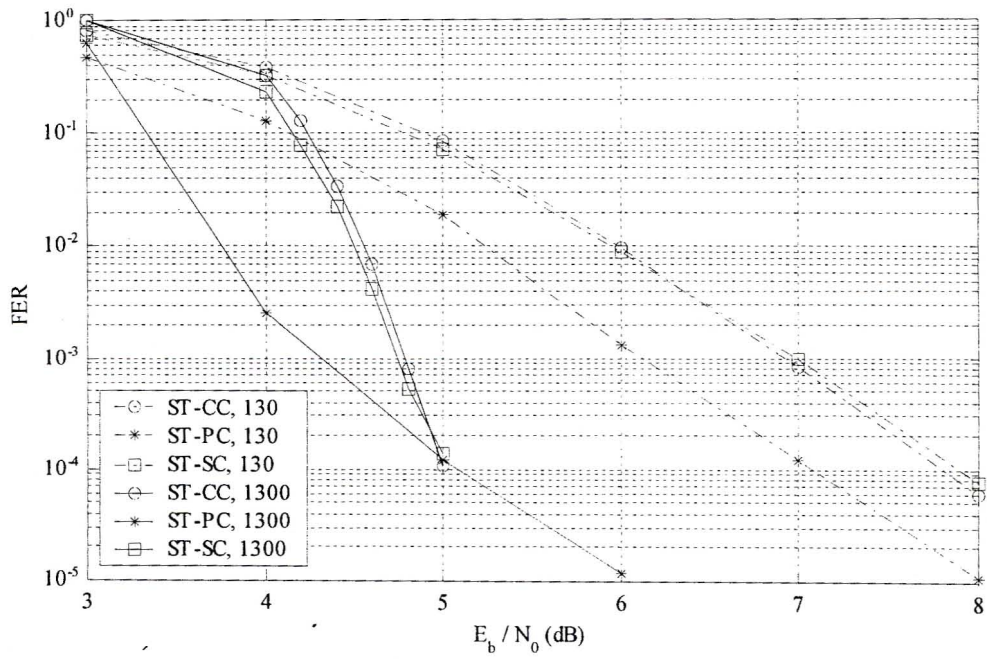
Figure 4.16: FER performance comparison in rapid fading channels.
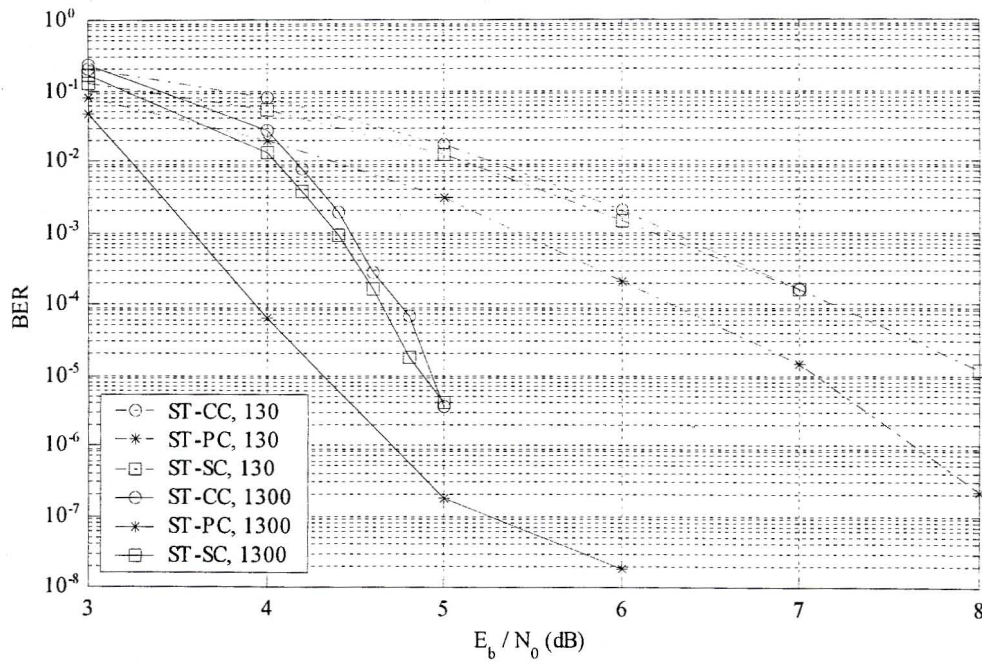
Figure 4.17: BER performance comparison in rapid fading channels.

performance of these schemes degrades due to the fading process [63, 65, 91]. This is also observed in the results shown in this chapter. It is also noted that system performance is worse in quasi-static fading channels than in rapid fading channels where more temporal diversity is available.

4.7   Analytical results

This section compares the proposed analytical results to simulation results for the ST-CC and ST-PC systems. Both systems use either a 4-PSK, 4-state non-recursive STTC (ST) or recursive STTC (RST). The ST-CC uses a rate-1/2 RSC outer code and the ST-PC system uses rate-2/3 RSC outer codes. All constituent codes are given in appendix C. In all cases a rapid fading channel is considered, the number of decoding iterations is 6, the frame size is 130 bits, two transmit and a single receive antenna are used.

A number of computational difficulties were experienced in the analysis. Firstly the bound and simulation results are only valid in the error floor region of the code. This error floor
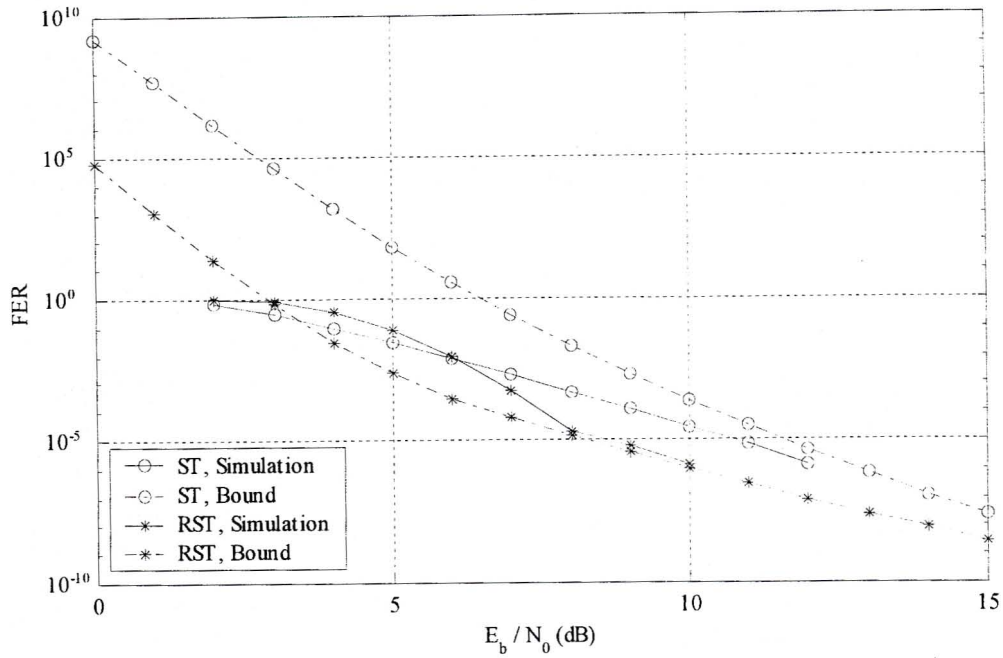
Figure 4.18: Analytical results for the ST-CC system.

occurs at very low FERs ($< 10^{-6}$) and it is extremely time intensive to obtain accurate simulation results in this region. For this reason it is sometimes not possible to observe the actual convergence of the bound and simulation results at high SNRs. Furthermore it is computationally intensive to enumerate the large number of error events required to obtain significant divergence of the union bound at low SNRs.

In Fig. 4.18 results are shown for the ST-CC code using ST and RST codes. The limiting function is set to $p_{lim} = 15$ for the STTC and $d_{lim} = 50$ for the CC. For the ST code the analysis gives an upper bound on system performance and is fairly tight (1 dB) at high SNRs. At low SNRs the analysis is very loose due to the divergence of the union bound. For the RST code a tight lower bound is observed in the error floor region at high SNRs. This could be attributable to the suboptimal iterative decoding algorithm used and the maximum likelihood assumption of the analysis. At low SNRs the bound gives lower FERs than the simulation results which could be due to an insufficient number of error events being enumerated. For both codes the proposed bound gives a fairly good approximation of the system performance at high SNRs.
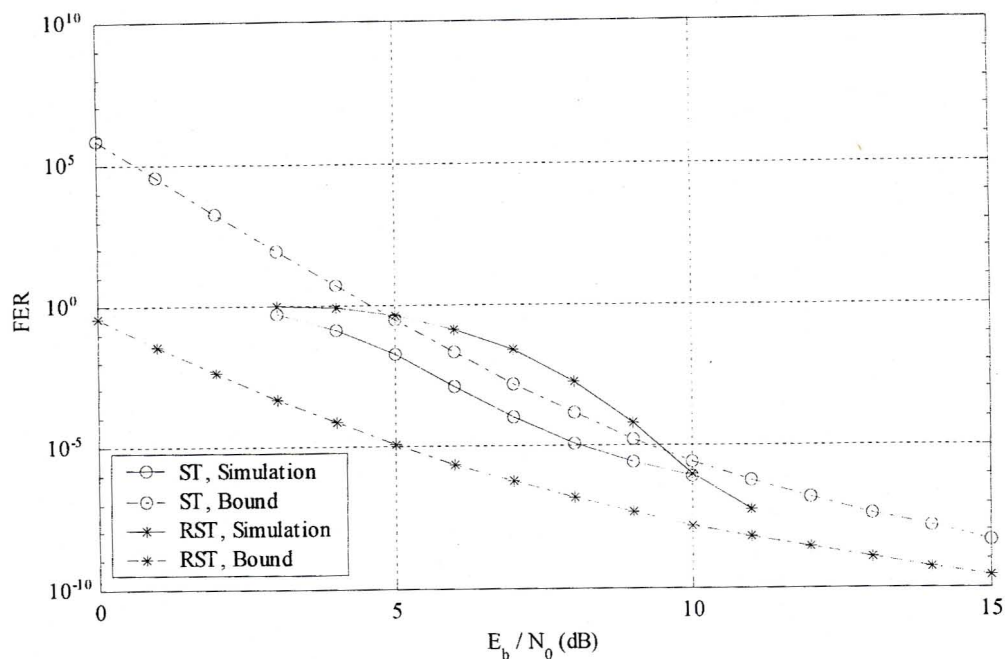
Figure 4.19: Analytical results for the ST-PC system.

The results for ST-PC are presented in Fig. 4.19. Here the limiting function is set to $p_{lim} = 10$ for the STTC and $d_{lim} = 20$ for the CC. The analysis for the ST code gives an upper bound on system performance and is fairly tight (1 dB) at high SNRs. At low SNRs the union bound diverges and becomes fairly loose. For the RST code, the error floor could not be accurately simulated but it is observed that the simulation results are tending towards the analytical results at high SNRs.

Comparing the analytical results for two systems it is observed that a large performance gain is achieved at high SNRs in using the ST-PC system over the ST-CC system for both ST and RST constituent codes. This is because the ST-PC system has a lower error floor than the ST-CC system. The analytical results presented here are very useful in observing the system behaviour at high SNRs where it is not practical to generate simulation results. At low SNRs, the simulation results indicate that both systems perform better using ST codes rather than RST codes. However, this is not true at high SNRs and the analytical bounds can be used to quickly observe the high SNR behaviour.

4.8 Summary

In this chapter an overview of concatenated convolutional codes was given and recent literature in the field of concatenated STTCs was reviewed. Two double concatenated architectures were proposed. The ST-PC system consisted of a PCCC outer code and a STTC inner code, while the ST-SC system consisted of a SCCC outer code and a STTC inner code. The system model for these two systems was presented and the encoding and decoding of each were discussed. The decoding of the constituent codes was explained where the additive bitwise SISO algorithm was used. The analysis of concatenated convolutional codes was explained and the necessity of the uniform interleaver was described. Using the notion of the uniform interleaver and the analytical model for STTCs proposed in chapter 3, an analytical model for the ST-CC and ST-PC systems was derived. The ST-CC system is a serial concatenation of a CC and a STTC.

Simulation results were presented for the cases of quasi-static and rapid Rayleigh fading, 130 bit and 1300 bit input frame sizes as well as recursive and non-recursive CCs and STTCs. At low to medium SNRs it was shown that RSC codes concatenated with non-recursive STTCs achieved the lowest FER for the proposed two systems. Interleaving gain, in terms of FER, was achieved for rapid fading channels but not for quasi-static fading channels.

The FER and BER performance of these two systems using the optimal encoder combinations was compared to the performance of the ST-CC. For quasi-static fading it was shown that the ST-CC and ST-PC systems achieved the lowest FER and BER for $N = 130$ and the ST-PC system achieved the lowest FER and BER for $N = 1300$. In the case of rapid fading for $N = 130$ the ST-PC system achieved the lowest FER and BER. For $N = 1300$ the ST-PC system resulted in the best performance at low to medium SNRs while the ST-SC gave the best performance at medium to high SNRs.

The proposed analysis was shown to accurately model the performance of the ST-CC and ST-PC systems at high SNRs. At low to medium SNRs, the bound was inaccurate but this is consistent with the behaviour of the union bound. Some computational difficul-

ties were experienced in generating simulation results at high SNRs and for this reason convergence of simulation and analytical results was not always observed. Furthermore it was computational intensive to generate a significant number of error events and in most cases significant divergence of the union bound was not seen.

In general it was shown that provided the constituent codes are chosen correctly, double concatenated STTCs have the potential to achieve lower FERs and BERs than simple concatenated STTCs in rapid fading channels but not in quasi-static fading channels.

Chapter 5

Turbo Coded Diversity for CDMA Systems

5.1 Introduction

In multiple access wireless communication systems such as cellular systems, many users share the same channel, possibly at the same time. In order to distinguish between users different multiple access techniques can be used.

Frequency division multiple access (FDMA) divides the available bandwidth into a number of frequency bands and assigns a single band to each user. All users transmit at the same time but only within their frequency band. The Advanced Mobile Phone System (AMPS) is based on FDMA. In a time division multiple access (TDMA) system each user is assigned an equal length time slot. Each user only transmits during this time slot but uses the full system bandwidth. A number of cellular communication systems are based on TDMA such as IS-54/IS-136 and Global System for Mobile Communication (GSM). In a code division multiple access system (CDMA) each user is assigned an orthogonal code. All users transmit at the same time using the full bandwidth of the system and are distinguished at the receiver by their orthogonal code. Systems based on CDMA include IS-95, Wideband CDMA and CDMA-2000. Of these 3 multiple access techniques, CDMA

has been chosen for 3rd generation wireless communication systems.

The increase in the demand for multi-media and internet services has placed a heavy burden on CDMA systems where very high data rates are now required. This chapter focuses on use of transmit antenna diversity to improve the performance of CDMA systems. The turbo transmit diversity direct-sequence/slow-frequency-hopped (DS/SFH) CDMA system from [82] is modified to include side information (SI) in the turbo decoder to improve system performance. Furthermore, a more realistic channel model is considered which introduces correlated Rayleigh fading and partial-band jamming. Possible applications of such a system include wireless LANs or mobile cellular systems.

Section 5.2 gives an overview of the various types of CDMA systems. Transmit antenna diversity, space-time transmit diversity and turbo decoding with SI is discussed in section 5.3. The DS/SFH CDMA system model using transmit antenna diversity and turbo coding is presented in section 5.4 where the transmitter, channel and receiver models are discussed in detail. The proposed modifications to the turbo decoder to utilise various types of SI are explained in section 5.5. Simulation results are presented in section 5.6 where the system performance is considered with various combinations of SI, with and without transmit antenna diversity, with different interleaver lengths and encoder memory, and in different fading channels.

5.2 CDMA systems

In this section, a basic overview of various CDMA systems is given and the advantages of hybrid DS/SFH CDMA are discussed.

A good overview of the main CDMA concepts and current CDMA cellular architectures is given in [83] and a tutorial describing the main CDMA concepts is given in [84]. In a CDMA system the transmission bandwidth B_t is much larger than the information bandwidth B_i. The processing gain G_p of a CDMA system is the ratio of B_t and B_i and is defined below.

$$G_p = \frac{B_t}{B_i} \qquad (5.1)$$

In general, a user's data is spread using a unique spreading or code sequence specific to that user and is often called a pseudo-noise (PN) sequence. The receiver knows the code sequences of all users and is able to extract the original information of the desired user using the code sequence specific to that user. CDMA systems have a number of advantages over FDMA and TDMA systems. These are: resistance to multipath fading; soft capacity limits where voice quality is traded for increased capacity; soft handoff; no frequency management between cells; takes advantage of voice inactivity; achieves higher capacity; privacy due to the spreading sequence; interference rejection; anti-jamming; low probability of interception due to low transmission power. On the other hand there are a few disadvantages such as the near-far effect and synchronisation to the PN sequences

There are many different types of CDMA systems as shown in Fig. 5.1. In direct-sequence CDMA (DS CDMA), the information bits are spread by a high rate code sequence. In frequency-hopping CDMA (FH CDMA), the carrier frequency at which the information signal is transmitted is changed according to a code sequence. In time-hopping CDMA (TH CDMA), the code sequence determines the burst times at which the information signal is transmitted. Hybrid CDMA systems combine 2 or more of the previously mentioned CDMA techniques in order to combine their advantages. Other hybrid CDMA systems combine CDMA techniques with other multiple access techniques such as TDMA and multi-carrier (MC) or multi-tone (MT) modulation. More detail on these different techniques including their advantages and disadvantages are discussed in [2, 83, 84].
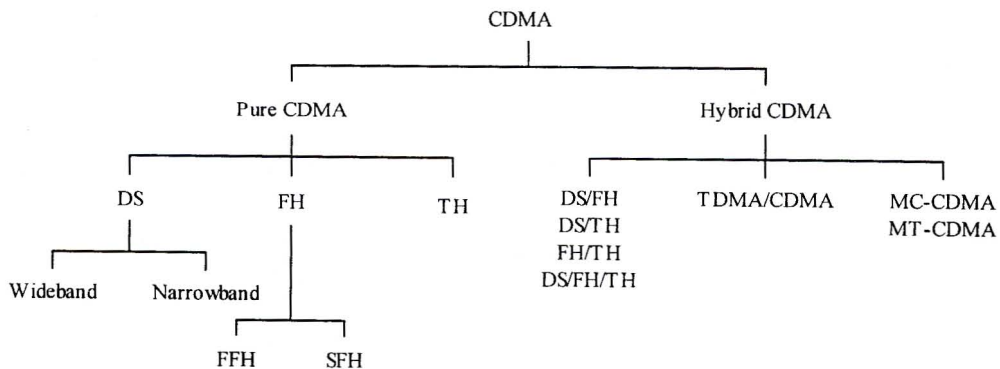
Figure 5.1: Classification of CDMA systems.

This chapter considers a hybrid DS/SFH CDMA system which has been considered by a

number of authors [85, 86, 87]. These systems have been shown to combine the advantages of both DS and FH systems. These being the anti-multipath interference and increased capacity of DS systems and the good immunity against partial-band-jamming and the absence of the near-far problem in FH systems.

5.3 Antenna diversity and coding for CDMA systems

This section discusses the use of coding and transmit antenna diversity to improve the performance of CDMA systems. Various transmit diversity and space-time transmit diversity techniques are discussed and the use of SI for turbo decoding is explained. Recent literature in the fields of space-time transmit diversity and side information is reviewed.

5.3.1 Transmit antenna diversity

Transmit antenna diversity can be used to improve the performance and spectral efficiency of CDMA systems and can be combined with the more traditional receive antenna diversity to achieve further gains in performance.

There are three main methods used to distinguish the signals transmitted simultaneously from multiple antennas. These are code division transmit diversity (CDTD), time division transmit diversity (TDTD) and CDTD, TDTD with pre-RAKE combining. A performance comparison of these transmit diversity techniques is presented in [88] for an IS-95 CDMA system using 2 transmit antennas.

With CDTD different orthogonal spreading codes are applied to each antenna (orthogonal-CDTD) or the same spreading code is applied to each antenna with an intentional delay (non-orthogonal-CDTD).

In TDTD only one antenna is allowed to transmit information at a time. A round-robin approach can be taken where the data is cycled over the antennas. Antenna selection is another approach to TDTD, which uses feedback from the receiver to determine the optimal antenna from which to transmit the information.

For CDTD, TDTD with pre-RAKE combining, each antenna convolves the transmitted signal with the complex conjugate of the channel gain. This method requires feedback to the transmitter.

5.3.2 Space-time transmit antenna diversity

As with space-time coding where system performance is improved by combining antenna diversity with channel coding, the performance of CDMA systems can also be improved by combining transmit antenna diversity with appropriate channel coding.

A basic ST coded CDMA system using transmit diversity combines FEC encoding with either CDTD or TDTD. This chapter will focus on CDTD schemes. In a CDTD scheme, the input data is FEC encoded, divided into n_T substreams, spread using orthogonal spreading codes and finally transmitted over the n_T transmit antennas. The received signal is a linear superposition of the n_T transmitted signals and the n_T substreams can be recovered by despreading this composite signal with the corresponding spreading code. These substreams are then decoded to obtain the original input data. A good comparison of CDTD and TDTD schemes using convolutional codes and turbo codes is given in [89].

Convolutional codes were combined with non-orthogonal CDTD in [90] in a DS CDMA system using BPSK modulation for an indoor wireless LAN. Both space and time diversity were achieved and it was shown that the proposed multi-antenna system with convolutional codes outperforms the same system using repetition codes and a conventional single antenna convolutionally coded system. In [91] a turbo transmit diversity scheme was proposed for a multiple satellite communication system. This scheme mapped the output of a turbo encoder to two transmit antennas using QPSK modulation. In [92] a DS CDMA turbo coded diversity system was considered which combined the turbo diversity scheme from [91] with the work in [90]. The output of a multiple turbo encoder was mapped to multiple transmit antennas where the signals on each antenna were distinguished using non-orthogonal CDTD. This work was extended in [82] to a DS/SFH CDMA system using orthogonal CDTD.

5.3.3   Turbo decoding with side information

The use of side information (SI) to improve the performance of turbo codes has been investigated in [93, 94, 95] for FH CDMA systems and in [96] for DS/SFH CDMA systems. It was shown that SI improves the decoding performance. Furthermore, employing SI only modifies the calculation of the branch transition probabilities and does not otherwise increase the complexity of the decoding algorithm.

In [93, 94] partial band interference SI was considered and the knowledge of the channel being jammed or unjammed was either available or unavailable to the turbo decoder. In [95] partial band interference and Rayleigh fading were considered. Turbo decoding considered 2 types of SI, knowledge that the transmitted bit was jammed or unjammed and knowledge of the Rayleigh fading amplitudes. In all cases it was shown the performance of the turbo decoder was improved by using SI. In [96] partial-band interference, multi-user interference and Rayleigh fading were considered. The performance of the decoder was considered with and without the knowledge of jamming, hitting and fading SI. In all cases the use of SI was shown to improve the system performance.

5.4   Turbo transmit diversity DS/SFH CDMA system model

In this section the system model for a DS/SFH CDMA system using transmit antenna diversity and turbo codes is presented. This system is based on the system proposed in [82] but here the channel model is extended to include partial-band jamming and correlated Rayleigh fading over time.

The DS/SFH CDMA system consists of K users transmitting asynchronously over a time correlated Rayleigh fading channel with partial band jamming and AWGN noise. The data stream of each user $k = \{1, \ldots, K\}$ is encoded using a rate $1/3$ turbo encoder [7, 8], DS/SFH spread, QPSK modulated and transmitted over the two antennas. Different spreading sequences are used on each antenna to distinguish the two signals. The antennas are assumed to be sufficiently separated to ensure spatially uncorrelated fading but

sufficiently close to ensure that the propagation delays for each antenna are the same. The received signal is despread, QPSK demodulated and fed to the turbo decoder which outputs an estimate of the original data stream of the desired user.

The following sections describe the transmitter, channel and receiver models used in this system.

5.4.1 Transmitter model

The transmitter model of user k is shown in Fig. 5.2. User k's binary data stream $u_k(t)$ of duration T_b is rate 1/3 turbo encoded to produce three output bit streams. The systematic output $x_k(t)$ is simply the original data stream while the non-systematic outputs $y_{1k}(t)$ and $y_{2k}(t)$ correspond to the encoded and interleaved encoded versions of $u_k(t)$ respectively. The turbo encoder has the same structure to that shown in Fig. 4.1.
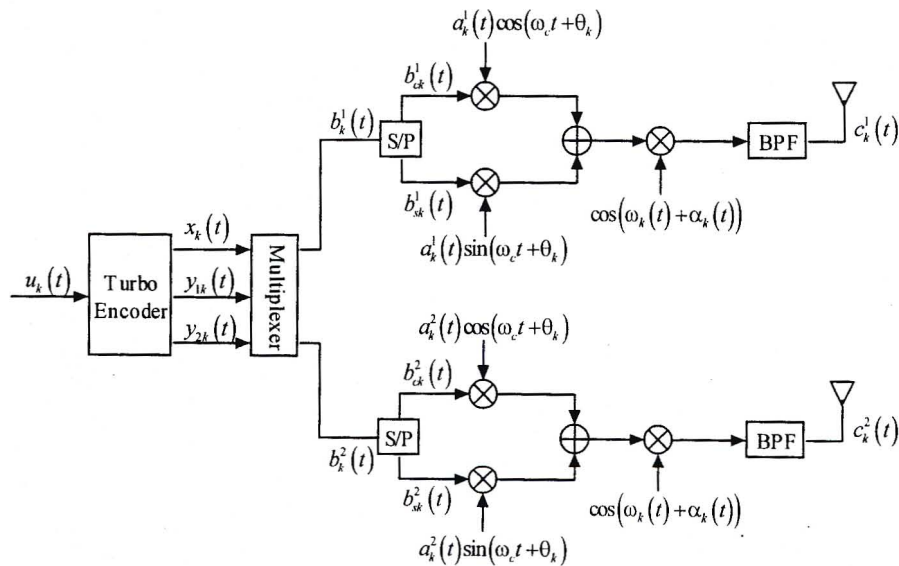
Figure 5.2: Transmitter block diagram.

After multiplexing and serial to parallel conversion the bit streams, of duration T_b, on the in-phase and quadrature branches of the QPSK modulator of antenna $l = \{1, 2\}$, $b^l_{ck}(t)$ and $b^l_{sk}(t)$ respectively, are expressed as follows.

$$b^1_{ck}(t) = b^2_{ck}(t) = \{x_k(1), x_k(2), x_k(3), x_k(4), \ldots\}$$

$$b_{sk}^2(t) \ = \ \{y_{1k}(1), y_{2k}(2), y_{1k}(3), y_{2k}(4), \ldots\}$$

$$b_{sk}^2(t) \ = \ \{y_{2k}(1), y_{1k}(2), y_{2k}(3), y_{1k}(4), \ldots\}$$

The non-systematic bit streams are transmitted alternatively on antenna 1 and 2 while the systematic bit stream is transmitted on both antennas.

The signals on the in-phase and quadrature branches of antenna l are multiplied by chipping sequence $a_k^l(t)$ of user k, antenna l. This sequence is periodical, has period N_c and chip duration T_c such that $T_b = N_c T_c$. Different chipping sequences are used on the two antennas so that these signals can be distinguished at the receiver. In general $b_{xk}^l(t)$ is given by (5.2) where $x = \{c, s\}$ and $a_k^l(t)$ by (5.3) where $P_{T_b}(t)$ and $P_{T_c}(t)$ are rectangular NRZ pulses of unit height and duration T_b and T_c respectively. Both $b_{xk}^l(i)$ and $a_k^l(i)$ belong to the set $\{-1, 1\}$.

$$b_{xk}^l(t) \ = \ \sum_i b_{xk}^l(i) P_{T_b}(t - iT_b) \tag{5.2}$$

$$a_k^l(t) \ = \ \sum_i a_k^l(i) P_{T_c}(t - iT_c) \tag{5.3}$$

The spread signal $a_k^l(t)b_{xk}^l(t)$ is QPSK modulated and frequency hopped by the pseudo-random hopping pattern $\omega_k(t)$ of user k. The hopping intervals are derived from a set of q available frequencies. After bandpass filtering, to remove unwanted frequency components, the transmitted signal of user k, antenna l can be expressed as follows.

$$
\begin{aligned}
c_k^l(t) \ = \ & \sqrt{P} \cdot a_k^l(t) \Big\{ b_{ck}^l(t) \cos\left[(\omega_k(t) + \omega_c)t + \alpha_k(t) + \theta_k\right] \\
& + b_{sk}^l(t) \sin\left[(\omega_k(t) + \omega_c)t + \alpha_k(t) + \theta_k\right] \Big\}
\end{aligned}
\tag{5.4}
$$

Here, θ_k is the random phase of user k, P is the total transmitted power which is equally divided between both antennas, ω_c is the carrier frequency and $\alpha_k(t)$ is the phase shift introduced by the frequency hopper which is assumed to remain constant during each hop.

5.4.2 Channel model

The link between the receiver and user k is characterised by a low-pass equivalent transfer function given by,

$$h_k(t) = \sum_{l=1}^{2} \beta_{kl} \delta(t - \tau_k) \exp(j\gamma_{kl}) \tag{5.5}$$

where kl refers to the transmission path of antenna l of user k, $j = \sqrt{-1}$ and $\delta(\cdot)$ is the delta dirac function. There are two antennas associated with user k, each assumed to have independent transmission paths. The l_{th} path of user k is characterised by three random variables; the path gain β_{kl}, the phase γ_{kl} and the delay τ_k. It is assumed that β_{kl} and τ_k are statistically independent for different values of k and l. The path gain β_{kl} is Rayleigh distributed with variance σ_r^2, γ_{kl} is uniformly distributed in $[0, 2\pi]$ and τ_k is uniformly distributed in $[0, T_b]$.

Correlated Rayleigh random variates over time are generated using the Filtered White Gaussian Noise (WGN) method described in [97]. In this method two independent zero-mean WGN processes are filtered and added in quadrature. The real and imaginary parts of the time samples of the complex Gaussian process have an autocorrelation sequence.

$$R[d] = J_0(2\pi f_m |d|) \tag{5.6}$$

Here f_m is the maximum Doppler frequency normalised by the sampling rate and d is the separation between samples.

The channel introduces AWGN with two-sided power spectral density $N_0/2$. It is assumed that there exists a partial band jammer [93] that will evenly distribute its power over a fraction ρ of the total bandwidth. The partial band interference is modeled as a Gaussian random process and has two-sided power spectral density $N_j/2\rho$. There are two channel states for user k, jammed and unjammed, denoted by $J_k(t) = 1$ and $J_k(t) = 0$ respectively where the channel state is assumed to remain constant over the entire hop duration. The probability of hopping into a jammed state is ρ and into an unjammed state $1 - \rho$.

5.4.3 Receiver model

The signal arriving at the receiver is a linear superposition of the transmitted signals. The coherent receiver consists of a frequency dehopper, two QPSK demodulators, a demultiplexer and a rate 1/3 turbo decoder as shown in Fig. 5.3.

The received signal $r(t)$ is given by (5.7) below where $n(t)$ is AWGN with two-sided power
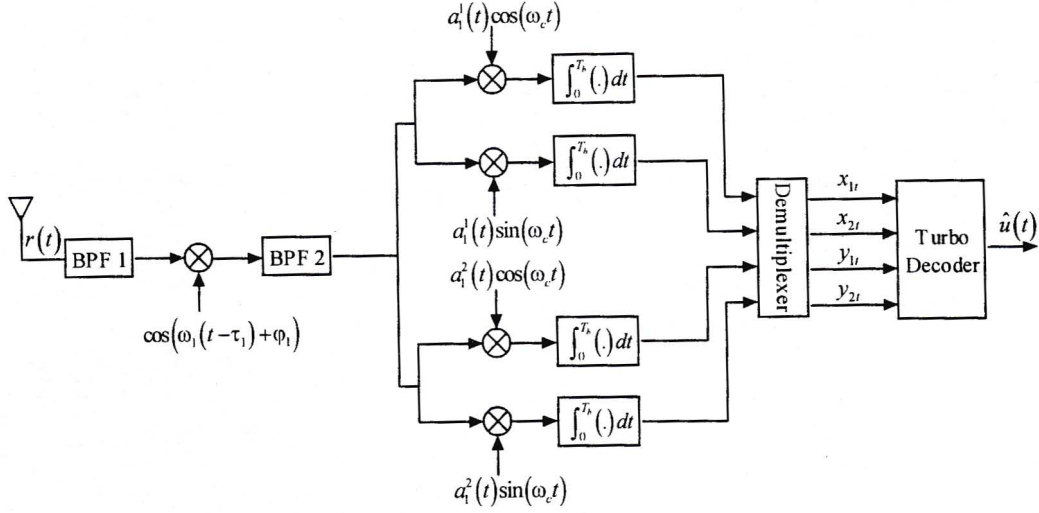
Figure 5.3: Receiver block diagram.

spectral density $N_0/2 + J_k(t)N_j/2\rho$.

$$r(t) = \sqrt{P} \sum_{k=1}^{K} \sum_{l=1}^{2} \beta_{kl} a_k^l(t - \tau_k) \Big\{ b_{ck}^l(t - \tau_k) \cos \left[(\omega_k(t - \tau_k) + \omega_c)t + \phi_{kl} \right] \qquad (5.7)$$
$$+ b_{sk}^l(t - \tau_k) \sin \left[(\omega_k(t - \tau_k) + \omega_c)t + \phi_{kl} \right] \Big\} + n(t)$$

The phase ϕ_{kl} is expressed as follows.

$$\phi_{kl} = \theta_k + \alpha_k(t - \tau_k) - [\omega_k(t - \tau_k) + \omega_c]\tau_k + \gamma_{kl} \qquad (5.8)$$

The calculation of the decision statistic from the received signal is well explained in [82, 85, 86] and only the details are presented here.

The frequency dehopper has an identical structure to that described in [86] and consists of two bandpass filters and a mixer. The first bandpass filter removes out-of-band thermal noise, the mixer performs appropriate frequency translation and the second bandpass filter removes the high frequency terms. It is assumed that the hopping pattern of the receiver is synchronised to that of user 1 and that the dehopper introduces a phase shift φ_1 which is assumed to be constant over the hopping interval. The output of the frequency dehopper $r_d(t)$ for user 1 is expressed as follows.

$$r_d(t) = \sqrt{P/4} \sum_{k=1}^{K} \sum_{l=1}^{2} \beta_{kl} a_k^l(t - \tau_k) \delta \left(\omega_1(t - \tau_1), \omega_k(t - \tau_k) \right) \Big\{ \qquad (5.9)$$
$$b_{ck}^l(t - \tau_k) \cos(\omega_c t + \Psi_{kl}) + b_{sk}^l(t - \tau_k) \sin(\omega_c t + \Psi_{kl}) \Big\} + n_d(t)$$

The phase term $\Psi_{kl} = \phi_{kl} + \varphi_1$ and $n_d(t)$ is AWGN with two-sided power spectral density $N_0/8 + J_k(t)N_j/8\rho$. The Kroneker function $\delta(\cdot, \cdot)$ is defined as $\delta(u, v) = 1$ for $u = v$ and $\delta(u, v) = 0$ for $u \neq v$ where u and v are both real valued. Thus the dehopper suppresses any signals at time t whose frequencies differ from $\omega_1(t - \tau_1)$. In this system the signals transmitted from both antennas of any of the non-reference users using a different hopping interval to the reference user are suppressed.

The impulse responses of the in-phase and quadrature branches of QPSK demodulator l of user 1 are matched to a T_b sec. time segment of $a_1^l(t)\cos(\omega_c t)$ and $a_1^l(t)\sin(\omega_c t)$ respectively. Consider the output of the in-phase integrator of user 1, antenna 1 and assume perfect synchronisation. Considering bit λ, the output of the in-phase integrator z_c^1 can be expressed as follows.

$$
\begin{aligned}
z_c^1 = {} & \sqrt{P/16} \sum_{k=1}^{K} \sum_{l=1}^{2} \beta_{kl} \Big\{ \\
& cos(\Psi_{kl}) \int_{\lambda T_b}^{(\lambda+1)T_b} a_1^1(t) a_k^l(t - \tau_k) b_{ck}^l(t - \tau_k) \delta\left(\omega_1(t), \omega_k(t - \tau_k)\right) dt \\
& + sin(\Psi_{kl}) \int_{\lambda T_b}^{(\lambda+1)T_b} a_1^1(t) a_k^l(t - \tau_k) b_{sk}^l(t - \tau_k) \delta\left(\omega_1(t), \omega_k(t - \tau_k)\right) dt \Big\} + n_c^1
\end{aligned}
\tag{5.10}
$$

Here n_c^1 is a zero-mean Gaussian random variable with variance $N_0/16 + J_k(t)N_j/16\rho$. In order to simplify the integration, the integral over T_b is split into 2 parts to account for hitting of the current bit λ of the reference user with the previous and current bits of the non-reference users. Because of the periodicity of the spreading code, the dependence of the integral on λ can be dropped and (5.10) can be re-written as follows.

$$
\begin{aligned}
z_c^1 = {} & \sqrt{P/16} \sum_{k=1}^{K} \sum_{l=1}^{2} \beta_{kl} \Big\{ \\
& cos(\Psi_{kl}) \left[d_1(b_{ck}^l(\lambda - 1)) b_{ck}^l(\lambda - 1) R_{kl}(\tau_k) + d_2(b_{ck}^l(\lambda)) b_{ck}^l(\lambda) \hat{R}_{kl}(\tau_k) \right] \\
& + sin(\Psi_{kl}) \left[d_1(b_{sk}^l(\lambda - 1)) b_{sk}^l(\lambda - 1) R_{kl}(\tau_k) + d_2(b_{sk}^l(\lambda)) b_{sk}^l(\lambda) \hat{R}_{kl}(\tau_k) \right] \Big\} + n_c^1
\end{aligned}
\tag{5.11}
$$

The functions $d_1(\cdot)$ and $d_2(\cdot)$ belong to the set $\{0, 1\}$ and account hitting between the reference and non-reference users. The correlation of the spreading sequences is expressed by the functions $R_{kl}(\tau_k)$ and $\hat{R}_{kl}(\tau_k)$ which are given below.

$$
R_{kl}(\tau_k) = \int_0^{\tau_k} a_1^1(t) a_k^l(t - \tau_k) dt
\tag{5.12}
$$

$$
\hat{R}_{kl}(\tau_k) = \int_{\tau_k}^{T_b} a_1^1(t) a_k^l(t - \tau_k) dt
\tag{5.13}
$$

The demodulated signals from each demodulator branch are demultiplexed and fed to the turbo decoder which outputs an estimate of the original information bit stream after a number of decoding iterations. The turbo decoder is similar to that shown in Fig. 4.2 and the decoding proceeds in a similar way to that described in section 4.2.

5.5   Turbo decoder with side information

The performance of the turbo decoder can be improved if side information other than the noise variance is available. The introduction of side information modifies only the transition probabilities of the channel and does not affect the complexity of the turbo decoding algorithm.

This section describes the proposed modification of the turbo transmit diversity DS/SFH system to incorporate jamming, hitting and fading SI into the turbo decoder. These modifications are based on the work described in [96] for a single antenna DS/SFH CDMA system.

5.5.1   The original turbo decoder

In this system the modified MAP decoding algorithm described in [91] is used. The calculation of the branch transition probabilities given below need to be modified to take into account the different forms of side information.

$$p(\underline{R}_t | d_t = i, S_t = m) \tag{5.14}$$

$$p(\underline{R}_{t+1} | d_{t+1} = i, S_{t+1} = S_f^i(m)) \tag{5.15}$$

Here $d_t = \{0, 1\}$ is the decoded bit, S_t is the encoder state, $S_f^i(m)$ is the state one would arrive at if one goes forward in time from state S_m on branch $d_t = i$ and $\underline{R}_t$ is the demodulator output at time t. The modification of (5.14) and (5.15) is very similar.

Consider the modification of (5.14) for the first component decoder of user 1 where the demodulator output $\underline{R}_t = (x_{1t}, x_{2t}, y_{1t})$ is used. Now (5.14) can be expanded as shown

below where the dependence of x_{1t} and x_{2t} on the current state can be dropped as these are the systematic bits and therefore independent of the encoder state.

$$p(\underline{R}_t|d_t, S_t) = p(x_{1t}|d_t)p(x_{2t}|d_t)p(y_{1t}|d_t, S_t) \tag{5.16}$$

The following section describes the calculation of these probabilities using the three forms of SI.

5.5.2 Modifications to the turbo decoder

This section describes the calculation of $p(x_{1t}|d_t)$ which is similar to the calculation of the other probabilities in (5.16).

The channel used in this chapter is assumed to be memoryless i.e. one bit per hop. The SI is either perfect (PSI), estimated (ESI) using the system parameters or not available (NSI). Three forms of side information are considered. Jamming SI reveals which bits have been jammed, hitting SI reveals the number of non-reference users using the same frequency bin as the reference user and fading SI gives the instantaneous Rayleigh fading amplitude $\beta_{kl}(t)$ of each bit.

Now consider the calculation of $p(x_{1t}|d_t)$ which for simplification purposes will be expressed as $p(x_t|d_t)$. For demodulated symbol x_t, let β_t denote the Rayleigh fading amplitude, J_t denote the channel state where the channel is jammed if $J_t = 1$ and unjammed if $J_t = 0$ and H_t denote the number of non-reference users hitting the reference user. In the PSI case the probabilities are evaluated directly, while in the ESI case the probabilities are calculated using the law of total probability and in the NSI case the side information is not considered at all.

The probability of the demodulated symbol x_t conditioned on the side information and d_t is expressed below.

$$p(x_t|J_t, H_t, \beta_t, d_t) \doteq \frac{1}{\sqrt{2\pi\sigma_0^2}} \exp\left(\frac{-[x_t - \beta_t(2d_t - 1)]^2}{2\sigma_0^2}\right) \tag{5.17}$$

$$\sigma_0^2 = \frac{T_b}{16}\left\{N_0 + J_t\frac{N_j}{\rho} + \frac{2PT_b\sigma_r^2}{3N_c}(H_t n_T + n_T - 1)\right\} \tag{5.18}$$

The partial band, multi-user and self interference as well as the AWGN are combined into a single Gaussian random variable with zero-mean and variance σ_0^2. The first term of (5.18) is the variance of the AWGN, the second the variance of the partial-band interference and the last the variance of the multi-user and self interference.

The probability distributions of the jamming, hitting and fading side information are given below.

$$p(J_t = j) = \begin{cases} 1 - \rho & \text{if } j = 0 \\ \rho & \text{if } j = 1 \end{cases} \tag{5.19}$$

$$p(H_t = h) = \binom{K-1}{h} (1/q)^h (1 - 1/q)^{K-1-h} \tag{5.20}$$

$$p(\beta_t = r) = \frac{r}{\sigma_r^2} \exp\left(-\frac{r^2}{2\sigma_r^2}\right) \tag{5.21}$$

Various combinations of jamming, hitting and fading SI are now considered to be perfect, estimated or not available.

Jamming PSI, Hitting PSI, Fading PSI

For the first case the knowledge of all forms of side information are available to the decoder and no estimation is required. The branch transition probabilities are calculated by substituting (5.17) to (5.21) into (5.22) below.

$$p(x_t, J_t, H_t, \beta_t | d_t) = p(J_t)p(H_t)p(\beta_t)p(x_t | J_t, H_t, \beta_t, d_t) \tag{5.22}$$

Jamming ESI, Hitting PSI, Fading PSI

In this case the knowledge of jamming SI is unavailable to the decoder and is thus estimated.

$$p(x_t, H_t, \beta_t | d_t) = p(H_t)p(\beta_t) \sum_{j=0}^{1} p(x_t | J_t = j, H_t, \beta_t, d_t)p(J_t = j) \tag{5.23}$$

Jamming PSI, Hitting ESI, Fading PSI

Here the knowledge of the hitting SI is unavailable to the decoder and is estimated as follows.

$$p(x_t, J_t, \beta_t | d_t) = p(J_t)p(\beta_t) \sum_{h=0}^{K-1} p(x_t | J_t, H_t = h, \beta_t, d_t)p(H_t = h) \qquad (5.24)$$

Jamming ESI, Hitting ESI, Fading PSI

In the last case the knowledge of jamming and hitting SI is not available to the decoder and both these forms of SI must be estimated.

$$p(x_t, \beta_t | d_t) = p(\beta_t) \sum_{h=0}^{K-1} \sum_{j=0}^{1} p(x_t | J_t = j, H_t = h, \beta_t, d_t)p(J_t = j)p(H_t = h) \qquad (5.25)$$

NSI cases

In order to observe the system performance with no jamming or no hitting SI, the corresponding term in (5.18) is removed and the corresponding probability $p(J_t)$ or $p(H_t)$ in (5.22) to (5.25) is set to 1. For the case of no fading SI the β_t term in (5.17) and $p(\beta_t)$ in (5.22) to (5.25) are set 1.

5.6 Simulation results

This section presents the simulation results for the proposed turbo transmit diversity DS/SFH CDMA system with side information. The effects of various combinations of side information (SI) are considered. The system performance with and without diversity is presented for the uncoded and coded cases. The effect of increasing the interleaver length and encoder memory is investigated. System performance in an AWGN, uncorrelated Rayleigh fading channel and time correlated Rayleigh fading channel is also considered.

The simulation results are generated using Monte-Carlo methods where (5.11) is evaluated for each branch of the demodulator. These outputs are then turbo decoded and the number

of bit and frame errors are recorded.

For all simulation results, the BER or FER is plotted against SNR per bit. In all cases, unless stated otherwise, the following parameters are used. The number of users K is 10. The number of transmit antennas n_T is 2 and receive antennas is 1. The number of frequency bins q is 3 and the number of data bits per hop is 1. The signal to jamming ratio (SJR) is 5dB where the fraction of the total bandwidth jammed ρ is 0.3. The length of the spreading sequence of each user is 31 where Gold codes [98, Chap. 8] are generated using the octal polynomials (45,75). The correlated Rayleigh random variables are generated using a carrier frequency of 1 GHz, a FIR filter length of 33, a mobile velocity of 10 m.s^{-1}. This corresponds to a normalised Doppler frequency of 0.002. The rate 1/3 turbo encoder uses rate 1/2, recursive systematic convolutional encoders using the (7,5) octal generator polynomials and a pseudo-random interleaver of length $N = 100$. The 1st encoder is terminated and the 2nd is left un-terminated. The number of decoding iterations is 5 and perfect SI for jamming, hitting and fading is assumed i.e. the (pJ,pH,pF) case.

In Fig. 5.4 the BER performance of the coded system with various combinations of SI is considered. The jamming (J), hitting (H) or fading (F) SI is either perfect (p), estimated (e) or not available (n). The jamming and hitting SI are estimated using equations 5.17 to 5.25.

The (nJ,nH,nF) case, where no SI except the variance of the AWGN is available to the decoder, results in the worst performance. By including fading SI the system performance is improved. Hitting SI only improves the system performance at higher SNRs when the multiple-access interference is more dominant than the AWGN. For both the cases of no hitting SI, a performance degradation from 10 dB is observed. At lower SNRs, hitting SI does not improve system performance because the multi-access interference is negligible compared with the AWGN. Jamming SI gives a larger performance gain than hitting SI. This gain however is inversely proportional to the SJR whereby a higher SJR would cause the performance gain due to jamming SI to diminish. Perfect and estimated hitting SI result in a similar performance gain which indicates that the estimate of the multi-access interference is fairly accurate. Perfect jamming SI results in lower BERs than estimated
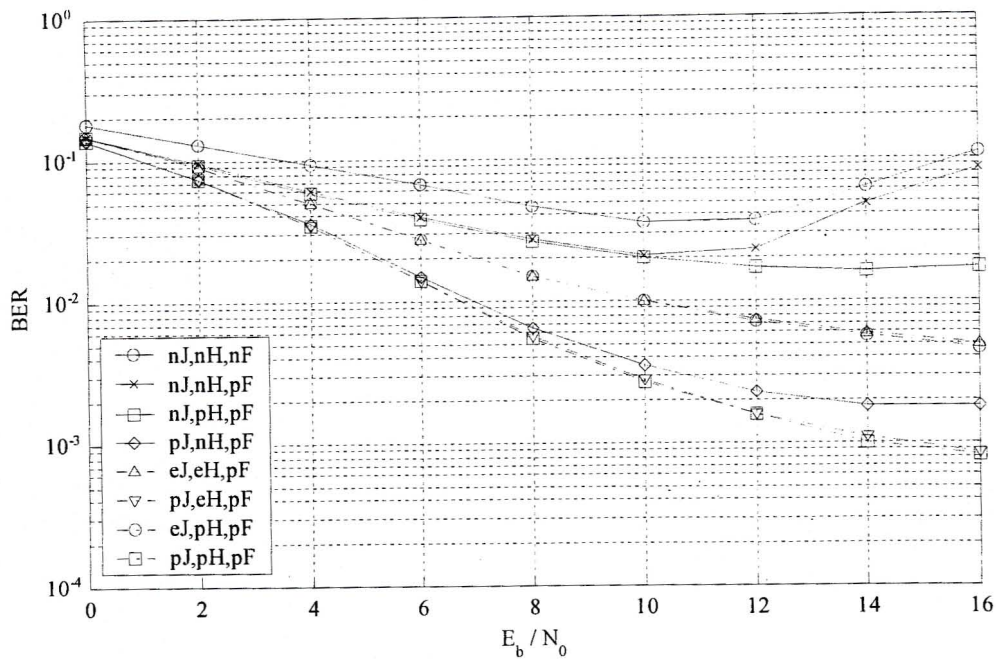
Figure 5.4: Effect of jamming, hitting and fading SI.

jamming SI. The lowest BER is achieved by using perfect SI i.e. the (pJ,pH,pF) case. Note that the (pJ,pH,pF) system has a performance gain of 5 dB over the (nJ,nH,nF) system at a BER of 2×10^{-2}.

The uncoded and coded system performance with diversity ($n_T = 2$) and without diversity ($n_T = 1$) is presented in Fig. 5.5 for the BER and in Fig. 5.6 for the FER. When no diversity or coding is employed, the data bits are transmitted using BPSK modulation. For the uncoded system with diversity, the input data is duplicated, transmitted over both antennas using BPSK modulation and combined at the receiver using maximal ratio combining. The coded system without diversity uses a rate 1/2 punctured turbo encoder where the systematic bits are transmitted on' the in-phase and the parity bits on the quadrature branches of the QPSK modulator. The total transmitted power P for all the systems with and without diversity is the same. For both the coded and uncoded systems, it is clear that employing transmit diversity improves the BER and FER performance where larger performance gains are achieved for the coded cases.

The effect of interleaver size N and constituent encoder memory m of turbo encoder is
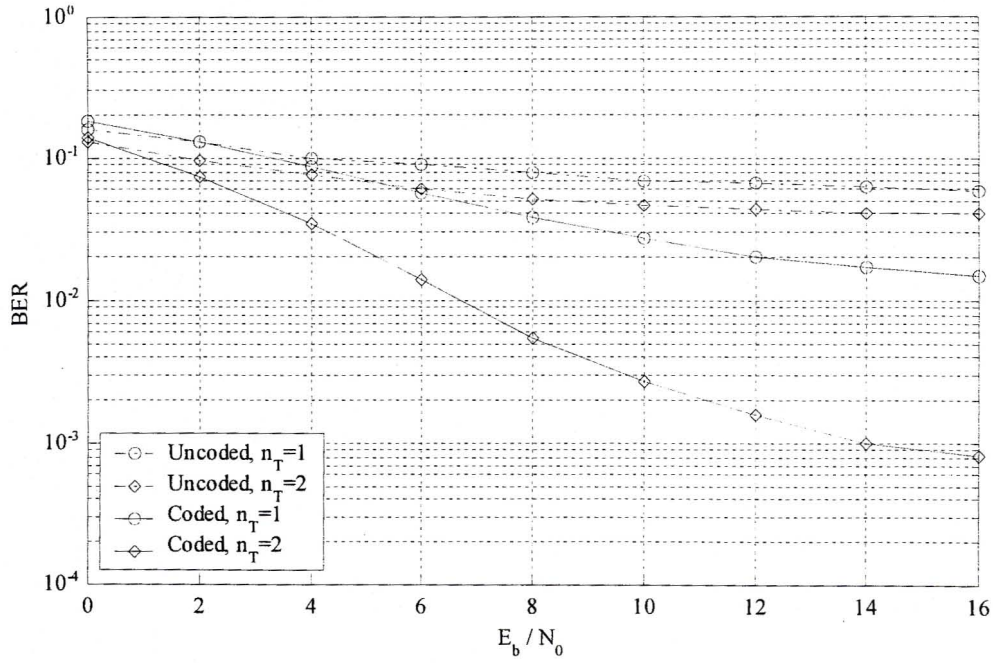
Figure 5.5: BER performance with and without diversity.
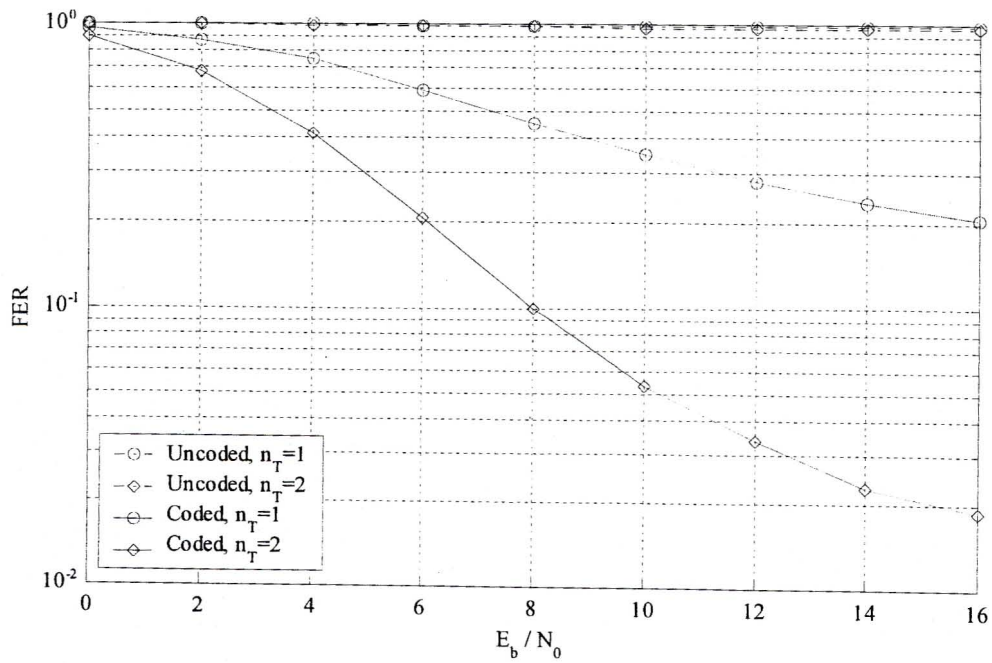
Figure 5.6: FER performance with and without diversity.
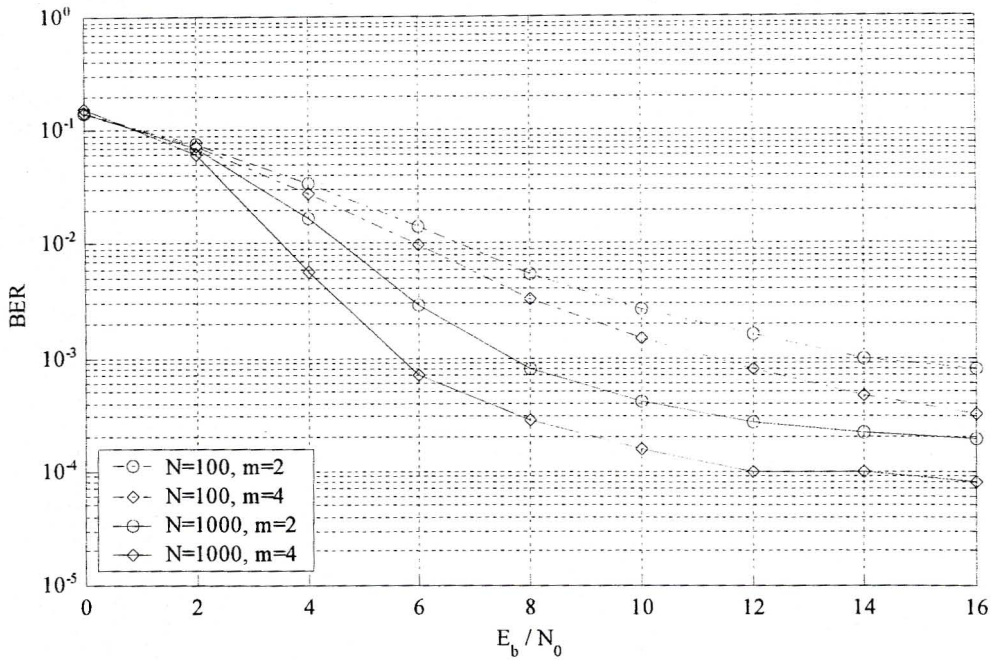
Figure 5.7: Comparison of turbo encoder parameters.

considered in Fig. 5.7. For the encoder with $m = 4$ the octal polynomials (37,21) are used. Increasing the interleaver size from $N = 100$ to $N = 1000$, improves the system performance for both $m = 2$ and $m = 4$. Performance gain is also achieved by increasing the encoder memory for both interleaver sizes.

In Fig. 5.8 the system performance in AWGN, uncorrelated Rayleigh fading and time correlated Rayleigh fading is presented for the coded and uncoded systems. In all cases partial-band jamming and AWGN are still present. When no coding is employed, the system performance in an uncorrelated and a correlated fading channel is identical but inferior to system performance in an AWGN channel. When coding is employed, the BER is highest in a correlated fading channel due to the longer fades resulting in burst errors. Performance improves in an uncorrelated Rayleigh fading channel and improves further in an AWGN channel.

In all the results presented in this section a flattening of the BER performance curve is observed from about 10 dB. This is largely due to the multi-user and self interference becoming more significant than the AWGN.
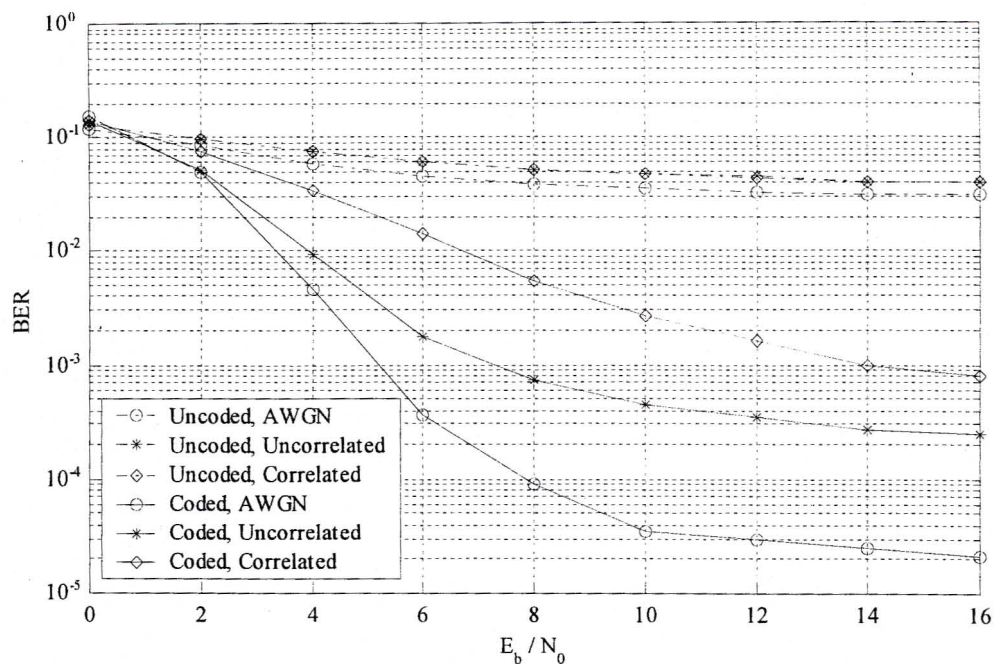
Figure 5.8: System performance in different channels.

5.7   Summary

In this chapter the performance of a DS/SFH CDMA system employing transmit antenna diversity and turbo coding with side information (SI) was investigated. An overview of multiple access techniques and CDMA systems was given. Various areas of research aiming to improve the performance of CDMA systems such as transmit antenna diversity, space-time antenna diversity and turbo coding with side information were discussed. The system model was presented and modifications to the turbo decoder to take advantage of jamming, hitting and fading SI were described.

Simulation results were presented to investigate the performance of the system. Results showed that jamming, hitting and fading SI improved the system performance where jamming SI gave the largest performance gain. Estimated and perfect hitting SI gave similar performance gains while perfect jamming SI resulted in larger performance gains than estimated jamming SI. The diversity system outperformed the equivalent system without diversity for the coded and uncoded cases although performance gains were more

evident in the coded cases. The performance of the turbo decoder was improved by increasing the interleaver size and encoder memory. It was shown that correlation in time degraded system performance.

Chapter 6

Conclusions

This dissertation focused on the use of coded transmit antenna diversity to improve the performance and capacity of single user and multiple user wireless communication systems without sacrificing system power or bandwidth. The results presented in chapters 2 through 5, were generated using custom built software simulation environments.

Chapter 1 described the necessity for and requirements of 3G cellular systems. Some current cellular proposals were discussed where CDMA had received the strongest support from industry. It was established that the ability of future wireless systems to deliver high quality, high data rate, power and bandwidth efficient services is integral to their future progress and development. A basic communication system was described and various methods to improve system performance, such as error correcting codes, modulation and diversity, were discussed. Antenna diversity can improve system reliability without sacrificing system power or bandwidth. Transmit diversity was shown to be a viable solution for improving the performance and capacity of systems where receive diversity is not effective such as the downlink in cellular systems. Furthermore transmit diversity can increase the capacity and performance of receive diversity systems. Space-time trellis codes, which merge channel coding with antenna diversity, were discussed and some current research issues were highlighted. Motivation for the research done and original contributions of this dissertation were presented.

Chapter 2 was a literature survey on MEA systems employing error control coding. A generalised system model was described. Theoretical results for channel capacity and FER were presented and it was shown that receive diversity alone cannot achieve the high capacities possible by MEA systems. Thus transmit diversity as well as receive diversity is essential in achieving high system capacities. An overview of existing MEA architectures using error control coding was given and it was discussed that STTCs give the best tradeoff between complexity and performance. Recent work in the field of STTCs was reviewed which included analytical techniques and the use of concatenated coding to improve the performance of STTCs. The STTC system architecture was described in detail and performance results for various codes were presented in quasi-static and rapid Rayleigh fading channels. These simulation results were compared to theoretical results which indicated that STTCs achieve maximum diversity gain but not maximum coding gain. These results demonstrated the need for concatenated STTCs to improve the coding gain of STTCs.

In chapter 3 a novel mathematical analysis for STTCs in quasi-static and rapid Rayleigh fading channels was proposed. Current analytical methods for STTCs were reviewed, but these did not sufficiently explain how the error events of a STTC were enumerated. The original Chernoff bound and a new bound on the PWEP of a particular codeword were discussed. The application of the union bound to the analysis of coded systems was described and it was discussed that the complexity of the analysis could be greatly reduced if error events were used. The state transition matrix method was modified to enumerate error events described by many parameters. The classification of the error events of a STTC in terms of parameters and calculation of the FER and BER from these enumerated error events was explained. The analytical results were compared with simulation results where the new bound on the PWEP was shown to be tighter than the Chernoff bound. In rapid fading channels the union bound agreed well with simulation results at high SNRs, but diverged at low SNRs. In quasi-static fading channels the union bound was very loose and the numerical bound was used which was shown to be accurate even at low SNRs.

Concatenated STTCs were considered in chapter 4 to improve the coding gain of STTCs.

Concatenated convolutional codes were discussed and recent literature on concatenated STTCs was presented. Two novel double concatenated STTC structures were proposed. A turbo code was serially concatenated with a STTC and a SCCC was concatenated with a STTC. An analysis for concatenated and double concatenated STTCs was derived by combining analytical methods for concatenated convolutional codes with the analysis proposed for STTCs in chapter 3. Simulation results showed that double concatenated STTCs outperform simple concatenated STTCs in rapid fading channels provided the correct constituent encoders are chosen. Marginal performance gains were observed in quasi-static fading channels. The proposed analytical model was shown to agree with simulation results at high SNRs, but not at low SNRs which is consistent with the behaviour of the union bound.

In chapter 5, a turbo transmit antenna diversity DS/SFH CDMA system was modified to incorporate side information (SI) in the turbo decoder to improve the system performance. The channel model was modified to include time correlated Rayleigh fading and partial-band jamming. Space-time transmit antenna diversity and turbo decoding with side information were briefly discussed. The system model and the modification of the turbo decoder to utilise jamming, hitting and fading SI were described. System performance was investigated, where it was shown that perfect and estimated jamming, hitting and fading SI improves system performance. Transmit antenna diversity was shown to give superior performance to the single antenna case for both the coded and uncoded systems.

Appendix A

List of acronyms

2G	Second Generation
3G	Third Generation
AMPS	Advanced Mobile Phone System
ARQ	Automatic Repeat Request
AWGN	Additive White Gaussian Noise
BER	Bit Error Rate
BLAST	Bell Laboratories Layered Space Time
bps	Bits Per Second
CC	Convolutional Code
CCDF	Complementary Cumulative Distribution Function
CDCM	Codeword Difference Covariance Matrix
CDMA	Code Division Multiple Access
CDTD	Code Division Transmit Diversity
CSI	Channel State Information
D-BLAST	Diagonally Layered BLAST
V-BLAST	Verticle BLAST
DPCCC	Double Parallel Concatenated Convolutional Code
DS	Direct Sequence
DSCCC	Double Serially Concatenated Convolutional Code

ESI	Estimated Side Information
ETSI	European Telecommunications Standards Institute
FDMA	Frequency Division Multiple Access
FEC	Forward Error Correction
FER	Frame Error Rate
FH	Frequency Hopped
GSM	Global System for Mobile Communication
HCCC	Hybrid Concatenated Convolutional Code
IMT-2000	International Mobile Telecommunications for the 21st century
IS-95	Interim Standard 95
ITU	International Telecommunications Union
MAP	Maximum a posteriori
MC	Multi-carrier
MEA	Multi-element Array
ML	Maximum-likelihood
MT	Multi-tone
NRC	Non-recursive Convolutional
NSI	No Side Information
PCCC	Parallel Concatenated Convolutional Code
PN	Pseudo-Noise
PSI	Perfect Side Information
PWEP	Pairwise Error Probability
RS	Reed-Solomon
RSC	Recursive Systematic Convolutional
SCCC	Serially Concatenated Convolutional Code
SFH	Slow Frequency Hopped
SI	Side Information
SISO	Soft-input Soft-output
SJR	Signal to Jamming Ratio
SNR	Signal to Noise Ratio
SOVA	Soft Output Viterbi Algorithm

ST	Space-time
STBC	Space-time Block Code
STC	Space-time Code
STTC	Space-time Trellis Code
TCM	Trellis Coded Modulation
TDMA	Time Division Multiple Access
TDTD	Time Division Transmit Diversity
TH	Time Hopping
UMTS	Universal Mobile Telecommunications System
UTRA	UMTS Terrestrial Radio Access
UTRA TDD	UTRA Time Division Duplex
WCDMA	Wideband Code Division Multiple Access

Appendix B

List of symbols

This appendix lists the more common symbols which are used throughout the dissertation.

$a_k^l(t)$	Spreading code for user k, antenna l
C	Channel capacity (bps/Hz)
c_{sf}^i	Transmitted symbol from antenna i for state s to state f transition
$\underline{c}_{sf}$	Vector of transmitted symbols for state s to state f transition
$\underline{c}_t$	Vector of transmitted symbols at time t
$c_k^l(t)$	Transmitted signal of user k from antenna l
c_t^i	Transmitted symbol from antenna i at time t
$\mathbf{c_0}$	All-zero codeword
$\mathbf{c}$	Valid correct transmitted codeword
$\mathbf{e}$	Valid incorrect decoded codeword
E_s	Energy of signal transmitted from antenna i
k	Number of encoder input bits for each time instance
K	Number of users
K_c	Constraint length of code
L	Input frame length in symbols
M	Constellation size (M-PSK)
m	Encoder memory

N	Input frame size in bits
n	Number of encoder output bits for each time instance
$n(i,\underline{d})$	Error event multiplicity
n_{TR}	Number of transmit and receive antennas ($n = n_T = n_R$)
$N_0/2$	Two-sided noise power spectral density
N_c	Length of spreading code
$N_j/2\rho$	Two-sided power spectral density of partial band jammer
n_R	Number of receive antennas
n_s	Number of encoder states
n_T	Number of transmit antennas
P	Total transmitted power in CDMA system
$P(\boldsymbol{c} \to \boldsymbol{e})$	PWEP of transmitting $\boldsymbol{c}$ and incorrectly decoding $\boldsymbol{e}$
P_b	Bit error rate
P_f	Frame error rate
q	Number of hopping intervals
R	Transmission rate (bps/Hz)
R_c	Code rate
r_t^j	Received signal at antenna j at time t
T_b	Bit duration of uncoded data stream
T_c	Chip duration
$u_k(t)$	Uncoded data stream of user k
$\alpha_k(t)$	Phase shift introduced by frequency hopper
α_t^{ij}	Path gain from transmit antenna i to receive antenna j at time t
$\boldsymbol{\alpha}$	Channel matrix for entire frame
$\boldsymbol{\alpha}_t$	Matrix of channel gains at time t
β_{kl}	Path gain for antenna l of user k
η_t^j	AWGN at receive antenna j at time t
γ_{kl}	Phase for antenna l of user k
θ_k	Random phase of user k
ρ	Fraction of total bandwidth occupied by partial band jammer
σ_r	Variance per dimension of α_t^{ij}

τ_k	Delay of user k
φ_1	Phase introduced by frequency dehopper
ω_c	Carrier frequency
$\omega_k(t)$	Hopping sequence of user k

Appendix C

Constituent codes

C.1 Space-time trellis codes

In this section the trellis diagrams for the constituent STTCs used in this dissertation are given. For all codes the number of input bits $k = 2$, the constellation size $M = 4$ and the number of transmit antennas $n_T = 2$. The general structure of such an encoder as well as the 4-PSK constellation used is given below in Fig. C.1.
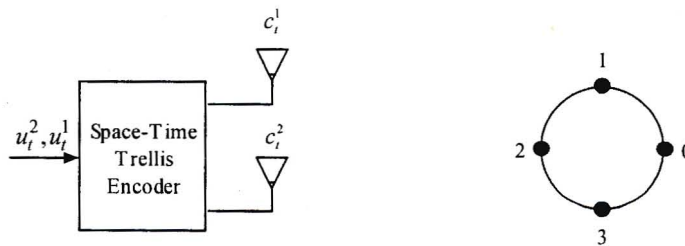
Figure C.1: General encoder structure with $k = 2$, $n_T = 2$ and $M = 4$.

In the following trellis diagrams, the encoder states are numbered along the right hand side of the trellis. The input output relationships $u_t^2 u_t^1 / c_t^1 c_t^2$ are given in the matrix to the left of the trellis where the transitions in the trellis diagram from top to bottom correspond to the matrix entries from left to right.

00/00 01/01 10/02 11/03

00/10 01/11 10/12 11/13

$u_t^2 u_t^1 / c_t^1 c_t^2$

00/20 01/21 10/22 11/23

00/30 01/31 10/32 11/33

0

1

State

2

3
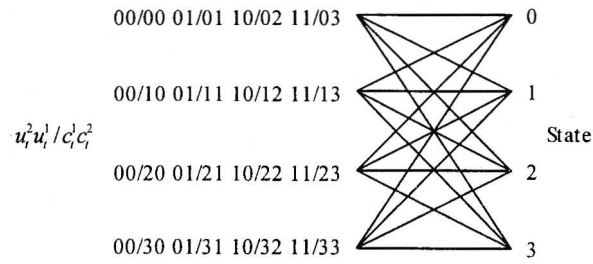
Figure C.2: Tarokh 4-state: $k = 2$, $m = 2$, $n_t = 2$, $M = 4$.

00/00 01/01 10/02 11/03

00/10 01/11 10/12 11/13

00/20 01/21 10/22 11/23

00/30 01/31 10/32 11/33

$u_t^2 u_t^1 / c_t^1 c_t^2$

00/22 01/23 10/20 11/21

00/32 01/33 10/30 11/31

00/02 01/03 10/00 11/01

00/12 01/13 10/10 11/11

0

1

2

3

State

4

5

6

7
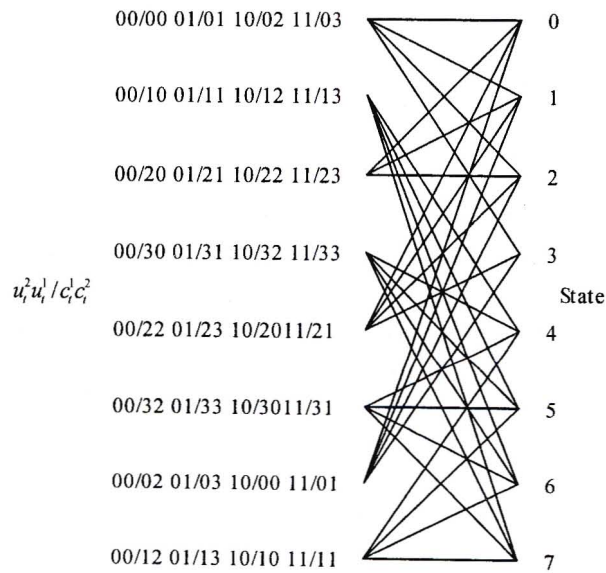
Figure C.3: Tarokh 8-state: $k = 2$, $m = 3$, $n_t = 2$, $M = 4$.

$u_t^2 u_t^1 / c_t^1 c_t^2$

00/00 01/01 10/02 11/03 — 0
00/12 01/13 10/10 11/11 — 1
00/20 01/21 10/22 11/23 — 2
00/32 01/33 10/30 11/31 — 3
00/20 01/21 10/22 11/23 — 4
00/32 01/33 10/30 11/31 — 5
00/00 01/01 10/02 11/03 — 6
00/12 01/13 10/10 11/11 — 7
00/02 01/03 10/00 11/01 — 8   State
00/10 01/11 10/12 11/13 — 9
00/22 01/23 10/20 11/21 — 10
00/30 01/31 10/32 11/33 — 11
00/22 01/23 10/20 11/21 — 12
00/30 01/31 10/32 11/33 — 13
00/02 01/03 10/00 11/01 — 14
00/10 01/11 10/12 11/13 — 15
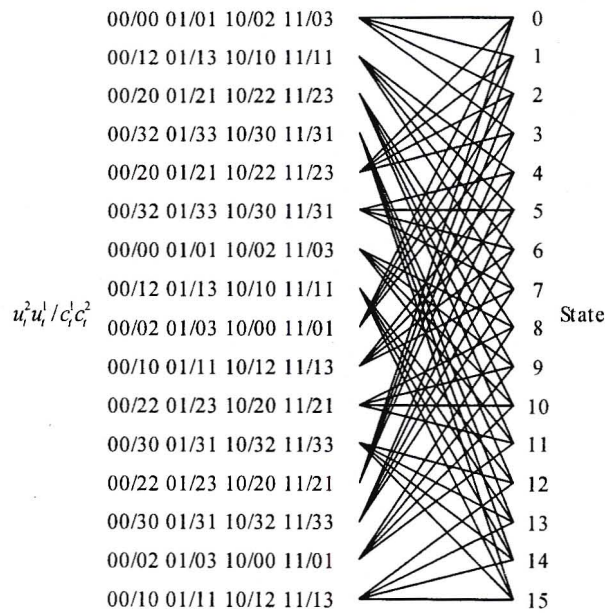
Figure C.4: Tarokh 16-state: $k = 2$, $m = 4$, $n_t = 2$, $M = 4$.

$u_t^2 u_t^1 / c_t^1 c_t^2$

00/00 01/22 10/02 11/20 — 0
00/12 01/30 10/10 11/32 — 1   State
00/21 01/03 10/23 11/01 — 2
00/33 01/11 10/31 11/13 — 3
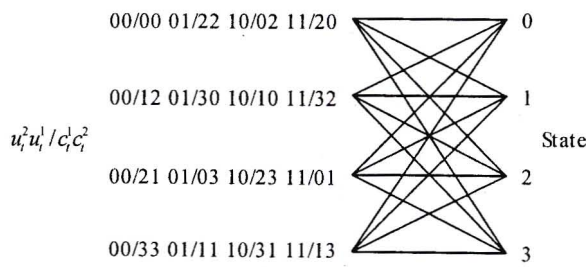
Figure C.5: Yan 4-state: $k = 2$, $m = 2$, $n_t = 2$, $M = 4$.

$u_t^2 u_t^1 / c_t^1 c_t^2$

00/00 01/01 10/02 11/03 — 0
01/10 10/11 11/12 00/13 — 1   State
10/20 11/21 00/22 01/23 — 2
11/30 00/31 01/32 10/33 — 3

Figure C.6: Recursive 4-state: $k = 2$, $m = 2$, $n_t = 2$, $M = 4$.

C.2   Convolutional codes

In this section the generating matrices for the constituent convolutional codes used in this dissertation are presented.

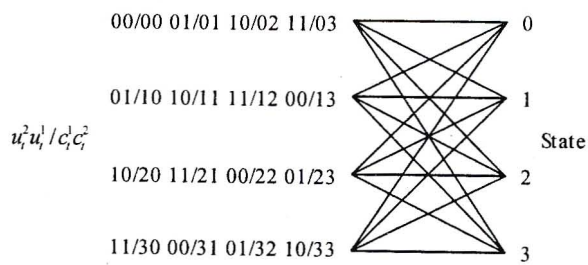$$G(D) = \left[1, \frac{1 + D^2}{1 + D + D^2} \right]$$

Recursive systematic, rate 1/2, 4-state.

$$G(D) = \left[1, \frac{1 + D^4}{1 + D + D^2 + D^3 + D^4} \right]$$

Recursive systematic, rate 1/2, 16-state.

$$G(D) = \left[\begin{array}{ccc} 1, & 0, & \frac{1+D^2}{1+D+D^2} \\ 0, & 1, & \frac{1+D}{1+D+D^2} \end{array} \right]$$

Recursive systematic, rate 2/3, 4-state.

$$G(D) = \left[\begin{array}{ccc} 1 + D, & D, & 1 \\ 1 + D, & 1, & 1 + D \end{array} \right]$$

Non-recursive, rate 2/3, 4-state.

Appendix D

Simulation description

The simulation results presented throughout this dissertation were generated using Monte-Carlo methods whereby the same simulation is repeated many times until a sufficient number of errors are generated. All simulations were developed by the author using the C++ programming language. The performance of many different systems are simulated in this dissertation and in this section the general structure of the simulation procedure is described.

A flow diagram describing the general simulation procedure for each system is shown in Fig. D.1. The system is initialised with the appropriate parameters. When a single ST encoder is employed, as discussed in chapters 2 and 3, the number of decoding iterations is 1. The flow diagram is clarified by the description of turbo codes given in section 4.2.1. For each data point on the BER or FER performance curve the following procedure is followed.
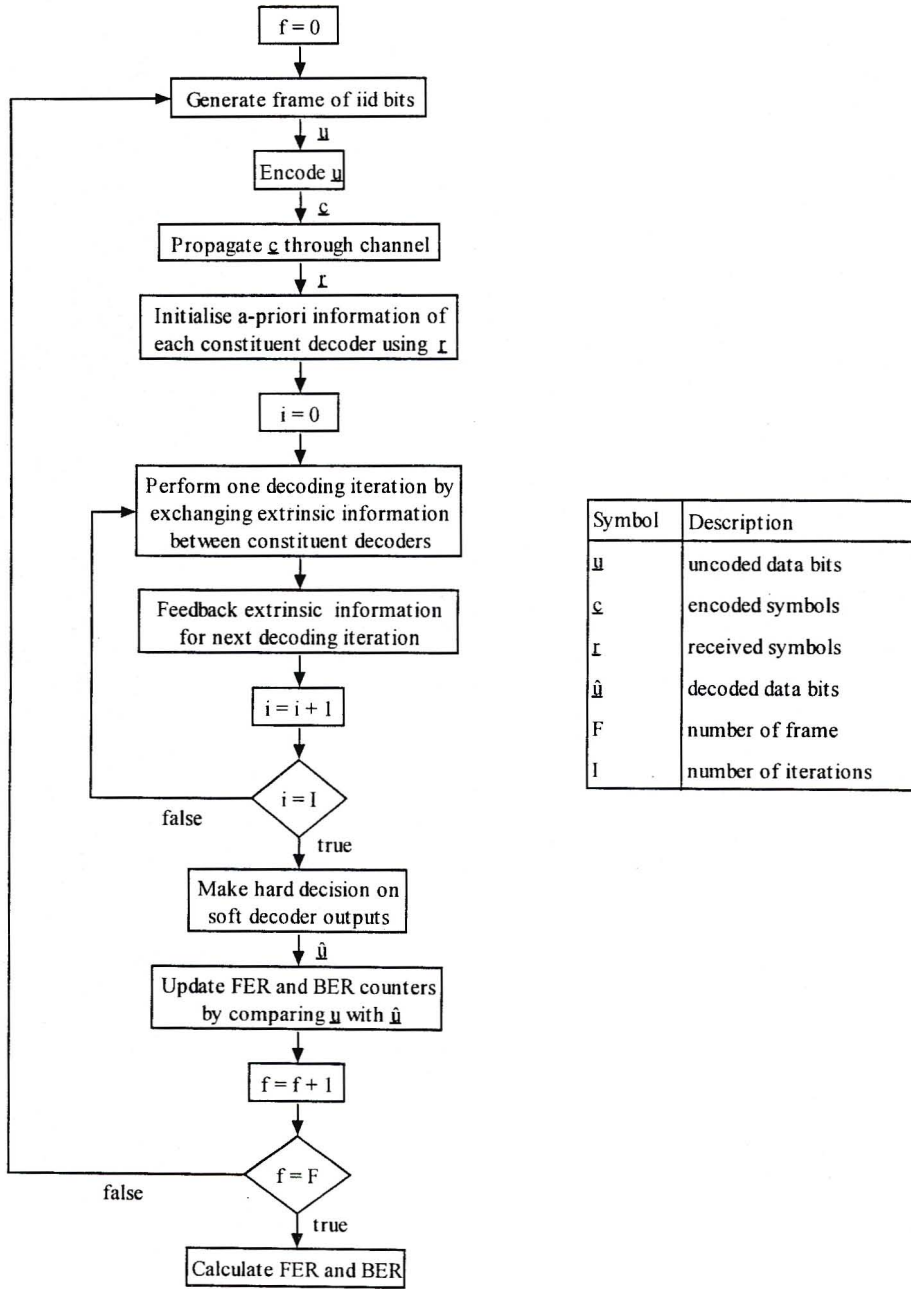
Figure D.1: Flow diagram for general code structure.

Bibliography

[1] CDMA Development Group, "3rd Generation Mobile Wireless - A Presentation on the Opportunities and Challenges of Delivering Advanced Mobile Communications Services," http://www.cdg.org/3GPavilion/overview.asp, 21 Sep. 2001.

[2] J. G. Proakis, *Digital Communications.* McGraw-Hill Companies, Inc., fourth ed., 2001.

[3] I. S. Reed and G. Solomon, "Polynomial codes over certain finite fields," *SIAM Journal on Applied Mathematics*, vol. 8, pp. 300–304, 1960.

[4] P. Elias, "Coding for noisy channels," *IRE Conv. Record*, vol. 4, pp. 37–47, 1955.

[5] A. J. Viterbi, "Error bounds for convolutional codes and an asymptotically optimum decoding algorithm," *IEEE Trans. Commun.*, vol. 13, pp. 260–269, Apr. 1967.

[6] G. D. Forney, "Concatenated Codes", Cambridge MA: MIT Press, 1966.

[7] C. Berrou, A. Glavieux and P. Thitimajshima, "Near Shannon limit error-correcting coding and decoding: Turbo codes," in *Proc. IEEE ICC '93*, Geneva, Switzerland, May 1993, pp. 1064–1070.

[8] C. Berrou, A. Glavieux and P. Thitimajshima, "Near optimum error correcting coding and decoding. Turbo-codes," *IEEE Trans. Commun.*, vol. 44, pp. 1261–1271, Oct. 1996.

[9] H. Taub and D. L. Schilling, *Principles of communication systems.* McGraw-Hill Book Company, second ed., 1986.

[10] G. Ungerboeck, "Trellis-coded modulation with redundant signal sets – Part II: State of the art," *IEEE Commun. Mag.*, vol. 25, pp. 12–21, Feb. 1987.

[11] P. Robertson and T. Woröz, "Bandwidth-efficient turbo trellis-coded modulation using punctured component codes," *IEEE J. Select. Areas Commun.*, vol. 16, pp. 206–218, Feb. 1998.

[12] S. Benedetto, D. Divsalar, G. Montorsi and F. Pollara, "Bandwidth efficient parallel concatenated coding schemes," *Electron. Lett.*, vol. 31, pp. 2067–2069, Nov. 1995.

[13] B. E. Wahlen and C. Y. Mai, "Turbo coding applied to pragmatic trellis-coded modulation," *IEEE Commun. Lett.*, vol. 4, pp. 65–67, Feb. 2000.

[14] Asha Mehrotra, *Cellular radio performance engineering*. Boston Mass. : Artec House, 1994.

[15] A. Klein, B. Steiner and A. Steil, "Known and novel diversity approaches as a powerful means to enhance the performance of cellular mobile radio systems," *IEEE J. Select. Areas Commun.*, vol. 14, pp. 1784–1795, Dec. 1996.

[16] I. E. Telatar, "Capacity of multi-antenna Gaussian channels," Tech. Rep. #BL0112170-950615-07TM, AT&T Bell Laboratories, 1995.

[17] T. L. Marzetta and B. M. Hochwald, "Capacity of a mobile multiple-antenna communication link in Rayleigh flat fading," *IEEE Trans. Inform. Theory*, vol. 45, no. 1, pp. 139–157, Jan. 1999.

[18] G. J. Foshcini and M. J. Gans, "On limits of wireless communications in a fading environment when using multiple antennas," *Wireless Personal Communications*, vol. 6, no. 3, pp. 311–335, Mar. 1998.

[19] G. J. Foschini, "Layered space-time architecture for wireless communication in a fading environment when using multiple antennas," *Bell Labs Tech. J.*, vol. 1, pp. 41–59, Autumn 1996.

[20] G. D. Golden, G. J. Foschini, R. A. Valenzuela and P. W. Wolniansky, "Detection algorithm and initial laboratory results using the V-BLAST space-time communications architecture," *Electron. Lett.*, vol. 35, pp. 14–15, Jan. 1999.

[21] V. Tarokh, N. Seshadri and A. R. Calderbank, "Space-time codes for high data rate wireless communication: performance criterion and code construction," *IEEE Trans. Inform. Theory*, vol. 44, pp. 744–765, Mar. 1998.

[22] V. Tarokh, H. Jafarkhani and A. R. Calderbank, "Space-time block codes from orthogonal designs," *IEEE Trans. Inform. Theory*, vol. 45, pp. 1456–1467, July 1999.

[23] A. F. Naguib, N. Seshadri and A. R. Calderbank, "Increasing data rater over wireless channels," *IEEE Signal Processing Magazine*, May 2000.

[24] D. Bevan and R. Tanner, "Performance comparison of space-time coding techniques," *Electron. Lett.*, vol. 45, pp. 1707-1708, Oct. 1998.

[25] E. Biglieri, G. Caire and G. Taricco, "Recent results on coding for multiple-antenna transmission systems," in *Proc. IEEE ISSSTA 2000*, New Jersey, USA, Sept. 2000, pp. 117–121.

[26] D. Cui, "Turbo space-time coded modulation: Principles and performance analysis," *PhD Dissertation*, Faculty of New Jersey Institute of Technology, May 2001.

[27] G. Caire, G. Taricco and E. Biglieri, "Bit-interleaved coded modulation," *IEEE Trans. Inform. Theory*, vol. 44, pp. 927–946, May 1998.

[28] A. Stefanov and T. M. Duman, "Turbo coded modulation system for systems with transmit and receive antenna diversity," in *Proc. IEEE GLOBECOM '99*, Rio de Janeiro, Brazil, Dec. 1999, pp. 2336–2340.

[29] G. J. Foschini, G. D. Golden, R. A. Valenzuela and P. W. Wolniansky, "Simplified processing for high spectral efficiency wireless communication employing multi-element arrays," *IEEE J. Select. Areas Commun.*, vol. 17, pp. 1841–1852, Nov. 1999.

[30] S. M. Alamouti, "A simple transmit diversity technique for wireless communications," *IEEE J. Select. Areas Commun.*, vol. 16, pp. 1451–1458, Oct. 1998.

[31] V. Tarokh, H. Jafarkhani and A. R. Calderbank, "Space-time block coding for wireless communications: Performance results," *IEEE J. Select. Areas Commun.*, vol. 17, pp. 451–460, Mar. 1999.

[32] B. M. Hochwald and T. L. Marzetta, "Unitary space-time modulation for multiple-antenna communications in Rayleigh flat fading," *IEEE Trans. Inform. Theory*, vol. 46, pp. 543–564, Mar. 2000.

[33] B. M. Hochwald and W. Sweldens, "Differential unitary space-time modulation," *IEEE Trans. Commun.*, vol. 48, pp. 2041–2052, Dec. 2000.

[34] V. Tarokh and H. Jafarkhani, "A differential detection scheme for transmit diversity," *IEEE J. Select. Areas Commun.*, vol. 18, pp. 1169–1174, July 2000.

[35] A. R. Hammons and H. E. Gamal, "On the theory of space-time codes for PSK modulation," *IEEE Trans. Inform. Theory*, vol. 46, pp. 524–542, Mar. 2000.

[36] S. Bäro, G. Bauch and A. Hansmann, "New trellis codes for space-time coded modulation," in *Proc. 3rd ITG Conference on Source and Channel Coding*, Munich, Germany, Jan. 2000, pp. 147–150.

[37] Q. Yan and R. S. Blum, "Optimum space-time convolutional codes," in *Proc. IEEE WCNC 2000*, Chicago, IL, Sep. 2000.

[38] Y. Gong and K. B. Letaief, "Performance of space-time trellis coding over Nakagami fading channels," in *Proc. IEEE VTC, 2001*, Rhodes, Greece, May 6-9, 2001.

[39] M. P. Fitz, J. Grimm and S. Siwamogsatham, "A new view of performance analysis techniques in correlated Rayleigh fading," in *Proc. IEEE WCNC '99*, New Orleans, LA, Sep 21-24, 1999.

[40] D. N. Rowitch, "Convolutional and Turbo Coded Multicarrier Direct Sequence CDMA and Applications of Turbo Codes to Hybrid ARQ Communication Systems," *PhD dissertation*, University of California, San Diego.

[41] D. Divsalar, S. Dolinar and F. Pollara, "Transfer function bounds on the performance of turbo codes," *JPL TDA Prog. Rep. 42-122*, pp. 44-55, 15 Aug. 1995.

[42] E. Malkamäki, H. Leib, "Evaluating the performance of convolutional codes over block fading channels," *IEEE Trans. Inform. Theory*, vol. 45, pp. 1643-1646, Jul. 1999.

[43] D. K. Aktas and M. P. Fitz, "Computing the distance spectrum of space-time trellis codes," in *Proc. WCNC 2000*, Chicago IL, Sep. 2000.

[44] R. Gozali and B. D. Woerner, "Upper bounds on the bit-error probability of space-time trellis codes using generating function techniques," in *Proc. IEEE VTC 2001*, Rhodes, Greece, May 6-9, 2001.

[45] A. P. des Rosiers and P. H. Siegel, "On performance bounds for space-time coded modulation on fading channels," in *Proc. International Symposium on Information Theory and Its Applications*, Honolulu, Hawaii, USA, Nov. 5-8, 2000.

[46] S. Benedetto, M. Mondin and G. Montorsi, "Performance evaluation of trellis-coded modulation schemes," *Proc. IEEE*, vol. 82, pp. 832–855, June 1994.

[47] G. D. Forney, "Geometrically uniform codes," *IEEE Trans. Inform. Theory*, vol. 37, pp. 1241–1260, Sep. 1991.

[48] A. Genz and A. Malik, "An adaptive algorithm for numerical integration over an N-dimensional rectangular region," *Journal of Computational and Applied Mathematics*, Vol. 6, pp. 295-302, 1980.

[49] P. Van Dooren and L. De Riddler, "An adaptive algorithm for numerical integration over an N-dimensional cube," *Journal of Computational and Applied Mathematics*, vol. 2, pp. 207-217, 1976.

[50] J. D. Anderson, "A turbo tutorial," Report TELE-15 ISSN 1396-1535, Institute of Telecommunication, Technical University of Denmark, Oct. 1999.

[51] W. E. Ryan, "A turbo tutorial," Submitted to *IEEE Globecom '97*, 1997

[52] B. Sklar, "A primer on turbo code concepts," *IEEE Commun. Mag.*, pp. 94–102, Dec. 1997.

[53] J. P. Woodard and L. Hanzo, "Comparative study of turbo decoding techniques: An overview," *IEEE Trans. Vehic. Tech.*, vol. 49, pp. 2208–2232, Nov. 2000.

[75] D. Tujkovic, "Space-time turbo coded modulation," in *Proc. Finnish Wireless Communications Workshop (FWCW)*, May 2000, pp.85–89.

[76] D. Tujkovic, "Recursive space-time trellis codes for turbo coded modulation," in *Proc. IEEE GLOBECOM '00*, San Francisco, CA, vol. 2, Nov. 2000, pp.1010–1015.

[77] Y. Wu, "Implementation of parallel and serial concatenated convolutional codes," *PhD dissertation*, Faculty of the Virginia Polytechnic Institute and State University, April 2000.

[78] D. Cui and A. Haimovich, "Design and performance of turbo space-time coded modulation," in *Proc. IEEE GLOBECOM '00*, San Fransisco, CA, Nov. 2000.

[79] S. Vishwanath, W. Yu, R. Negi and A. Goldsmith, "Space-time turbo codes: Decorrelation properties and performance analysis in fading channels," in *Proc. IEEE GLOBECOM '00*, San Fransisco, CA, Nov. 2000.

[80] S. Benedetto and G. Montorsi, "Average performance of parallel concatenated block codes," *Electron. Lett.*, vol. 31, pp. 156–158, Feb. 1995.

[81] S. Benedetto and G. Montorsi, "Performance evaluation of turbo-codes," *Electron. Lett.*, vol. 31, pp. 163–165, Feb. 1995.

[82] H. Xu and F. Takawira, "Turbo Coded/Diversity combining scheme for hybrid DS/SFH CDMA systems," in *Proc. Africon 1999*, Cape Town, SA, Sep. 1999, pp. 75–80.

[83] R. Prasad and T. Ojanperä, "An overview of CDMA evolution toward wideband CDMA," *IEEE Communications Surveys*, Fourth quarter 1998, vol. 1, no. 1.

[84] R. L. Pickholtz, D. L. Schilling and L. B. Milstein, "Theory of spread-spectrum communications - tutorial," *IEEE Trans. Commun.*, vol. COM-30, pp. 855–884, May 1982.

[85] R. Prasad, *CDMA for Wireless Personal Communications*. Artech House Publisher, London, 1996.

[86] J. Wang and M. Moeneclaey, "Hybrid DS/SFH-SSMA with predetection diversity and coding over indoor multipath Rician fading channels," *IEEE Trans. Commun.*, vol. 40, pp. 1654–1662, Oct. 1992.

[87] E. Geraniotis, "Noncoherent hybrid DS-SFH spread-spectrum multiple-access communications," *IEEE Trans. Commun.*, vol. COM-34, pp. 600–611, Sep. 1986.

[88] J.S. Thompson, P.M. Grant and B. Mulgrew, "Downlink transmit diversity schemes for CDMA networks," in *Proc. IEEE VTC Fall '99*, Amsterdam, Holland, Sept. 1999, pp. 1382–1386.

[89] P. van Rooyen, M. Lötter and D. van Wyk, *Space-time processing for CDMA mobile communications*. Kluwer Academic Publishers, 2000.

[90] K. Ban, M. Katayama, T. Yamazato and A. Ogawa, "Multi-antenna tranmission scheme for convolutionally coded DS/CDMA system," *IEICE Trans. Commun.*, vol. E80-A, pp. 2437–2444, Dec. 1997.

[91] S. A. Barbelescu, "Iterative decoding of turbo codes and other concatenated codes," *PhD thesis*, University of South Australia, Feb. 1996.

[92] D. J. van Wyk and L. P. Linde, "Turbo-code/multi-antenna diversity combining scheme for DS/CDMA systems," in *Proc. ISSSTA '98*, Sun City, South Africa, Sep. 1998, pp. 18–22.

[93] J. H. Kang and W. E. Stark, "Turbo codes for coherent FH-SS with partial band interference," in *Proc. IEEE MILCOM '97*, Monterey, CA, Nov. 1997.

[94] J. H. Kang and W. E. Stark, "Turbo codes for noncoherent FH-SS with partial band interference," *IEEE Trans. Commun.*, vol. 46, pp. 1451–1458, Nov. 1998.

[95] J. H. Kang and W. E. Stark, "Performance of turbo-coded FH-SS with partial-band interference and Rayleigh fading," in *Proc. IEEE MILCOM '98*, Boston, Massachusetts, Oct. 18-21, 1998.

[96] H. Xu and F. Takawira, "Performance of turbo-coded DS/SFH CDMA with partial-band interference and Rayleigh fading," in *Proc. ISSSTA 2000*, New Jersey, USA, Sep. 2000.

[97] D. Young and N. Beaulieu, "A quantitive evaluation of generation methods for cor-
related Rayleigh random variates," in *Proc. Globecom '98*, Sydney Australia, 8-12
Nov., vol.6, pp. 3332–3337.

[98] R. E. Ziemer and R. L. Petereson, *Digital communications and spread spectrum
systems*. New York, Macmillan, 1985.